ACR No. 4C11

NATIONAL ADVISORY COMMITTEE FOR AERONAUTICS

WARTIME REPORT

ORIGINALLY ISSUED
March 1944 as
Advance Confidential Report 4C11

WIND-TUNNEL INVESTIGATION OF SHIELDED HORN BALANCES AND TABS ON A 0.7-SCALE MODEL OF XF6F VERTICAL TAIL SURFACE

By John G. Lowry, James A. Maloney,
and I. Elizabeth Garner

Langley Memorial Aeronautical Laboratory
Langley Field, Va.

WASHINGTON

NATIONAL ADVISORY COMMITTEE FOR AERONAUTICS

ADVANCE CONFIDENTIAL REPORT

WIND-TUNNEL INVESTIGATION OF SHIELDED HORN BALANCES AND TABS ON A 0.7-SCALE MODEL OF XF6F VERTICAL TAIL SURFACE

By John G. Lowry, James A. Maloney,
and I. Elizabeth Garner

SUMMARY

An investigation was made in the LMAL 7- by 10-foot tunnel of a 0.7-scale model of the vertical tail surface of the Grumman XF6F airplane. The model was also utilized for a more general investigation of the effect on the hinge-moment characteristics of shielded horns of different chords, spans, and nose shapes and of trimming tabs of two nose shapes. An unshielded horn was tested for comparison with the shielded horn, and the results of the comparison are given.

Analysis of the data showed that for most tail surfaces it will be impossible to obtain by means of shielded horns a closely balanced surface and keep the rate of change of hinge-moment coefficient with angle of attack near zero without the addition of some other balancing device. With shielded horns, the rate of change of hinge-moment coefficient with rudder deflection could be reduced to about 50 percent of the unbalanced value without obtaining a positive value of the rate of change with angle of attack large enough to give steady oscillations of the airplane with free rudder. Pressure-distribution and tuft tests were made of the flow over horns of two nose shapes. Lower peak pressures and consequently higher critical speeds were obtained for the medium-nose horn than for the blunt-nose horn. The tests of the two trimming tabs showed that the shape of the tab nose made very little difference in the results.

INTRODUCTION

Tests were made in the LMAL 7- by 10-foot tunnel of a 0.7-scale model of the XF6F vertical tail surface. These tests were undertaken to obtain data for use in the design of shielded horns in general and to obtain data useful for the XF6F vertical tail in particular. Additional tests were made to determine tab characteristics for two different tabs and flow characteristics over several of the shielded horns.

The various shielded horn balances tested included models of the original horn on the XF6F airplane and of shielded horns of four chords, each of which was tested with two different spans and nose shapes. The variation in horn size covers the range from no balance to overbalance. Flow characteristics were determined by tuft tests of two of the smaller horns and pressure-distribution tests of two of the larger horns. The pressure-distribution data show the local velocity distribution of the two nose shapes tested. For convenience, the term "shielded horn" will generally be referred to as "horn," followed by a designation to indicate the horn size and nose shape.

Tests were made of an unshielded horn balance to determine whether any correlation between shielded and unshielded horns was possible. These tests were also the logical extension of those of the short-span shielded horns.

Characteristics of the tab were determined in order to have information useful in the design of any balancing or unbalancing device that uses tabs, as well as to have the characteristics of the particular trimming tabs tested. A round-nose tab of the same plan form and size as the original tab was tested to determine the variations in characteristics, if any, from the original tab. The round-nose tab represented the type of tab usually used on wind-tunnel models. Both tabs were tested sealed and unsealed.

APPARATUS AND METHODS

The model was mounted vertically in the LMAL 7- by 10-foot tunnel with one end adjacent to the floor of the

tunnel, which acted as a reflection plane. (See figs. 1 and 2.) The model was supported entirely by the balance frame (fig. 1) with a small clearance at the tunnel floor in order that all the forces and moments acting on the model could be measured. Provisions were made for changing the angle of attack of the model and the deflection of the rudder while the tunnel was in operation. The hinge moments of the moving surfaces were measured by means of electrical strain gages mounted within the model, and the rudder deflections were measured by an electrical position indicator attached to the rudder and mounted within the surface. For the pressure-distribution tests, the pressures were recorded photographically from a multiple-tube manometer located outside the tunnel.

The 0.7-scale model of the XF6F vertical tail surface was built by the National Advisory Committee for Aeronautics and conformed to the dimensions of figure 3. The airfoil sections used (fig. 3) were modified NACA 16-series airfoils with the portion rearward of the rudder hinge line faired to a flat contour. The tip contour was changed somewhat from the shape used on the airplane in that it was built with semicircular sections through the tip to allow for changing the horn shape and size easily. The trailing edges of the cover plates were 0.61 inch ahead of the rudder hinge line from the root section to station 47.93 and tapered from 0.61 inch at station 47.93 to 0.35 inch at the tip. The rudder was sealed with a flexible seal for most of the tests; the hinges, however, were not sealed. Some geometric characteristics of the model are given in the table in figure 3.

Several different arrangements of shielded horn balances were made for the model and are shown in figure 4. Horn 2-a (fig. 4(i)) represents the horn on the XF6F airplane with the exception of the tip fairing. The other shielded horns were tested with two different nose shapes. The blunt-nose horns are of airfoil contour from the hinge line to the point of tangency with the leading-edge radius. The medium nose shapes were made to the ordinates given in table I. The variations tested included horns of four chords and two spans and cover the range from no balance, plain rudder, to a condition of overbalance. The gap between the horn nose and fin extension was similar to the one on the airplane for horn 2-a and was maintained for all other horn arrangements. The gap between the inboard end of the horn

and fin was 0.22 inch, which corresponds to the gap on the XF6F vertical tail.

The unshielded horn tested is shown in figure 5 and was made to the same span as horns 1, 2, 3, and 7. The shape of the horn is the same as the airfoil tip shape and has the same gap between the horn and fin as the shielded horns.

The plan form and geometric characteristics of the tabs tested are given in figure 3 and the sections of the tabs are given in figure 6. The original tab represents the tab on the XF6F rudder. The leakage through the piano hinge was simulated by a piece of gauze. The round-nose tab was constructed as shown in figure 6 and had provisions for sealing. Both tabs were sealed with a flexible seal for some tests.

Horns 8-a and 8-b were modified for pressure-distribution tests by placing a row of orifices 5.97 inches from the inboard end of the horn, as shown in figure 7. The chordwise locations of the orifices are given in figure 7 and are the same for both horns, except that orifice 1 on horn 8-a was eliminated from horn 8-b. These orifices were connected to copper tubes that were in turn connected to leads from the manometer. The copper tubes were kept within the model until they were a few inches from the tunnel floor. When pressure-distribution tests were made, time was allowed for conditions in the tunnel and for the manometer to become stable before the pressures were photographed.

A dynamic pressure of 16.37 pounds per square foot, which corresponds to a velocity of about 80 miles per hour and to a test Reynolds number of about 2,300,000 based on the model mean chord of 3.16 feet, was maintained for nearly all tests. In some cases it was not possible to maintain the dynamic pressure at 16.37 pounds per square foot because of the high drag at large angles of attack and rudder deflections, for which the dynamic pressure was decreased and corresponding corrections were made in the computations.

RESULTS AND DISCUSSION

Coefficients and Symbols

The coefficients and symbols used in the report are defined as follows:

C_L	lift coefficient (L/q_oS)
C_D	drag coefficient (D/q_oS)
C_{D_i}	induced-drag coefficient
C_m	pitching-moment coefficient (M/q_oSc)
C_h	hinge-moment coefficient $(H/q_ob\bar{c}^2)$
P	pressure coefficient $\left[(p-p_o)/q_o\right]$
L	lift of model
D	drag of model
M	pitching moment about mounting-axis center line
H	moment about control-surface hinge line
S	area
q_o	dynamic pressure of free air stream $\left(\frac{1}{2}\rho V_o^2\right)$
b	span
c	chord (for movable surfaces, measured from hinge line to trailing edge)
c'	mean chord
$\bar{c}$	root-mean-square chord
B	balance coefficient $\left(\sqrt{S_Hc_H'/S_rc_r'}\right)$
p	static pressure at an orifice
p_o	static pressure of free air stream
ρ	mass density of air

V local velocity at a point

V_o free-stream velocity

α angle of attack of model

δ control-surface deflection relative to surface to which control surface is hinged, positive when trailing edge is moved left

$$c_{h_\alpha} = \left(\frac{\partial c_h}{\partial \alpha}\right)_{\delta_r, \delta_t}$$

$$c_{h_\delta} = \left(\frac{\partial c_h}{\partial \delta}\right)_{\alpha, \delta}$$

$$c_{L_\alpha} = \left(\frac{\partial c_L}{\partial \alpha}\right)_{\delta_r, \delta_t}$$

$$c_{L_\delta} = \left(\frac{\partial c_L}{\partial \delta}\right)_{\alpha, \delta}$$

Δc_{h_α} c_{h_α} of rudder with shielded horn - c_{h_α} of plain rudder

$\Delta c_{hr_{\delta_r}}$ $c_{hr_{\delta_r}}$ of rudder with shielded horn - $c_{hr_{\delta_r}}$ of plain rudder

All parameters have an angle range of about $\pm 5^\circ$.

Subscripts:

r rudder

t tab

H horn

Symbols or coefficients without subscript refer to complete vertical tail surface.

Corrections

All the coefficients have been corrected for the effect of the jet boundaries. No corrections have been made for the effect of gap between the root section and the floor or the leakage around the support strut. The over-all corrections applied (by addition) to the tunnel data are as follows:

$$\Delta\alpha = 1.53C_{L_{corrected}} \quad \text{(in deg)}$$

$$\Delta C_L = -0.012C_L$$

$$\Delta C_{D_i} = 0.0233C_L{}^2$$

$$\Delta C_m = 0.00447C_L$$

$$\Delta C_h = kC_L$$

where

Horn	k
None	0.0085
1	.0083
2	.0080
3	.0075
4	.0082
5	.0077
6	.0067
7	.0078
8	.0072
Unshielded	.0065

The results of the pressure-distribution tests have not been corrected as described.

The results of this investigation represent the aerodynamic characteristics of a semispan tail surface and will have to be changed to the proper aspect ratio if applied to a vertical tail surface. The effect of the horn and of tab deflection on the hinge-moment characteristics should, however, be applicable to any control surface of similar plan form without correction for aspect ratio. The absolute values of hinge-moment, lift, and drag coefficients should, however, be corrected if applied to a vertical tail surface for the purpose of estimating airplane characteristics.

Plain Rudder

Tests were made of the plain rudder to obtain a basis for the effect of the horns on the hinge-moment characteristics. These tests included tests of the rudder unsealed (fig. 8) and tests of the rudder sealed (fig. 9). Sealing the rudder had no effect on the lift characteristics but did change the value of $C_{h_r \delta_r}$ from -0.0084 to -0.0077.

Tests were made of the sealed rudder to determine the effect of fixing the transition at or near the leading edge of the surface (fig. 10). The transition was fixed by roughening the first 5 percent of the fin with No. 60 emery dust. The main effects of the roughness were to decrease slightly the slope of the lift curve C_{L_α}, to decrease the effectiveness of the rudder $C_{L_{\delta_r}}$, and to decrease the maximum lift coefficient. The hinge-moment characteristics were not appreciably affected by roughening the leading edges of the fin.

Shielded Horns

Original horn.- The results of the tests of the original horn (horn 2-a) are presented in figure 11. This horn represented the horn on the XF6F vertical tail except for the shape through the tip. A few tests were made of a horn of the same size and nose shape except that the radius on the outboard leading edge was eliminated, with the result that this horn had the same plan form as the other horns tested. The data of this modification were not noticeably different from the data of horn 2-a and are therefore not presented.

Modified horns.- The hinge-moment characteristics (fig. 12) indicate that the addition of the horn results in a positive increase in the slope of the hinge-moment-coefficient curves for both α and δ_r throughout the unstalled range of α or δ_r. The curves of hinge-moment coefficient against rudder deflection show no discontinuity when the horn unports, that is, when the chord line of the horn projects beyond the surface of the fin. Comparison of increments of hinge-moment coefficient for any of the various horns shows that the increment is linear with rudder deflection or angle of

attack through the unstalled range. A comparison of the individual curves of figures 12(a) and 12(b) indicates that, although the use of some of the larger horns gives a large positive increase in $C_{h_{r\delta_r}}$ over the small deflection range, the values of C_{h_r} for these horns in the stalled range with large rudder deflection are increased.

In order to obtain a more comprehensive comparison of the shielded horns, the values of ΔC_{h_α} and $\Delta C_{h_{r\delta_r}}$ were plotted against balance coefficient B of reference 1 in figure 13. The curves for the unshielded horns of reference 1 have been included for comparison. The data of figure 13 indicate that the values of ΔC_{h_α} and $\Delta C_{h_{r\delta_r}}$ increase evenly with balance coefficient. The values of ΔC_{h_α} are independent of nose shape for a given value of B, but the values of $\Delta C_{h_{r\delta_r}}$ are larger for the blunt nose than for the medium nose. The values of ΔC_{h_α} for the shielded horns are about 60 percent as great as for the unshielded horns in the range tested. The values of $\Delta C_{h_{r\delta_r}}$ are less for the shielded horns for values of B below 0.35 but are higher than for the unshielded horns for values of B greater than 0.35.

A comparison of the lift characteristics for several arrangements of shielded horns (table II) indicates that there are only small changes in C_{L_α} and $C_{L_{\delta_r}}$ with horn shape or size. A large part of the variations shown may be the result of experimental error. The test data are not presented for the lift characteristics, which were very similar to the characteristics of the plain rudder. The nose shape of the horn had little effect on the value of $C_{L_{\delta_r}}$ taken from deflections of $\pm 10^\circ$, but the medium nose in some cases gave a value of $C_{L_{\delta_r}}$ based on deflections of $\pm 4^\circ$ about 5 to 10 percent less than those based on deflections of $\pm 10^\circ$. This effect was, however, limited to small deflections and did not affect the values of C_L at large values of δ_r.

Complete force tests were made of the XF6F vertical tail with horns 8-a and 8-b to determine the characteristics of a horn giving closer balance than horn 2-a. The results of these tests are presented in figures 14 and 15 and can be used to estimate the hinge-moment-coefficient curves for other horns by interpolating between the values for horn 8 and horn 2 and/or the plain rudder from the curves of figure 13.

Dynamic-stability estimates.- Closely balanced rudders are desirable, but balancing the XF6F rudder with a shielded horn leads to a positive value of C_{h_α}. The oscillatory characteristics of the XF6F airplane were estimated by the method of reference 2. It was assumed that the rudder had no moment of inertia and that the rudder was mass-balanced, although the rudder was known to have some mass overbalance on the airplane. The assumption of no inertia tends to overestimate the stabilizing effect on the oscillations whereas the assumption that the rudder is mass-balanced tends to underestimate the effect. (See reference 2.) It appears that all of the horns except 6 and 8 would fall in the completely damped region; all of the horns except 3, 6, and 8 could be further balanced by use of balancing tabs without going out of the region of complete damping.

From reference 2 it appears that if the rudder is to be closely balanced - that is, $C_{h_{r_{\delta_r}}}$ approaches zero - C_{h_α} must be held near zero if complete damping is to be obtained. A comparison of the values of ΔC_{h_α} and $\Delta C_{h_{r_{\delta_r}}}$ at a constant value of B from figure 13 indicates that ΔC_{h_α} increases about seven-tenths as fast as $\Delta C_{h_{r_{\delta_r}}}$; thus, if complete balance is to be obtained by use of shielded horn alone, the unbalanced control must have the ratio $C_{h_\alpha}/C_{h_{r_{\delta_r}}} = 0.7$. Inasmuch as this ratio appears to give a value of C_{h_α} higher than found with most control surfaces, some other type of balance is required to reduce $C_{h_{r_{\delta_r}}}$ to give the ratio desired. Several types of balancing device may be used

including internal balances, overhang, or balancing tabs; however, any balancing device that reduces C_{h_α} about the same amount as $C_{h_{r_{\delta_r}}}$ cannot be used. The results of this study indicated that for the XF6F vertical tail surface it is possible to reduce $C_{h_{r_{\delta_r}}}$ to about 50 percent of the unbalanced value without obtaining positive values of C_{h_α} large enough to give steady oscillations.

Tuft study.- Figures 16 and 17 give some of the results of the tuft study of horns 2-c and 2-d, respectively. These photographs show the flow characteristics over the two horns at several rudder deflections and two angles of attack. The results indicate little difference between the two nose shapes, blunt-nose horn 2-c and medium-nose horn 2-d, except at zero rudder deflection and zero angle of attack, for which the medium nose shows unsteady flow over the leading edge of the horn. The photograph of horn 2-c with $\alpha = 0^\circ$ and $\delta_r = 0^\circ$ is not shown, as the tufts all lay straight back. Figure 18 shows the flow over the tip of the tail surface at several angles of attack with the rudder neutral.

Pressure distribution.- The pressure-distribution diagrams (figs. 19 to 28) give the pressures over the upper and lower surfaces of horns 8-a and 8-b for several angles of attack and rudder deflections. The pressures are plotted normal to the chord line of the rudder and horn. Although taken at only one spanwise location, these pressure curves should be useful in the design of shielded horns, as they give a general distribution of the loads over the horn.

The curves indicate that, in general, the medium-nose shielded horn 8-b gave lower peak pressures and consequently higher critical speeds than the blunt-nose horn 8-a. Additional pressure data were taken that showed a considerable hysteresis in stall characteristics, but the force tests failed to show this effect in the rudder hinge moments. This effect might result because the rudder shows a hysteresis that compensates for the change in flow over the horn. No results that show this effect are presented because pressure tests of the rudder are not available and the over-all hinge-moment coefficients were not changed.

The pressure plots can also be used to determine the local velocity ratio over the shielded horn by means of the equation

$$V/V_o = \sqrt{1 - P}$$

where

V local velocity at a point

V_o free-stream velocity

By using the curve of figure 22 of reference 3 and the peak pressures found from the pressure-distribution tests of horns 8-a and 8-b, the curves of figure 29 were estimated. Although the test points shown in figure 22 of reference 3 do not fall on the curve, later tests of symmetrical airfoils show good agreement with the curve. The curves of figure 29 show that the reduction of critical Mach number with rudder deflection is much less for the medium-nose than for the blunt-nose horn, as would be expected. Inasmuch as no pressure measurements were made over the complete tail surface, it is impossible to determine whether these pressures are critical for the tail assembly or for the horn only. Figure 29 does, however, indicate the critical speeds of the various horns plotted against rudder deflection and may be useful in determining the horn nose shape.

Unshielded Horn

The results of the tests of the unshielded horn on the model of the XF6F vertical tail surface (fig. 30) show irregularities in the hinge-moment-coefficient curves not found in the curves for shielded horns (figs. 11 and 14). The values of $\Delta C_{h_{r\delta_r}}$ and ΔC_{h_α} for the unshielded horn are plotted in figure 13 and agree quite well with the unshielded horns of reference 1. The value of $\Delta C_{h_{r\delta_r}}$ falls within the range of B for which there is little difference between the shielded and unshielded horns and therefore agrees quite well with the medium-nose shielded horns.

The unshielded horn tested was expected to be too large for the XF6F vertical tail but was tested solely to obtain a comparison between shielded and unshielded

horns of the same span. If an unshielded horn were used, it would have to be considerably smaller and would have to have an auxiliary balance device to reduce the negative value of $C_{h_r \delta_r}$.

Tab Characteristics

The results of the tests of the original tab are presented in figures 31 to 36 and of the round-nose tab, in figures 37 to 44. The original tab is less effective in the negative rudder deflection range when the tab is deflected negatively than when the tab is deflected positively or when the round-nose tab is used. With both the original and the round-nose tabs, the tab and rudder hinge-moment coefficients indicate that, in the high negative rudder and tab deflection range and with α near 25°, the tab stalls and shows little change in hinge-moment coefficient C_{h_t} with rudder deflection and in rudder hinge-moment coefficient C_{h_r} with tab deflection. As δ_t is reduced to zero, the condition eases and is improved when the tab is deflected positively. In fact, when δ_t is 20°, there is a very large increase in C_{h_t} as the rudder is deflected from -20° to -32°.

Both the original and the round-nose tabs were sealed for some tests to determine the effect of the seal. Sealing the original tab appears to have changed $\left(\partial C_{h_r}/\partial \delta_t\right)_{\alpha, \delta_r}$ from -0.020 to about -0.025 and $C_{h_{t_{\delta_t}}}$ from -0.0070 to -0.0065. Sealing the round-nose tab changed $\left(\partial C_{h_r}/\partial \delta_t\right)_{\alpha, \delta_r}$ from -0.025 to about -0.032 and $C_{h_{t_{\delta_t}}}$ from -0.0055 to -0.0045.

The data presented for the two trimming tabs are applicable to a rudder with any of the horn modifications tested. These data should be useful in the design of any tab device to reduce the amount of overbalance or to be used as an unbalancing tab. The data were taken on the rudder with no horn in order that the tab effects would be more easily distinguished, as the hinge-moment-coefficient curves for the unbalanced rudder are, in general, more regular.

CONCLUSIONS

An investigation was made in the LMAL 7- by 10-foot tunnel of a 0.7-scale model of the vertical tail surface of the Grumman XF6F airplane. Tests to determine the effect on the hinge-moment characteristics of an unshielded horn, of shielded horns of different chords, spans, and nose shapes, and of trimming tabs of two nose shapes indicated the following conclusions:

1. The addition of the shielded horns gave a change in hinge-moment variation with angle of attack about 60 percent as great as unshielded horns for the same balance coefficient. (The balance coefficient is the square root of the ratio of the product of the horn area and mean chord of the horn to the product of the rudder area and mean chord of the rudder.) For the shielded horns, the change in hinge-moment variation with rudder deflection was less than for the unshielded horn for horns of small balance coefficient and greater for horns of large balance coefficient. The ratio of the change in hinge-moment variation with angle of attack to change with rudder deflection was about 0.7 for the shielded horns.

2. For the XF6F vertical tail surface the rate of change of hinge-moment coefficient with rudder deflection could be reduced with shielded horns to about 50 percent of the unbalanced value without obtaining a positive value of the rate of change with angle of attack large enough to give steady oscillations of the airplane with free rudder.

3. For most tail surfaces it will be impossible to obtain a closely balanced surface by means of shielded horns and keep the rate of change of hinge-moment coefficient with angle of attack near zero without the addition of some other balancing device of which the main function is to reduce the negative hinge moment due to deflection.

4. The pressure-distribution tests showed that, in general, the medium-nose horn gave lower peak pressures and consequently higher critical speeds than the blunt-nose horn.

5. The two tabs tested gave approximately the same results.

Langley Memorial Aeronautical Laboratory,
National Advisory Committee for Aeronautics,
Langley Field, Va.

REFERENCES

1. Lowry, John G.: Résumé of Hinge-Moment Data for Unshielded Horn-Balanced Control Surfaces. RB No. 3F19, NACA, 1943.

2. Greenberg, Harry, and Sternfield, Leonard: A Theoretical Investigation of the Lateral Oscillations of an Airplane with Free Rudder with Special Reference to the Effect of Friction. NACA ARR, March 1943.

3. Stack, John, Lindsey, W. F., and Littell, Robert E.: The Compressibility Burble and the Effect of Compressibility on Pressures and Forces Acting on an Airfoil. Rep. No. 646, NACA, 1938.

TABLE I.- ORDINATES FOR MEDIUM NOSE SHAPES

[Spanwise stations in in. from root section.
Chordwise stations and ordinates in in.]

Horns 1 and 4		
Chordwise station	Ordinates	
	Spanwise station 41.01	54.62
0	0	0
.03	.152	.071
.08	.247	.115
.13	.314	.146
.23	.414	.193
.43	.556	.259
.93	.778	.363
1.43	.916	.427
2.43	1.050	.489
2.93	1.066	.496
3.43	1.050	.489
3.76	1.020	.475

Horns 2 and 5		
Chordwise station	Ordinates	
	Spanwise station 41.01	54.62
0	0	0
.02	.100	.047
.05	.186	.086
.12	.242	.113
.22	.326	.152
.72	.576	.268
1.22	.732	.341
1.72	.845	.393
2.29	.942	.439
2.72	.999	.465
3.72	1.090	.507
4.72	1.133	.528
5.22	1.138	.530
5.72	1.133	.528
6.72	1.090	.507
7.52	1.020	.475

Horns 3 and 6		
Chordwise station	Ordinates	
	Spanwise station 41.01	54.62
0	0	0
.05	.142	.066
.20	.284	.132
.30	.345	.161
.80	.554	.258
1.30	.694	.323
1.80	.800	.373
2.30	.887	.413
3.30	1.019	.474
4.30	1.111	.517
5.30	1.172	.546
6.30	1.206	.562
6.80	1.216	.566
7.30	1.218	.567
8.30	1.206	.562
9.30	1.172	.546
10.30	1.111	.517
10.80	1.069	.498
11.28	1.020	.475

Horns 7 and 8		
Chordwise station	Ordinates	
	Spanwise station 41.01	54.62
0	0	0
.04	.142	.066
.17	.284	.132
.25	.345	.162
.68	.554	.258
1.10	.694	.323
1.53	.800	.373
1.95	.887	.413
2.80	1.019	.474
3.65	1.111	.517
4.50	1.172	.546
5.35	1.206	.562
5.77	1.216	.566
6.20	1.218	.567
7.05	1.206	.562
7.90	1.172	.546
8.74	1.111	.517
9.17	1.069	.498
9.58	1.020	.475

TABLE II.- SUMMARY OF CHARACTERISTICS OF SHIELDED HORNS ON 0.7-SCALE MODEL OF XF6F VERTICAL TAIL SURFACE

Horn	B	S_H/S_r	C_{L_α}	C_{L_δ}	C_{h_α}	C_{h_δ}
None	0	0	0.053	0.034	-0.0020	-0.0077
1-a	.106	.038	.052	.034	-.0014	-.0074
1-b	.106	.038	.052	.035	-.0016	-.0075
2-a	.210	.075	.052	.034	-.0007	-.0062
2-c	.210	.075	.050	.036	-.0010	-.0065
2-d	.210	.075	.052	.036	-.0006	-.0070
3-a	.310	.111	.053	.035	.0010	-.0037
3-b	.310	.111	.053	.034	.0008	-.0045
4-a	.151	.076	.054	.036	-.0013	-.0072
4-b	.151	.076	.053	.036	-.0017	-.0075
5-a	.303	.151	.054	.036	.0001	-.0037
5-b	.303	.151	.055	.036	.0005	-.0045
6-a	.453	.226	.054	.036	.0034	.0019
6-b	.453	.226	.053	.037	.0040	0
7-a	.268	.094	.054	.037	-.0002	-.0058
7-b	.268	.094	.054	.036	-.0003	-.0060
8-a	.386	.187	.053	.036	.0018	-.0013
8-b	.386	.187	.053	.036	.0017	-.0026

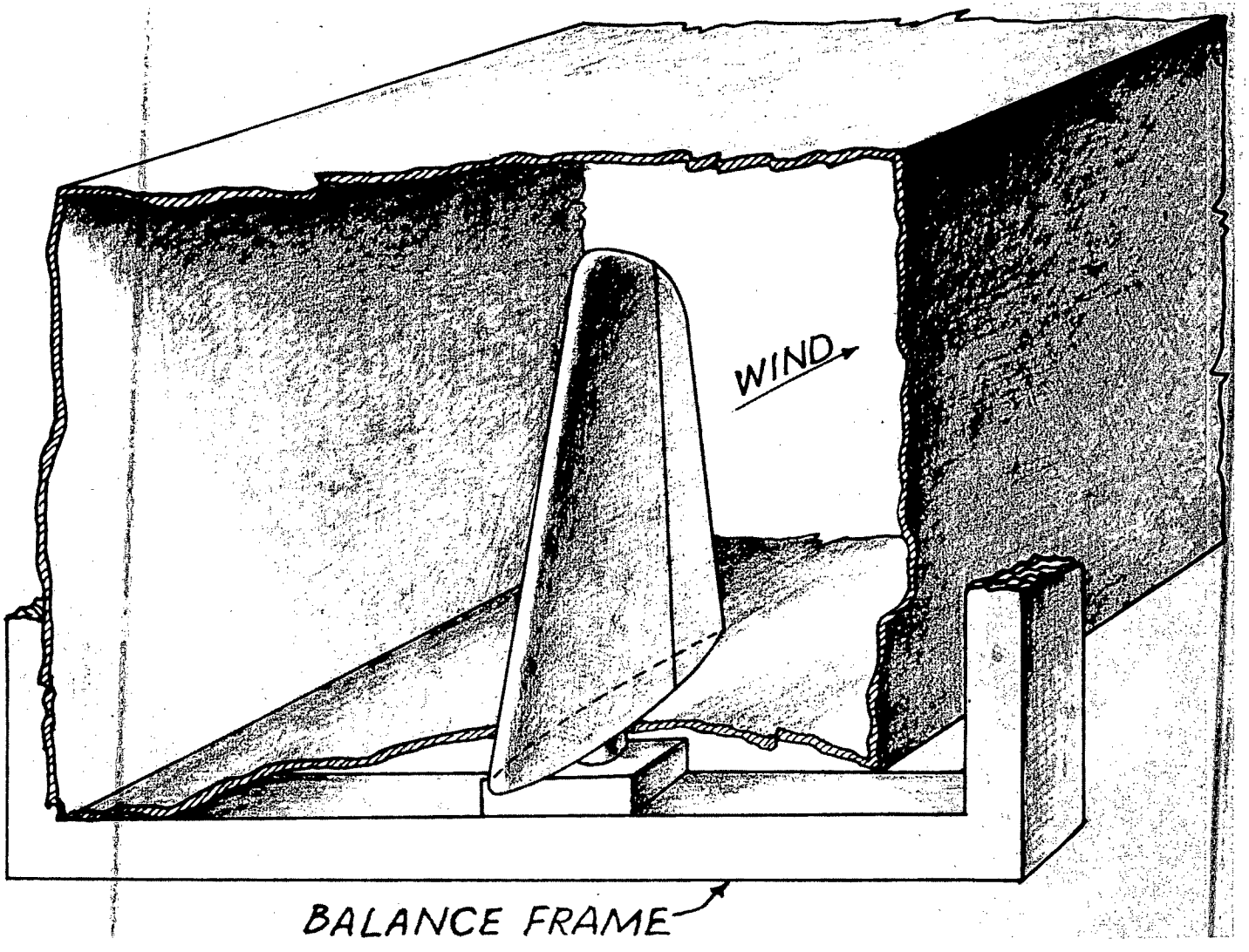

Figure 1.- Vertical-tail-surface setup in LMAL 7- by 10-foot tunnel

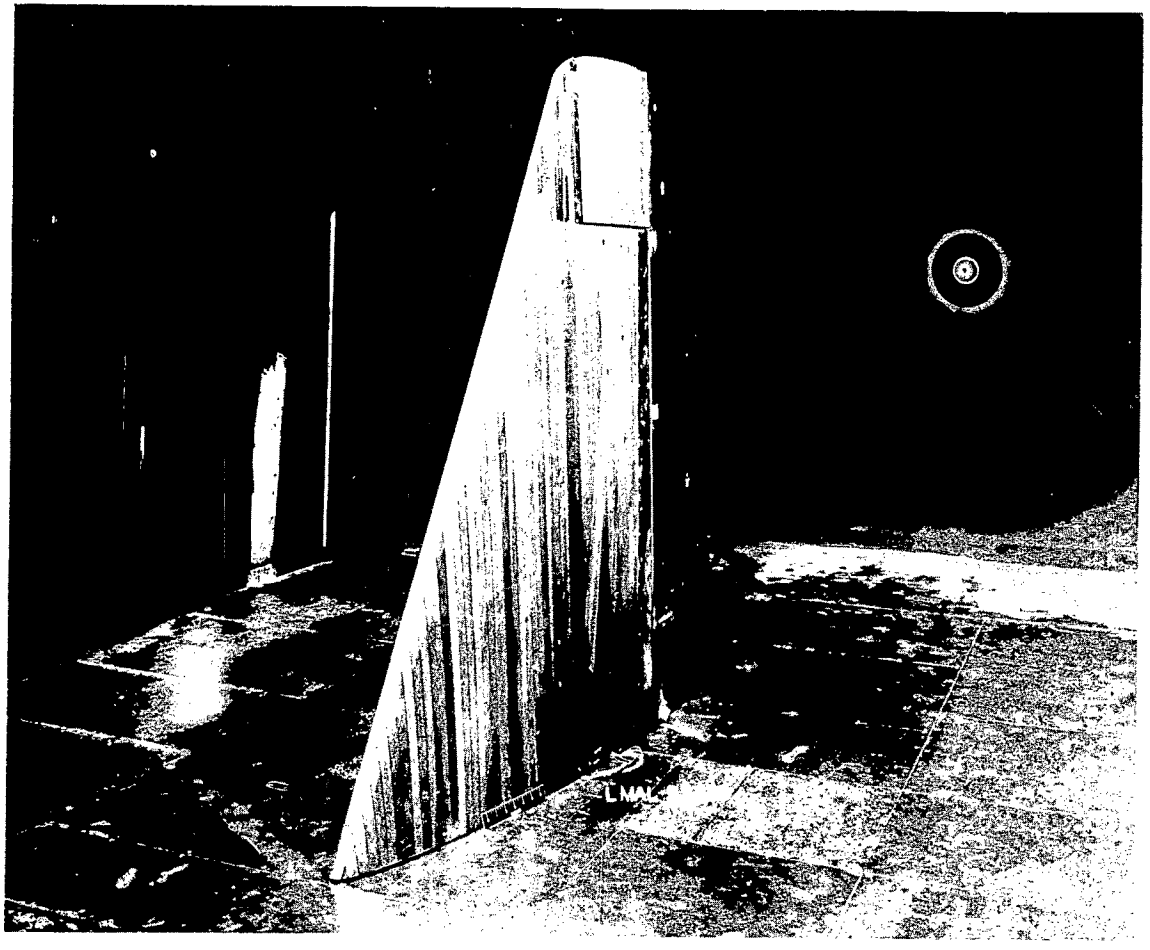

Figure 2.- Three-quarter front view of installation of 0.7-scale model of XF6F vertical tail surface in LMAL 7- by 10-foot tunnel.

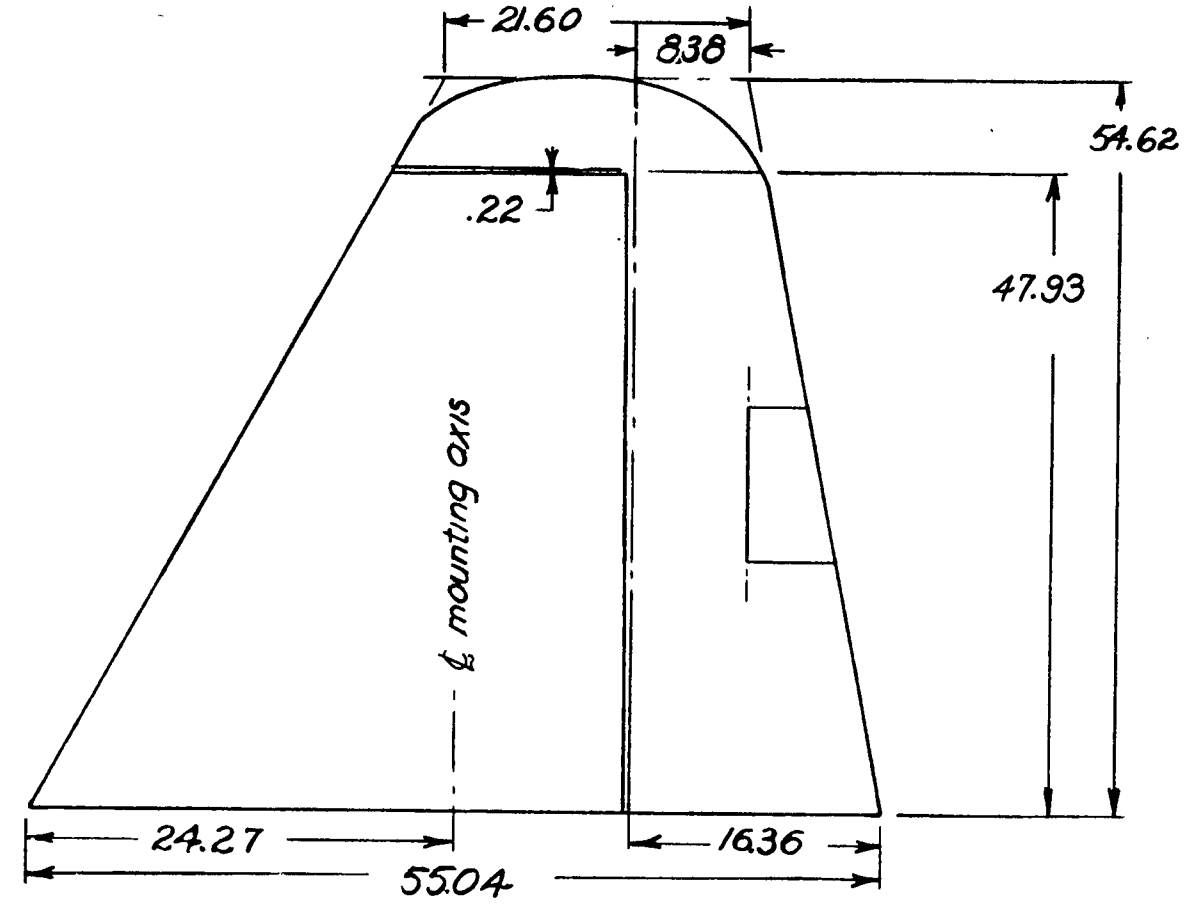

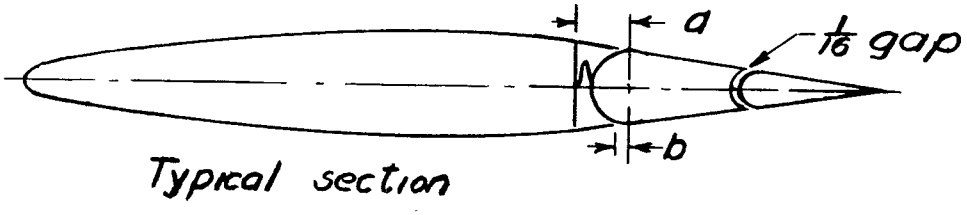

	Station 0	Station 47.93
a	3.03	1.33
b	.61	.61

Figure 5.- The 0.7-scale model of XF6F vertical tail surface with unshielded horn. (All dimensions are in in.)

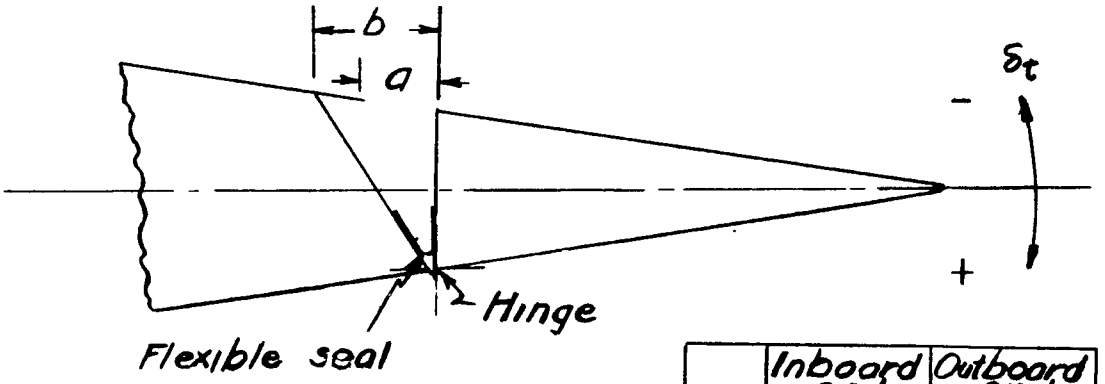

	Inboard end (in.)	Outboard end (in.)
a	0.65	0.37
b	.90	.53

(a) Original tab.

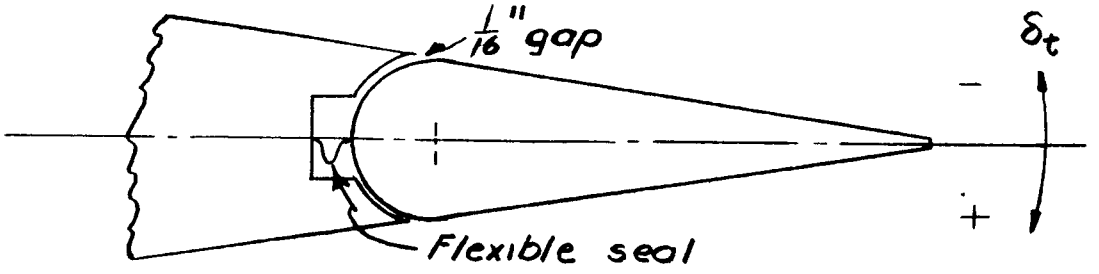

(b) Round-nose tab.

Figure 6.- Tabs tested on 0.7-scale model of XF6F vertical tail surface.

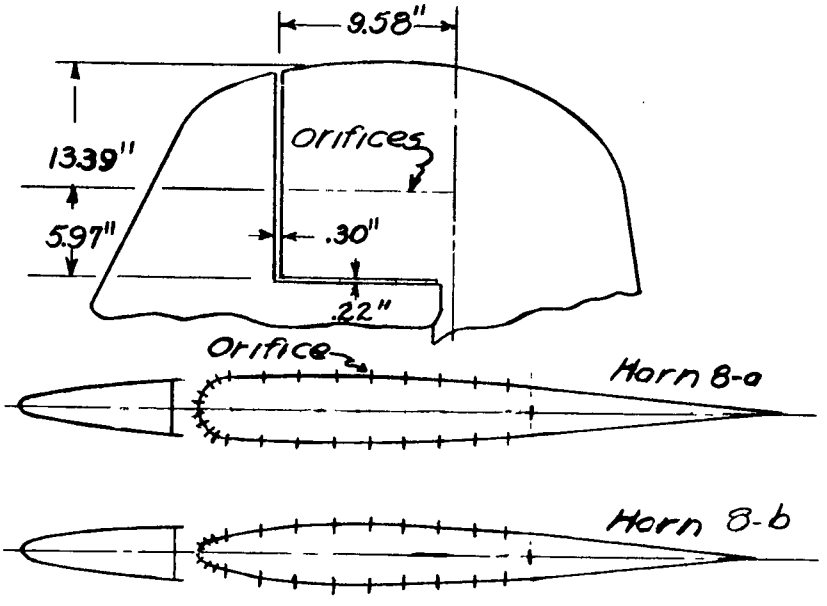

Horn 8-a Orifice location in in. from horn L.E.	
Orifice	Location
0	0
1	.03
2	.13
3	.25
4	.50
5	1.00
6	2.00
7	3.00
8	4.00
9	5.00
10	6.00
11	7.00
12	8.00
13	9.00

Horn 8-b Orifice location in in. from horn L.E.	
Orifice	Location
0	0
1	.13
2	.25
3	.50
4	1.00
5	2.00
6	3.00
7	4.00
8	5.00
9	6.00
10	7.00
11	8.00
12	9.00

Figure 7.- Location of pressure orifices on horns 8-a and 8-b on 0.7-scale model of XF6F vertical tail surface.

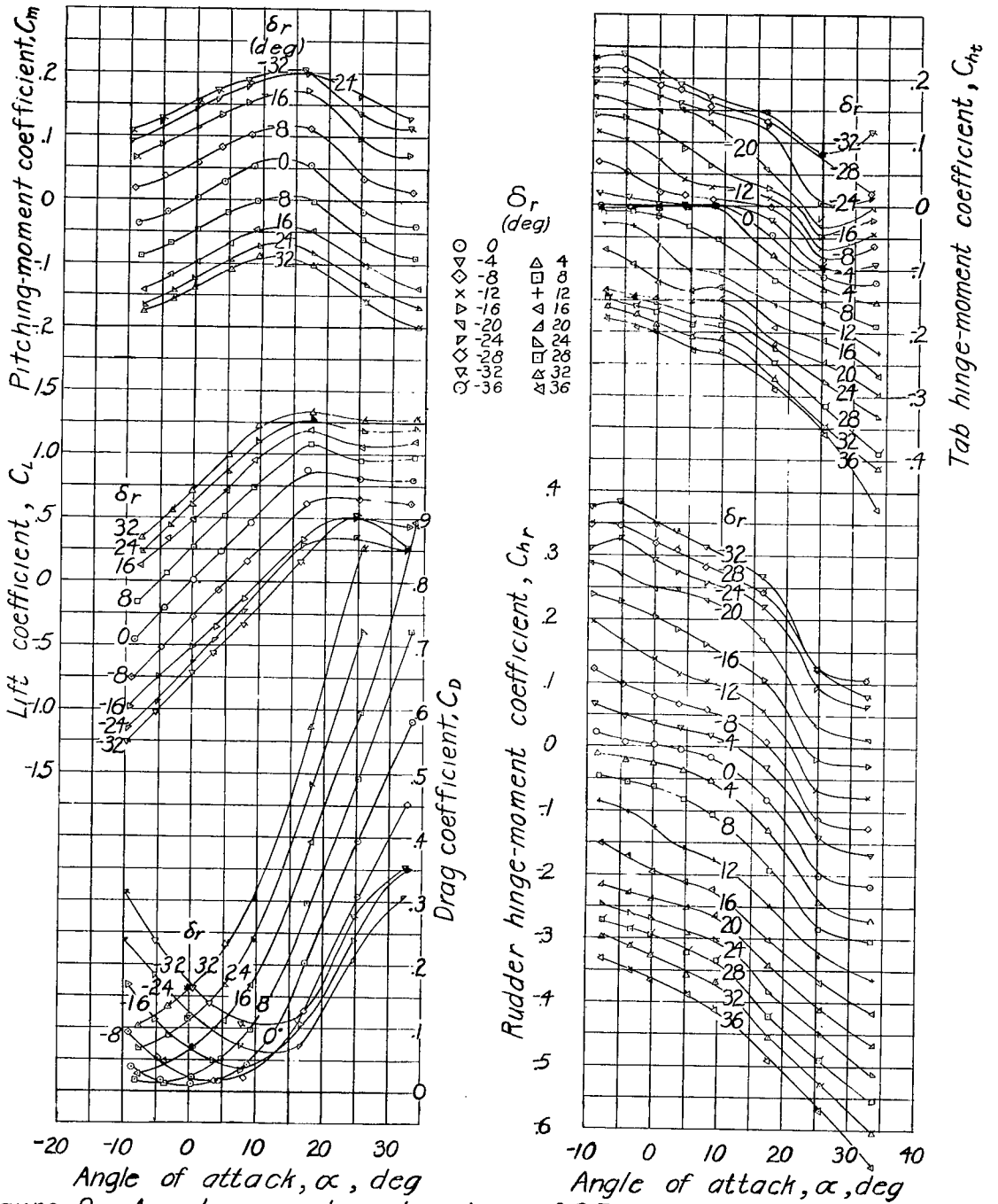

Figure 8.- Aerodynamic characteristics of 0.7-scale model of XF6F vertical tail surface. Plain rudder. $\delta_t = 0°$.

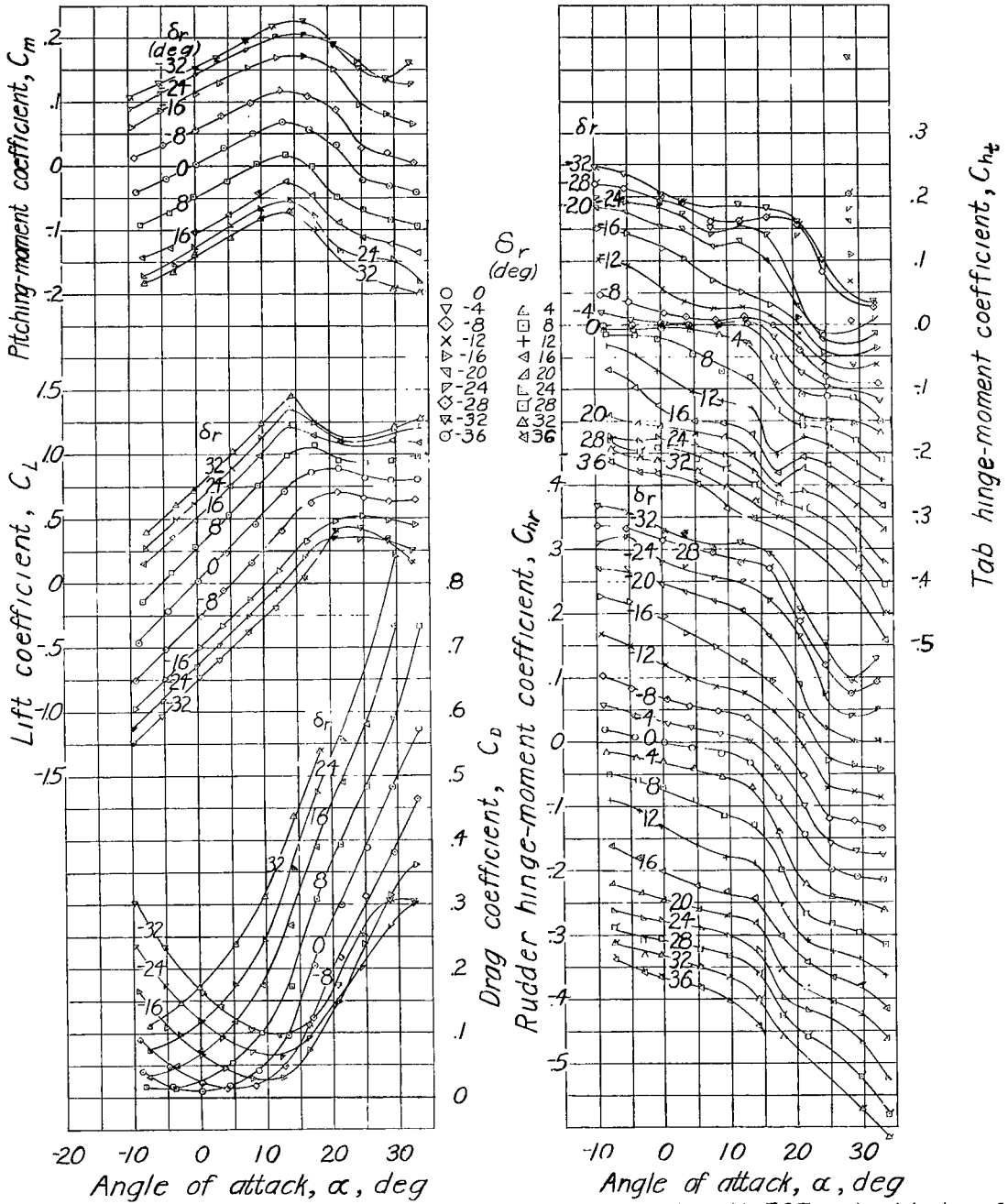

Figure 9.-Aerodynamic characteristics of 0.7-scale model of XF6F vertical tail surface. Plain sealed rudder. Original tab; $\delta_t = 0°$.

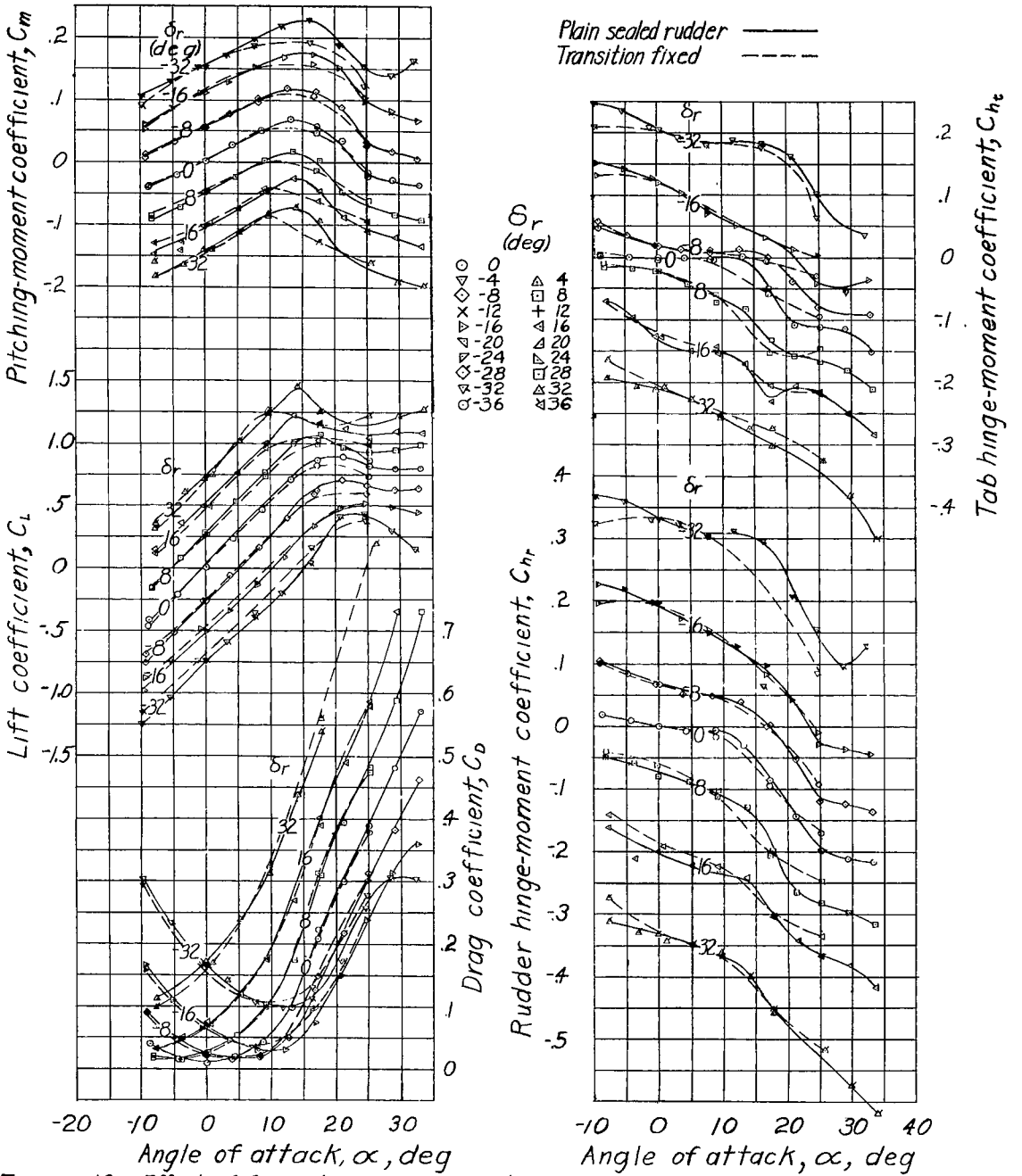

Figure 10.- Effect of fixing transition on the aerodynamic characteristics of 0.7-scale model of XF6F vertical tail surface. Plain sealed rudder. Original tab; $\delta_t = 0°$.

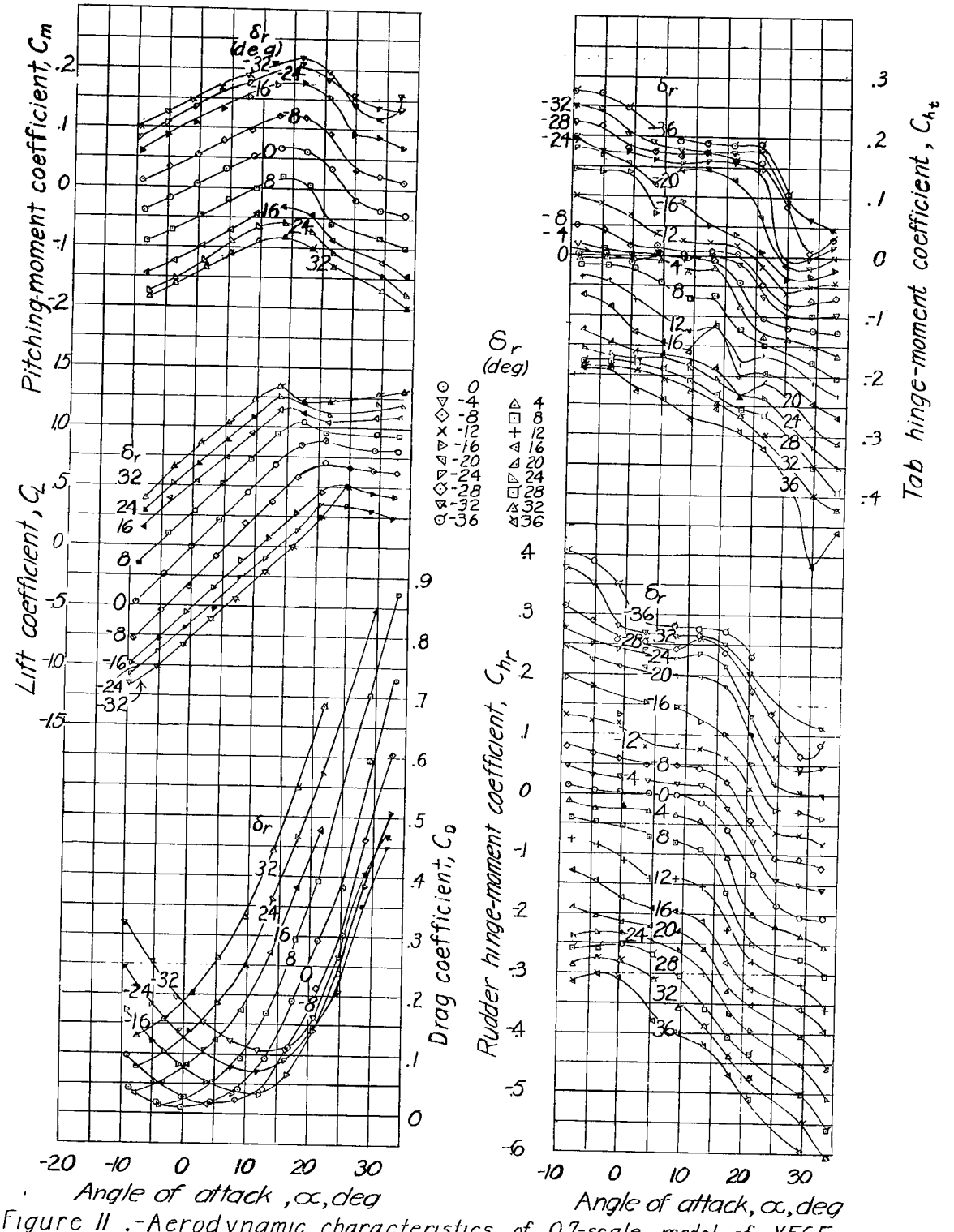

Figure 11.-Aerodynamic characteristics of 0.7-scale model of XF6F vertical tail surface with shielded horn 2-a. Rudder gap sealed.

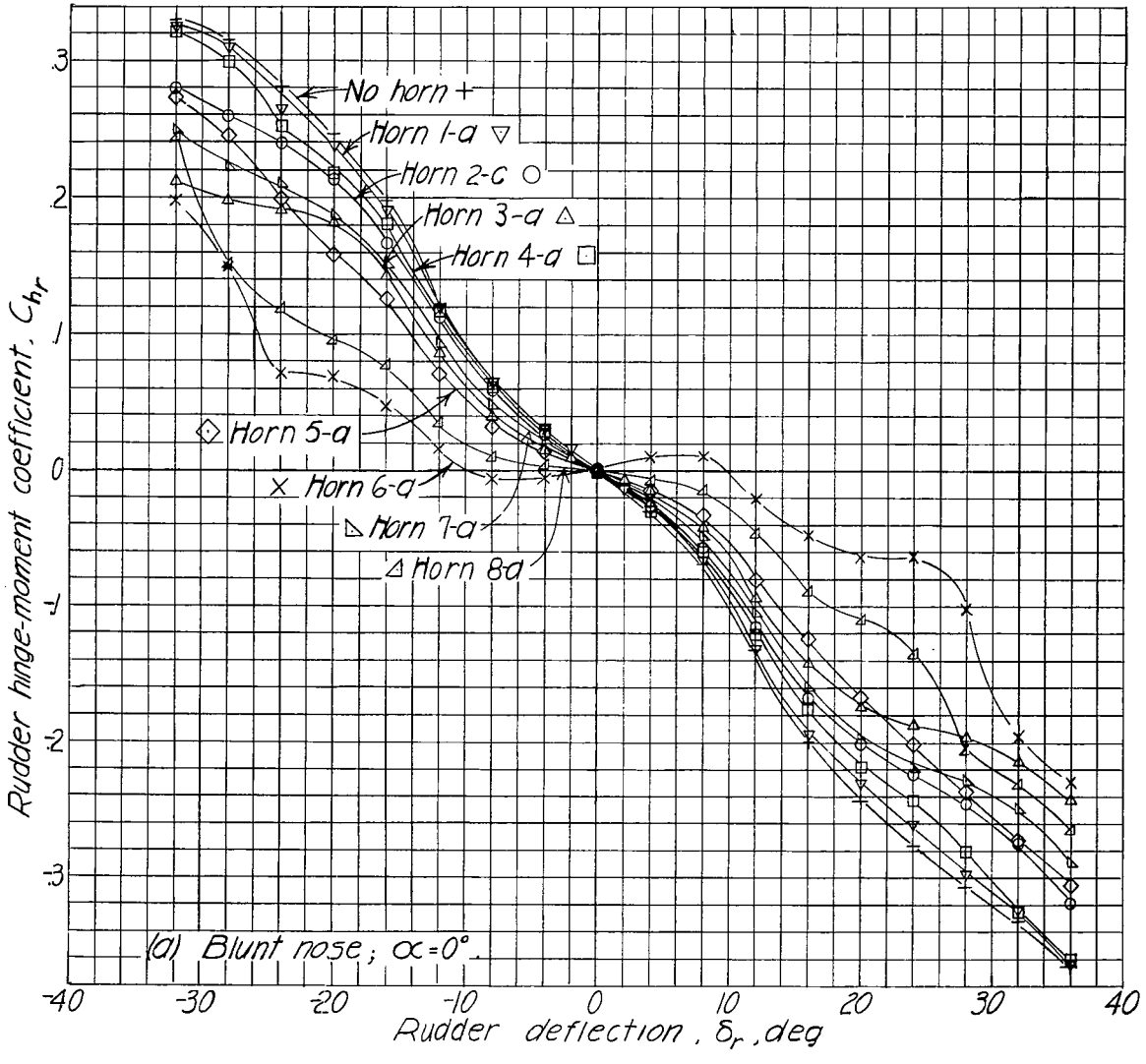

Figure 12.-Hinge-moment characteristics of the 0.7-scale model of XF6F vertical tail surface with several shielded-horn balances. Rudder gap sealed.

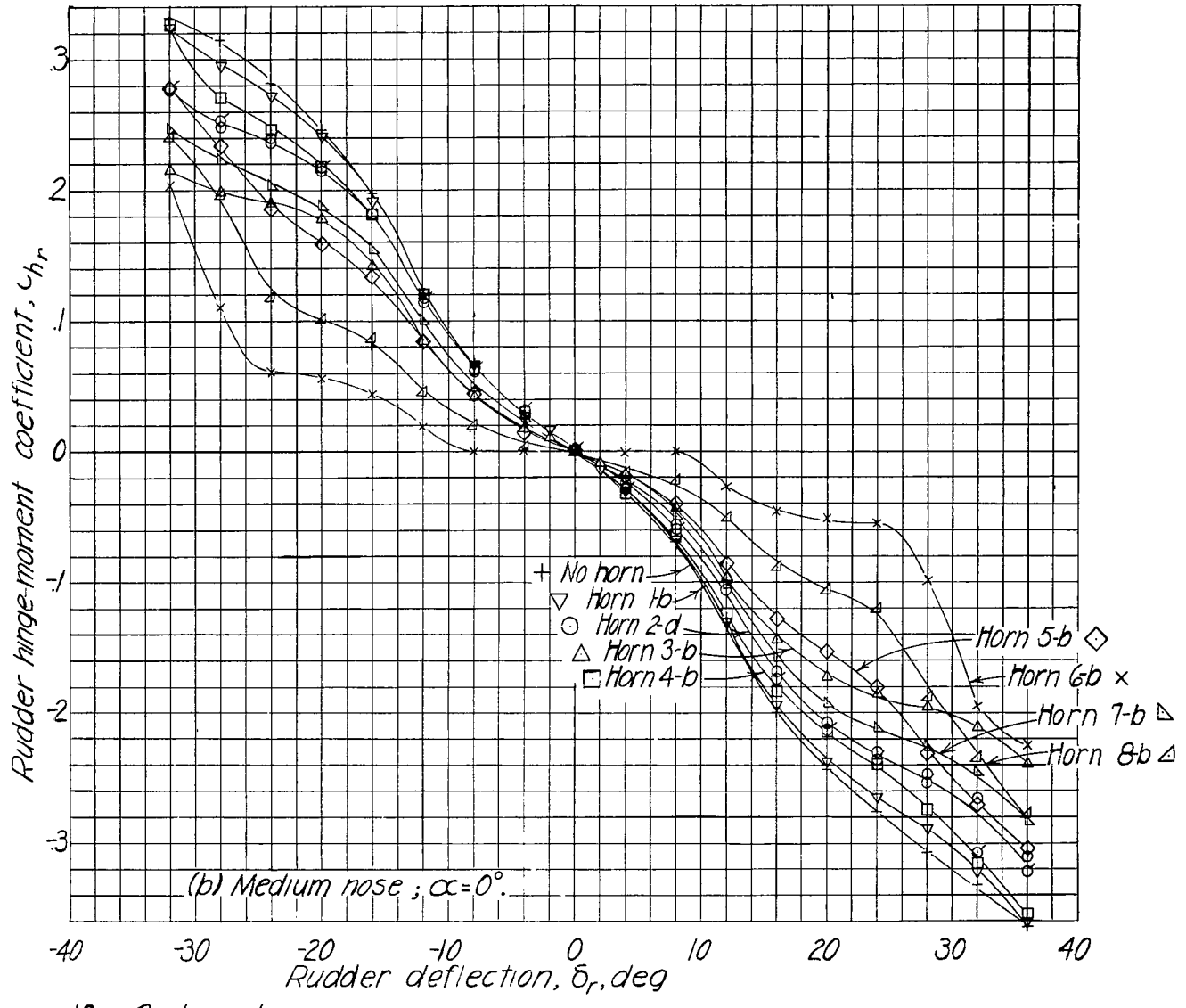

Figure 12.- Continued.

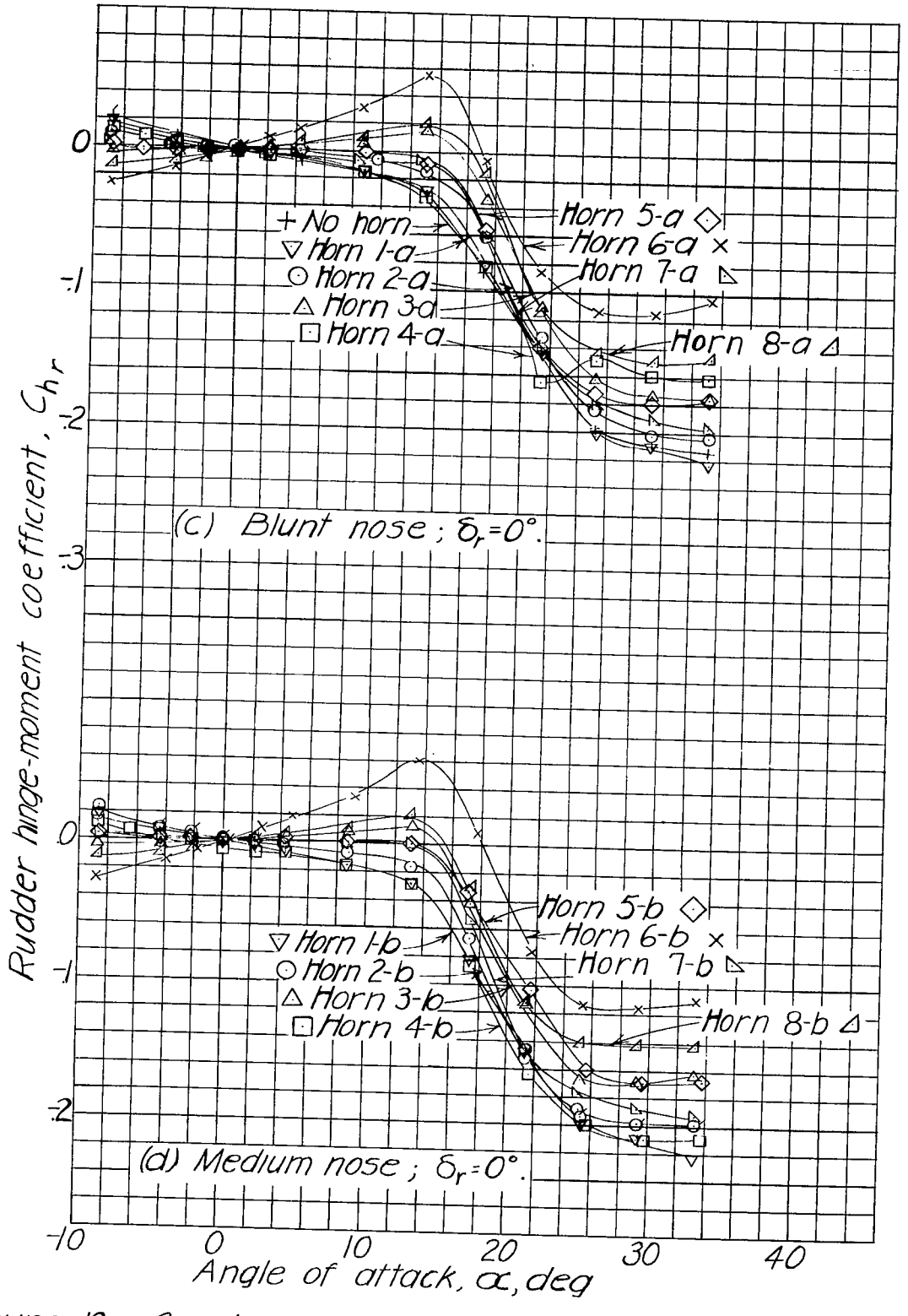

Figure 12.- Concluded.

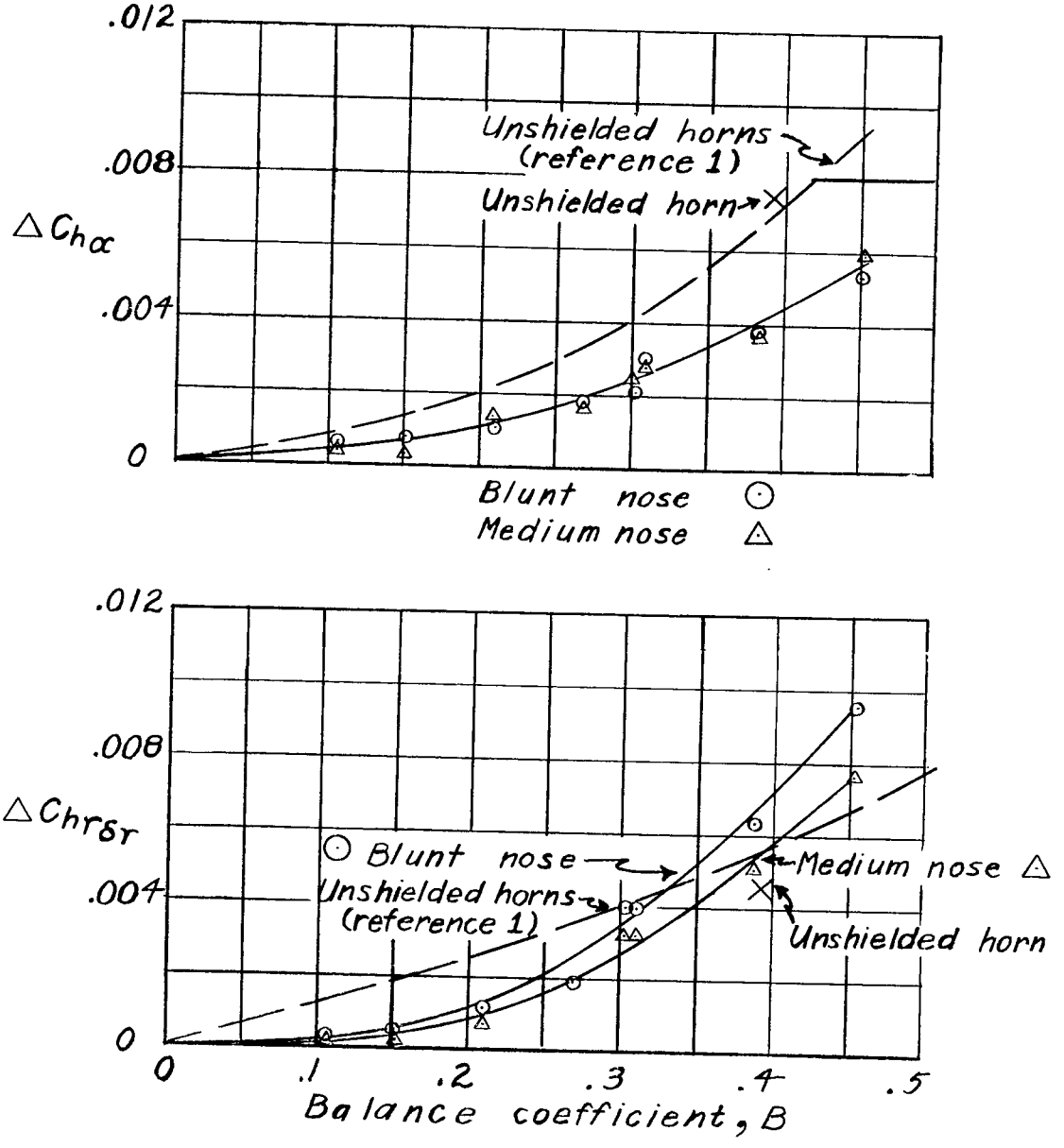

Figure 13.- Variation of ΔC_{h_α} and $\Delta C_{h_{r_{\delta r}}}$ with balance coefficient B. Shielded horns on 0.7-scale model of XF6F vertical tail.

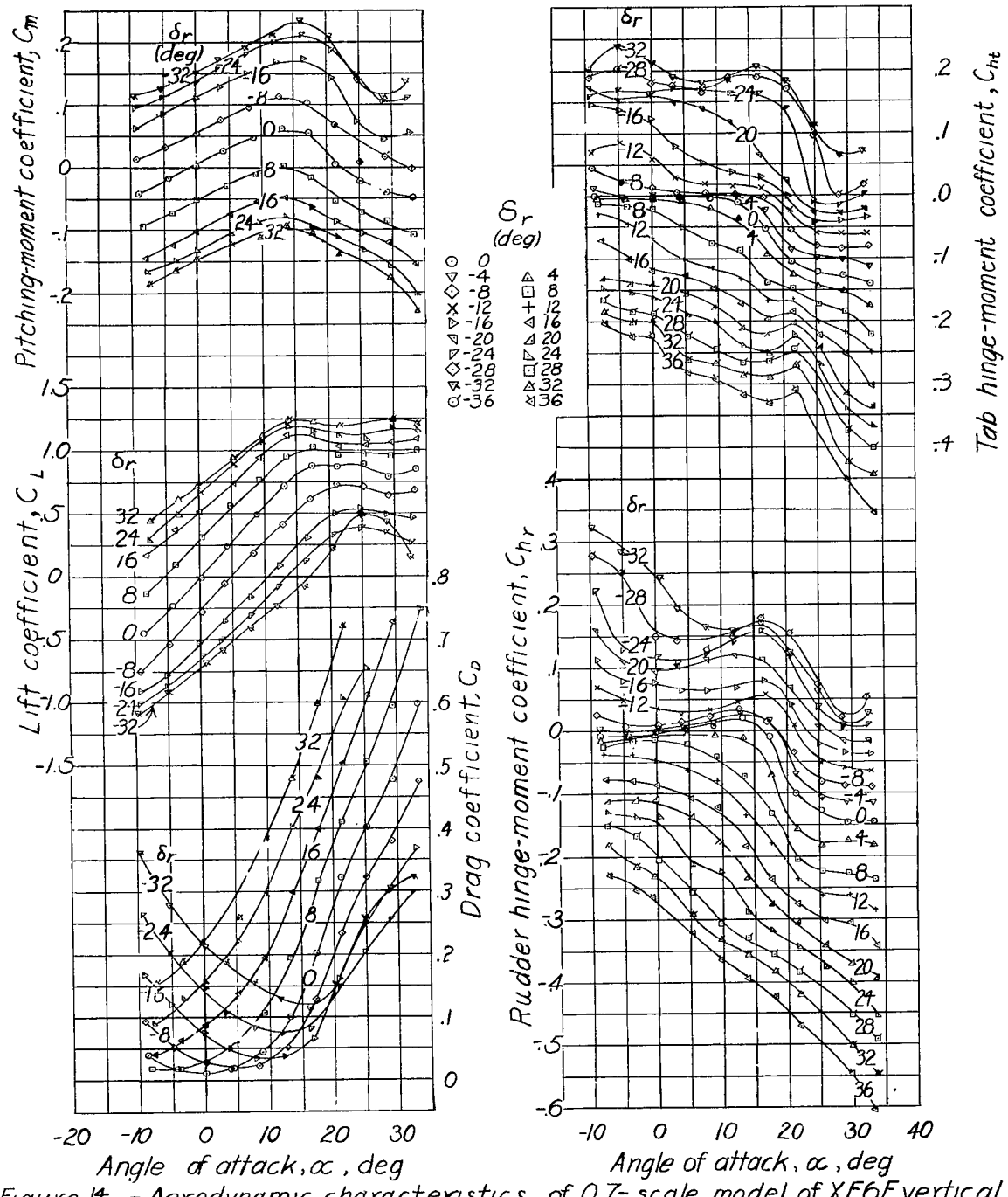

Figure 14 .- Aerodynamic characteristics of 0.7-scale model of XF6F vertical tail surface with shielded horn 8-a. Rudder gap sealed.

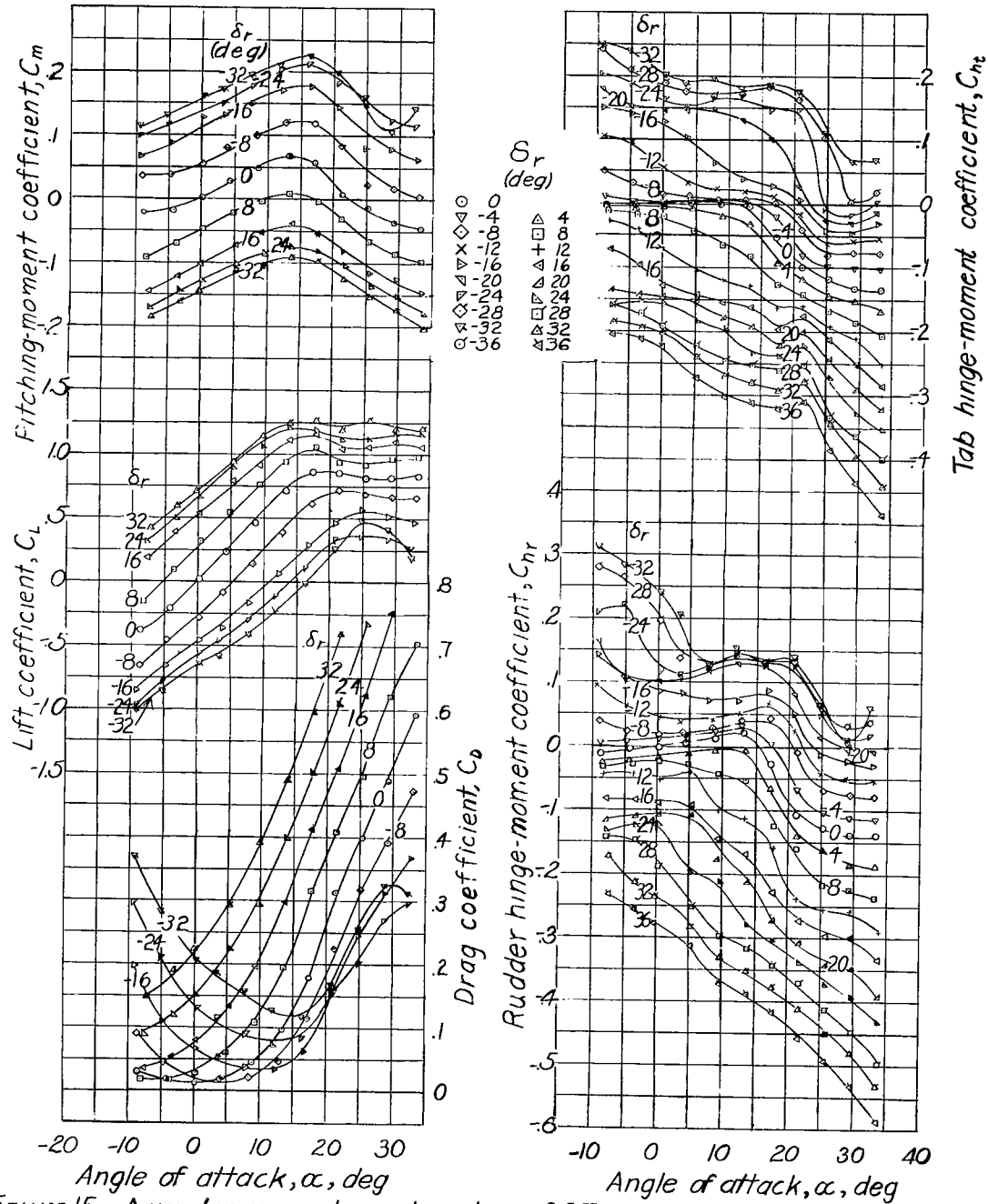

Figure 15.-Aerodynamic characteristics of 0.7-scale model of XF6F vertical tail surface with shielded horn 8-b. Rudder gap sealed.

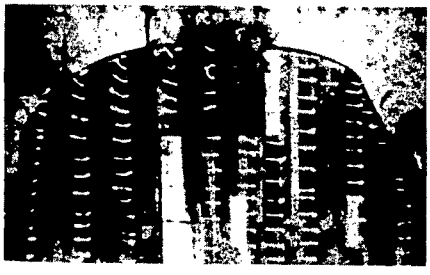

(a) $\alpha = 0^{\circ}; \delta_r = -24^{\circ}$.

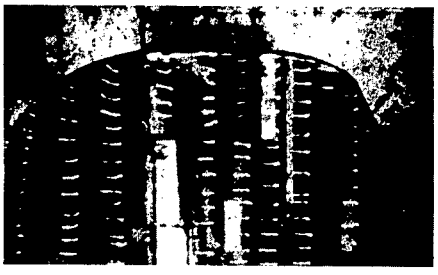

(b) $\alpha = 0^{\circ}; \delta_r = -12\frac{1^{\circ}}{2}$.

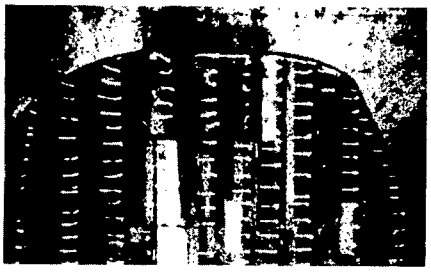

(c) $\alpha = 0^{\circ}; \delta_r = -6^{\circ}$.

(d) $\alpha = 0^{\circ}; \delta_r = -3\frac{1^{\circ}}{2}$.

(e) $\alpha = 0^{\circ}; \delta_r = 24^{\circ}$.

Figure 16.- Tuft study over upper surface of 0.7-scale model of XF6F vertical tail with horn 2-c.

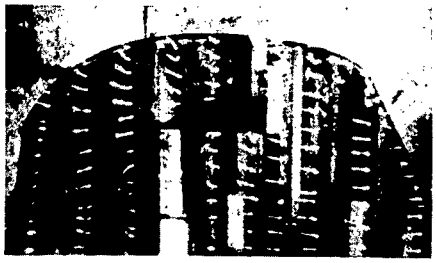

(f) $\alpha = 12^{\circ}; \delta_r = -36^{\circ}$.

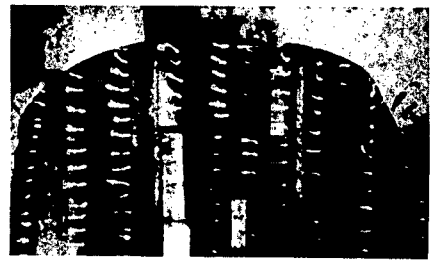

(g) $\alpha = 12^{\circ}; \delta_r = -16^{\circ}$.

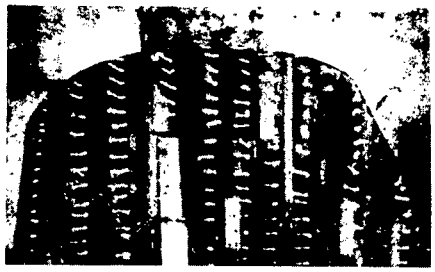

(h) $\alpha = 12^{\circ}; \delta_r = -8^{\circ}$

(i) $\alpha = 12^{\circ}; \delta_r = 0^{\circ}$.

(j) $\alpha = 12^{\circ}; \delta_r = 24^{\circ}$.

Figure 16.- Concluded.

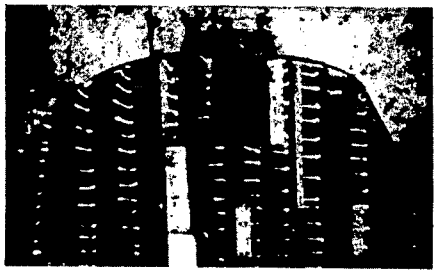

(a) $\alpha = 0^{\circ}; \delta_r = -24^{\circ}$.

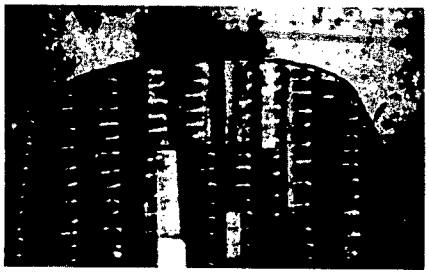

(b) $\alpha = 0^{\circ}; \delta_r = 0^{\circ}$.

(c) $\alpha = 0^{\circ}; \delta_r = 8^{\circ}$.

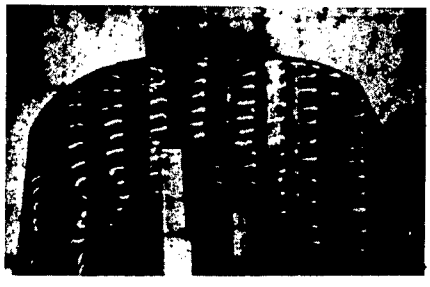

(d) $\alpha = 0^{\circ}; \delta_r = 16^{\circ}$.

(e) $\alpha = 0^{\circ}; \delta_r = 24^{\circ}$.

Figure 17.- Tuft study over upper surface of 0.7-scale model of XF6F vertical tail with horn 2-d.

(f) $\alpha = 12^{\circ}; \delta_r = -32^{\circ}$.

(g) $\alpha = 12^{\circ}; \delta_r = -16^{\circ}$.

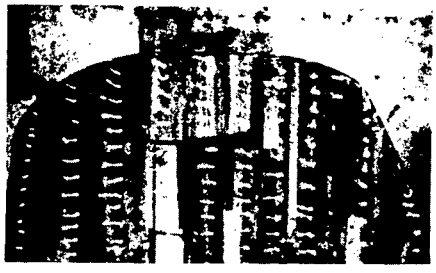

(h) $\alpha = 12^{\circ}; \delta_r = -8^{\circ}$.

(i) $\alpha = 12^{\circ}; \delta_r = 0^{\circ}$.

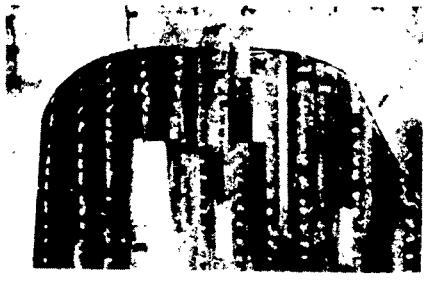

(j) $\alpha = 12^{\circ}; \delta_r = 24^{\circ}$.

Figure 17.- Concluded.

(a) $\alpha = 0°$.

(b) $\alpha = 4°$.

(c) $\alpha = 8°$.

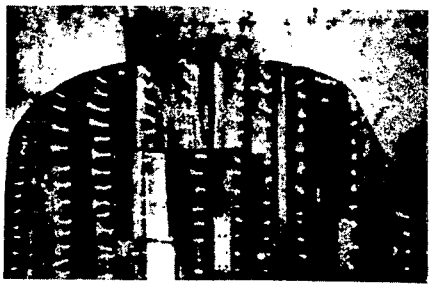

(d) $\alpha = 12°$.

Figure 18.- Tuft study over upper surface of 0.7-scale model of XF6F vertical tail with horn 2-d. Rudder neutral.

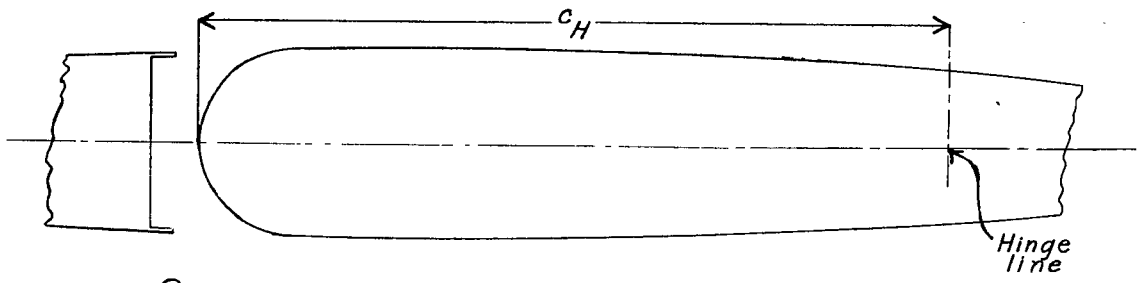

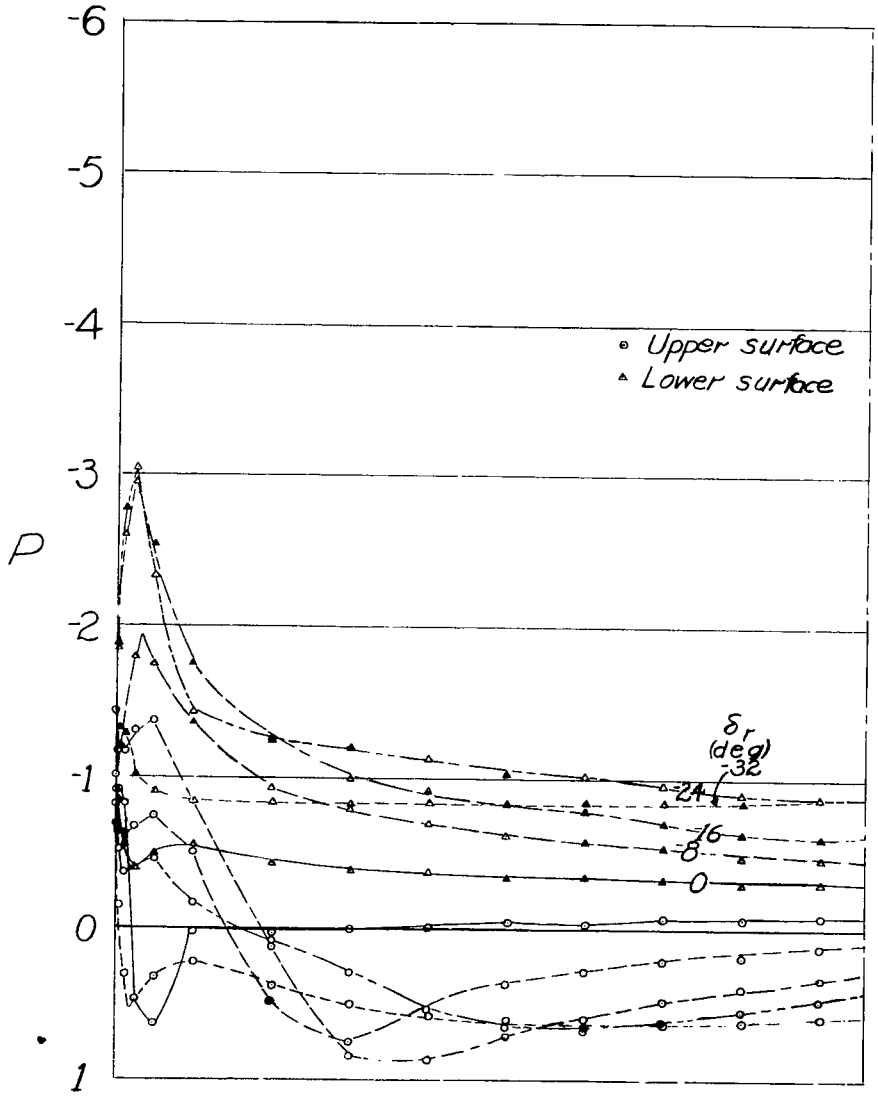

Figure 19.- Pressure distribution over horn 8-a on 0.7-scale model of XF6F vertical tail. $\alpha = -8°$.

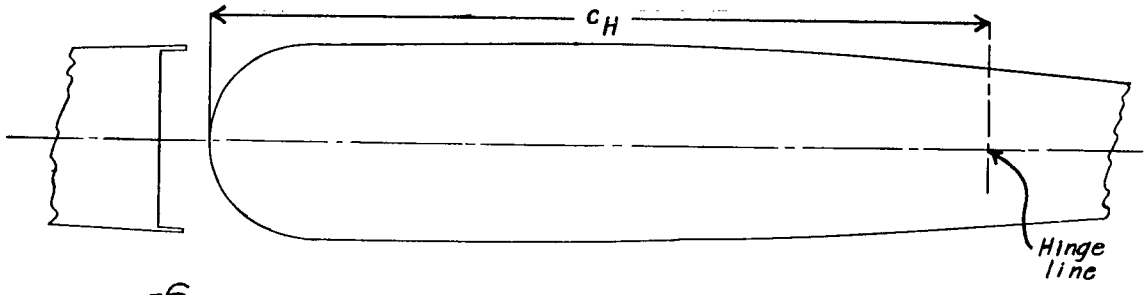

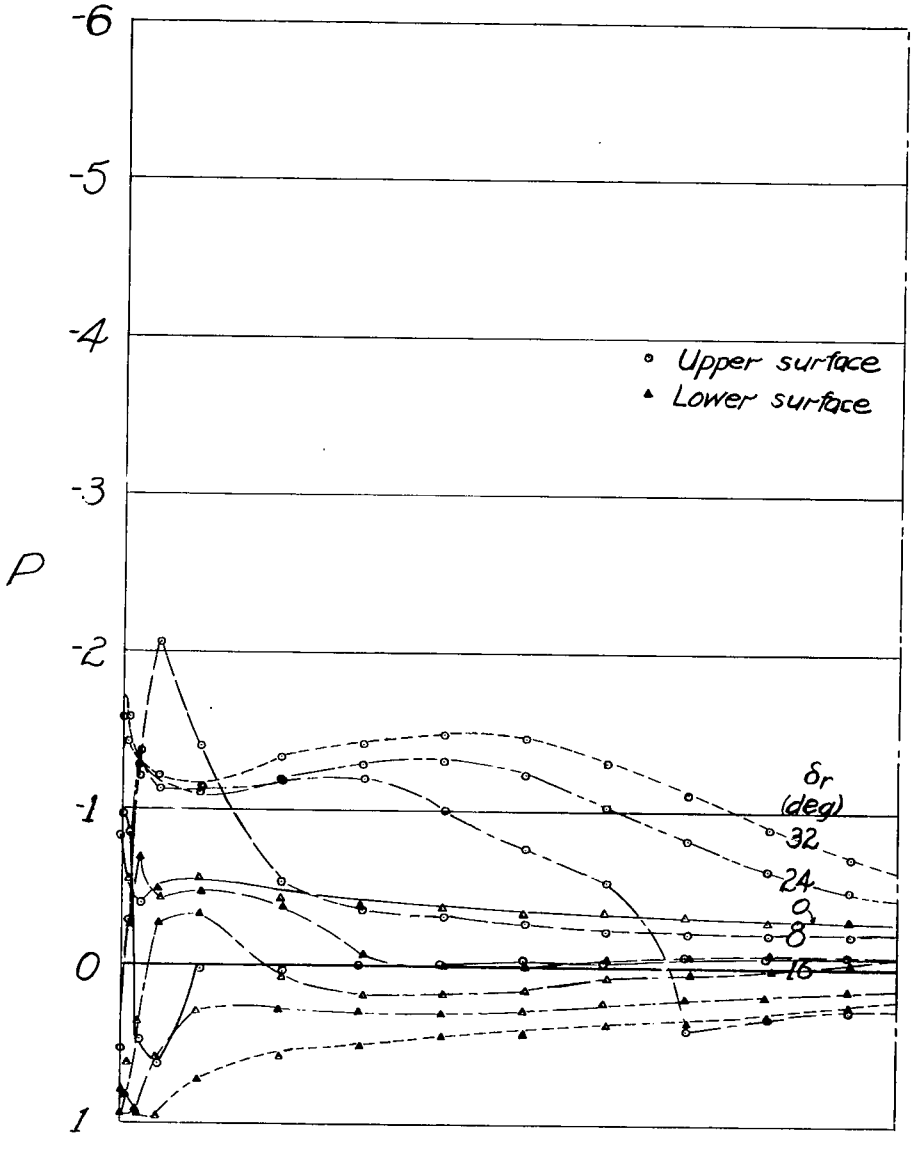

Figure 19.- Concluded.

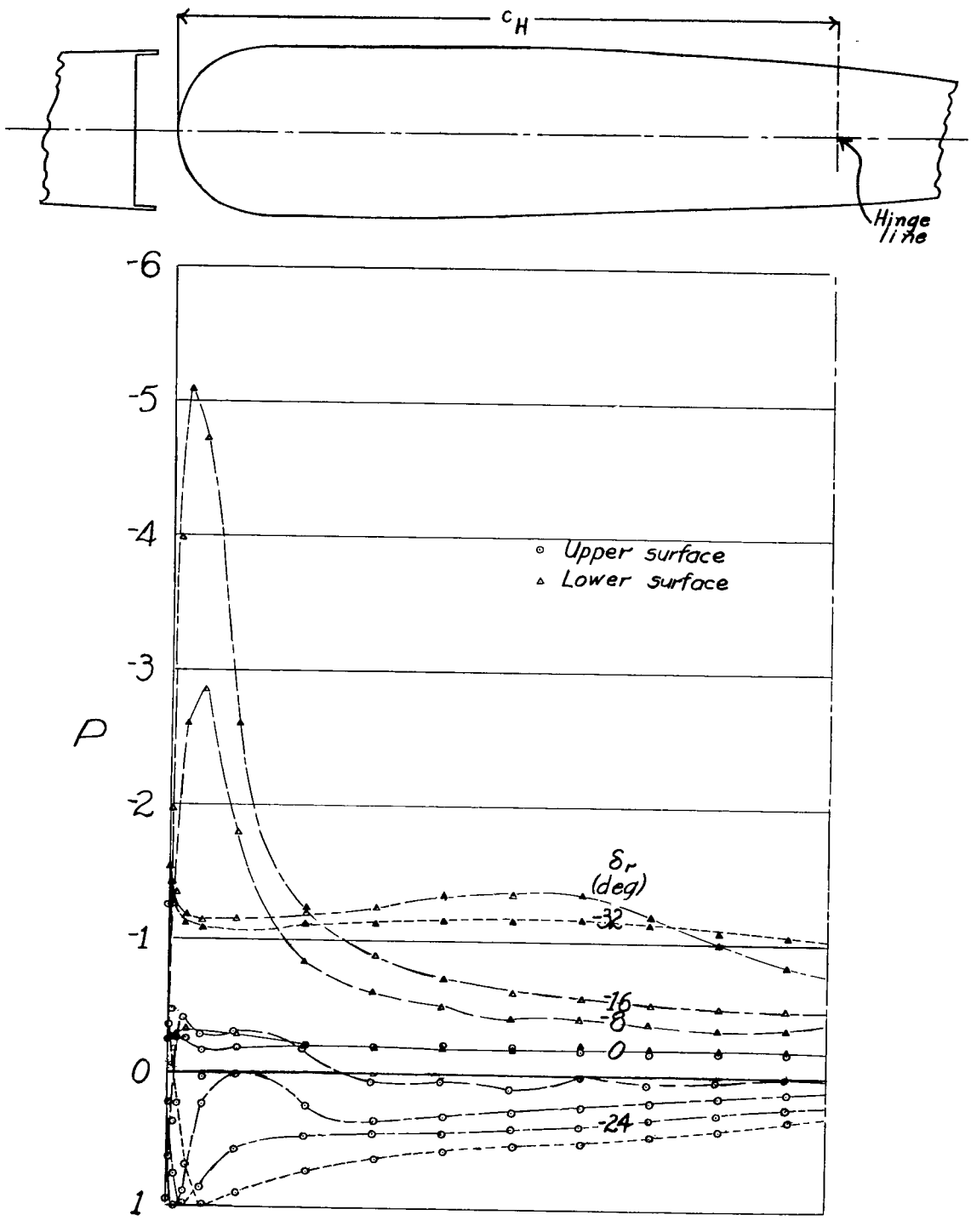

Figure 20.- Pressure distribution over horn 8-a on 0.7-scale model of XF6F vertical tail. α - 0°.

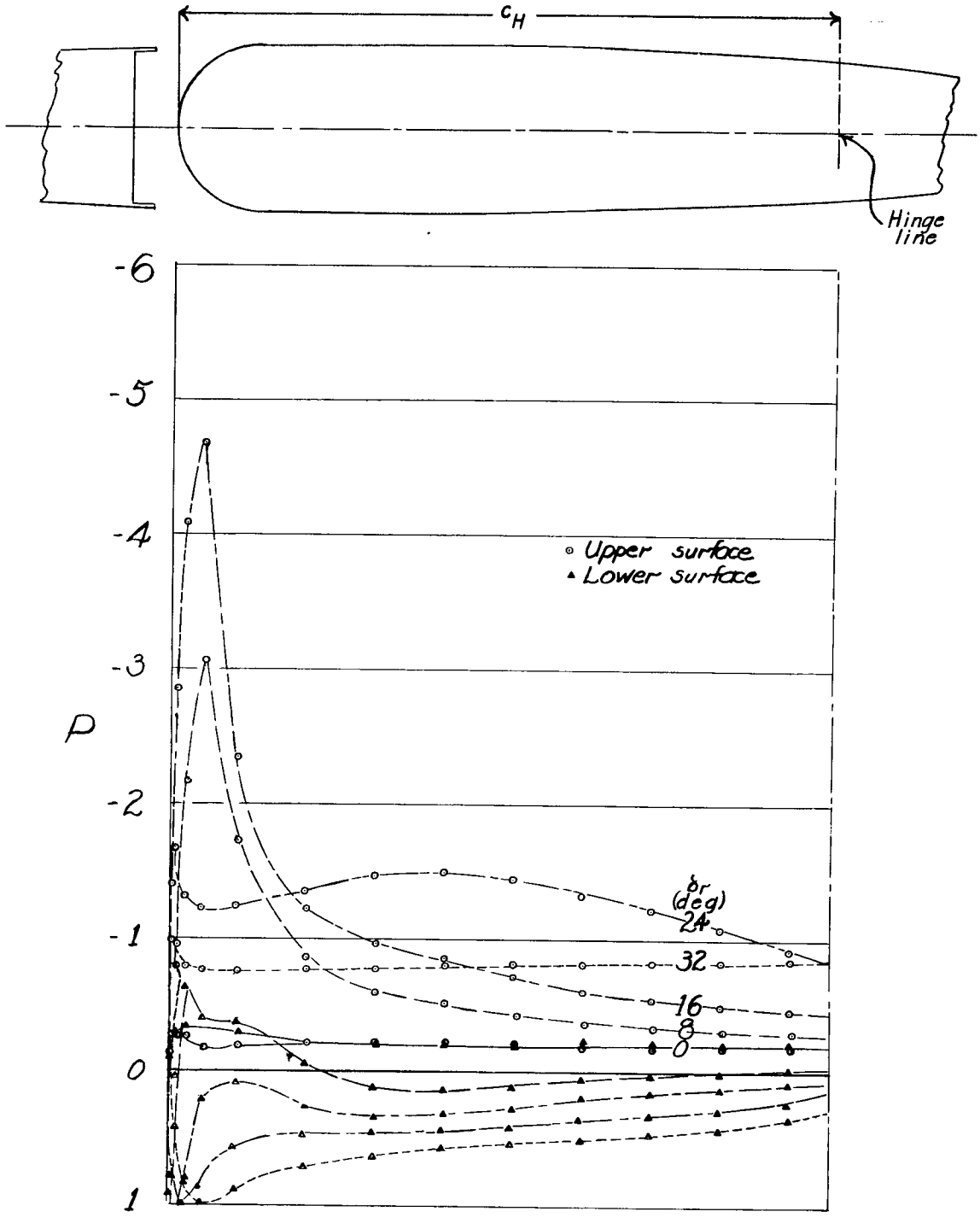

Figure 20- Concluded.

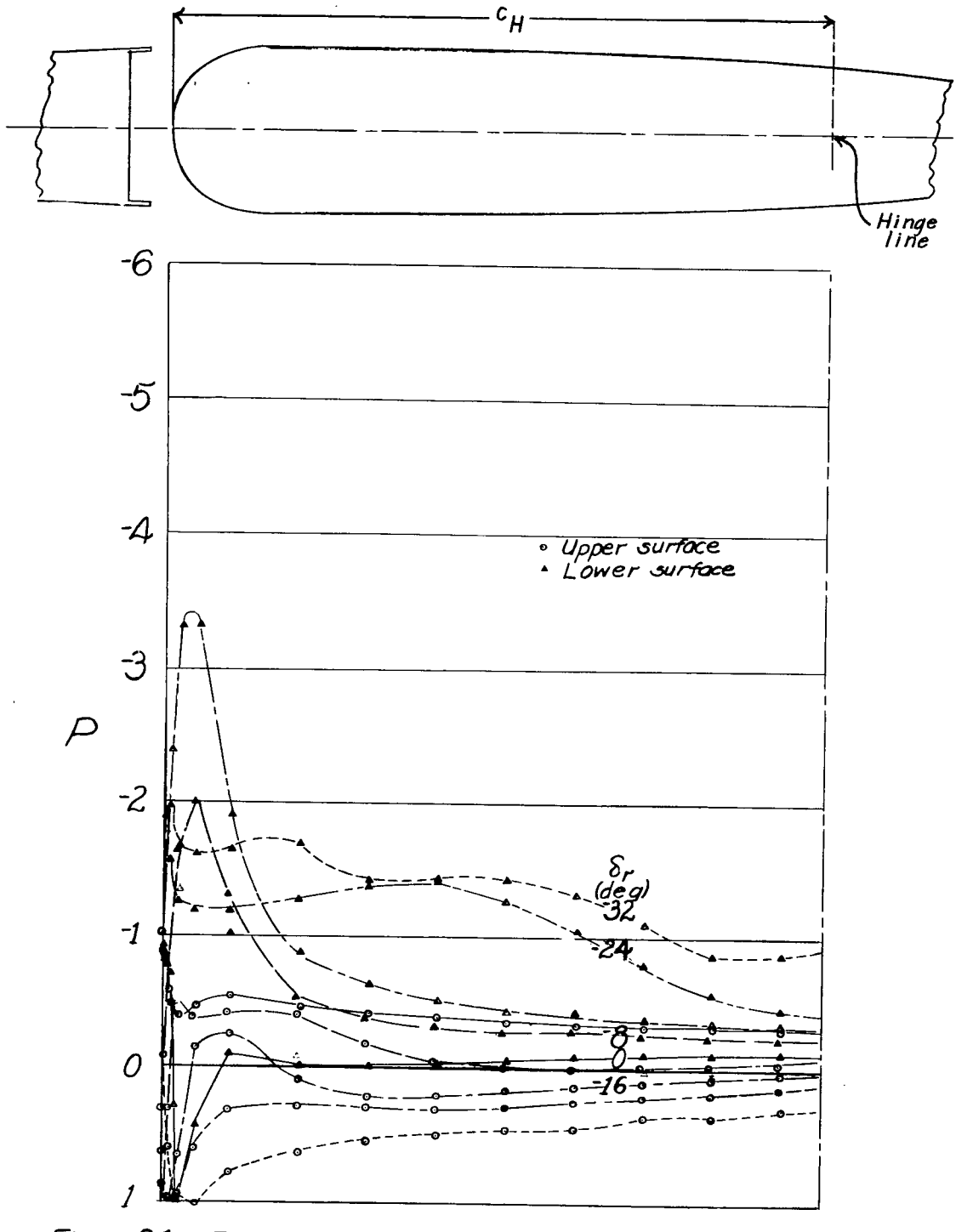

Figure 21.- Pressure distribution over horn 8-0 on 0.7-scale model of XF6F vertical tail. $\alpha = 8°$.

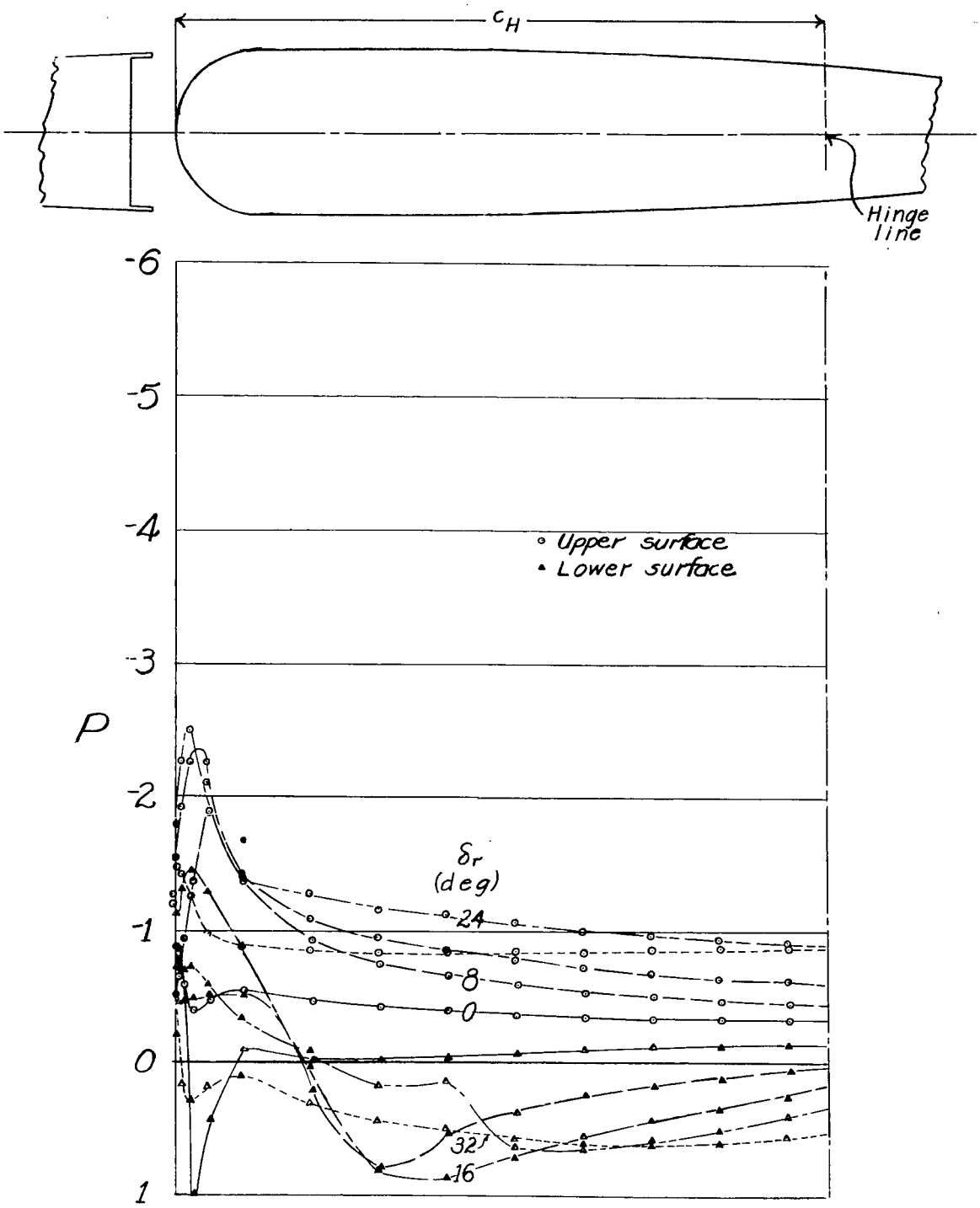

Figure 21.- Concluded

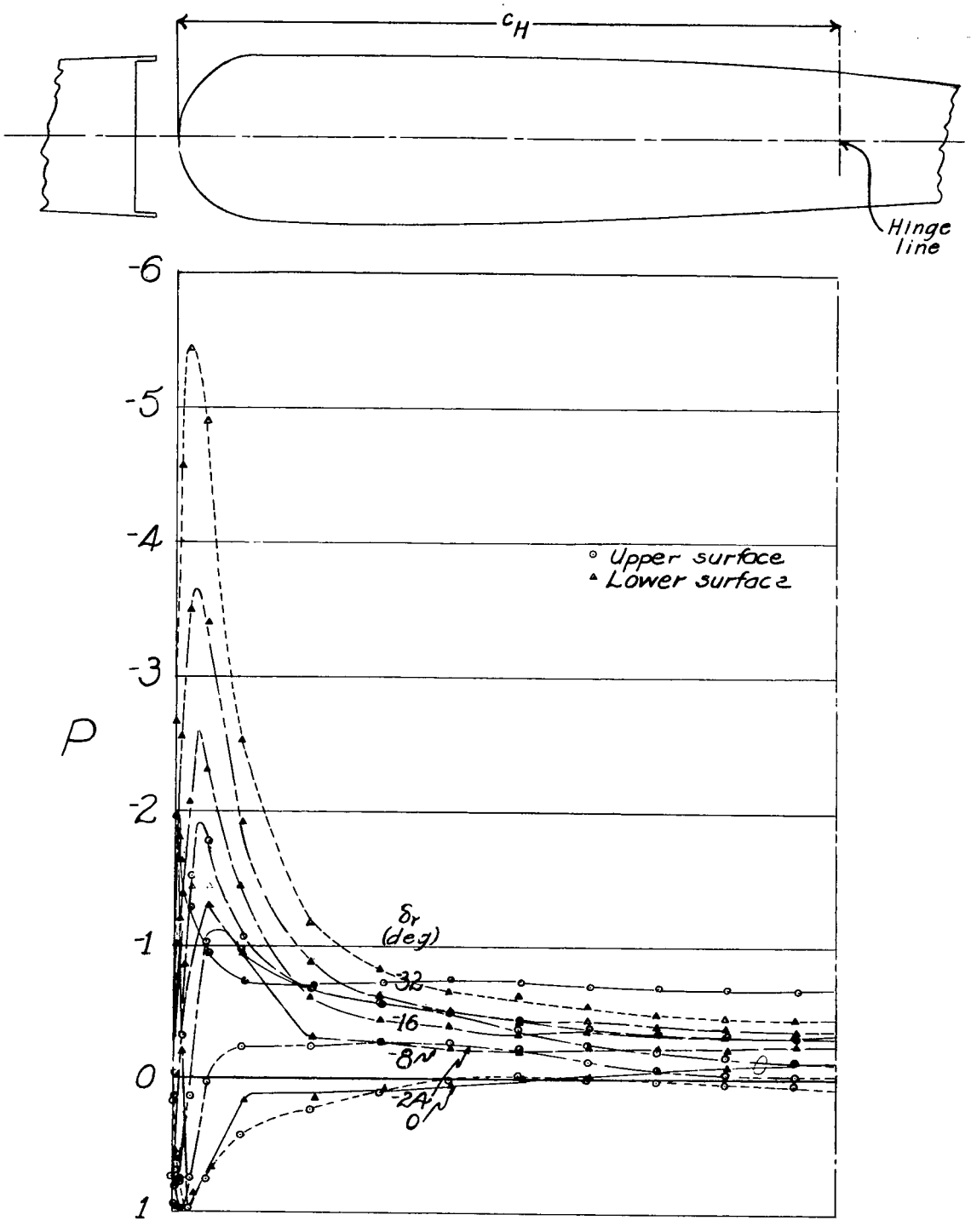

Figure 22.- Pressure distribution over horn 8-0 on 0.7-scale model of XF6F vertical tail. $\alpha = 16°$.

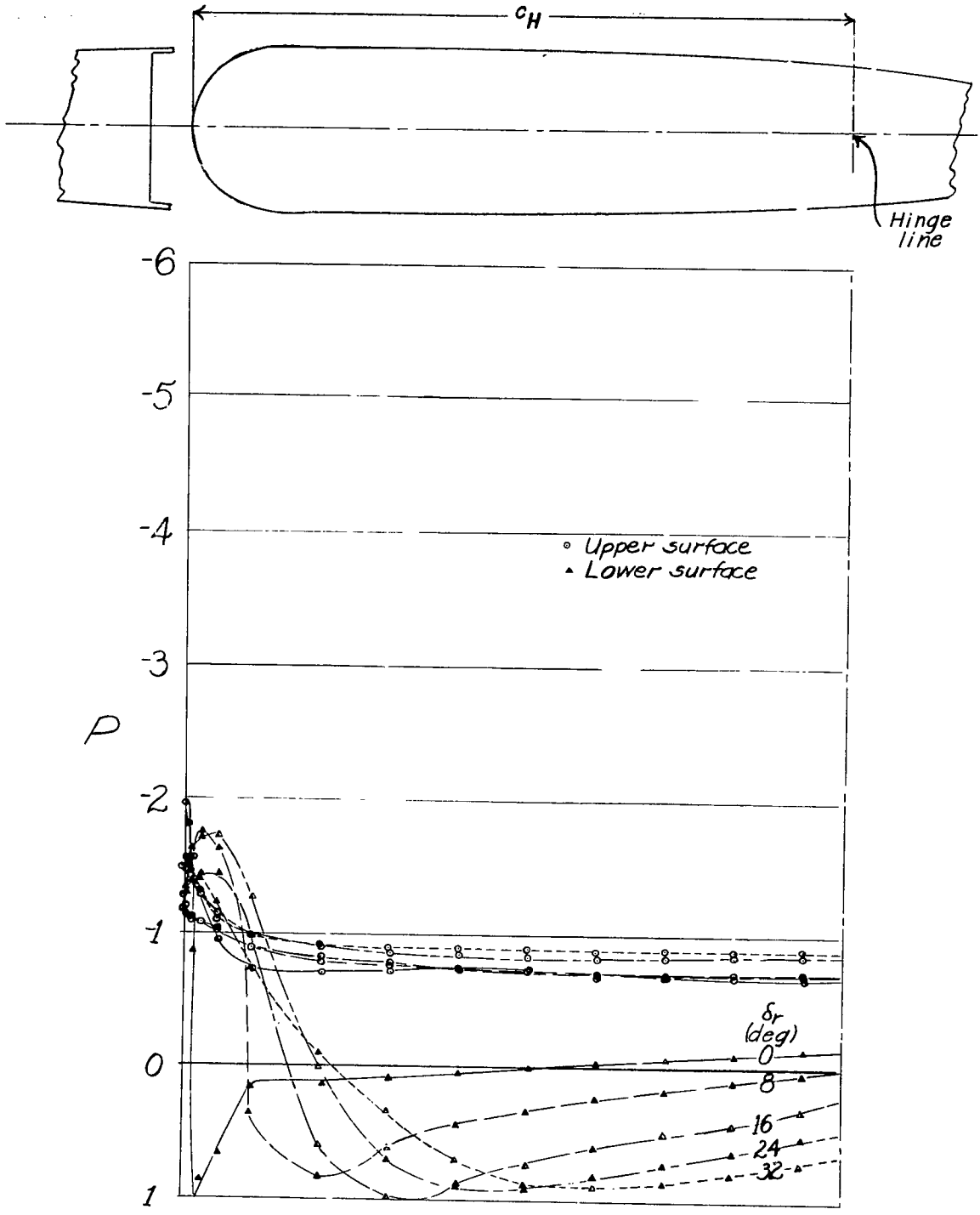

Figure 22.- Concluded.

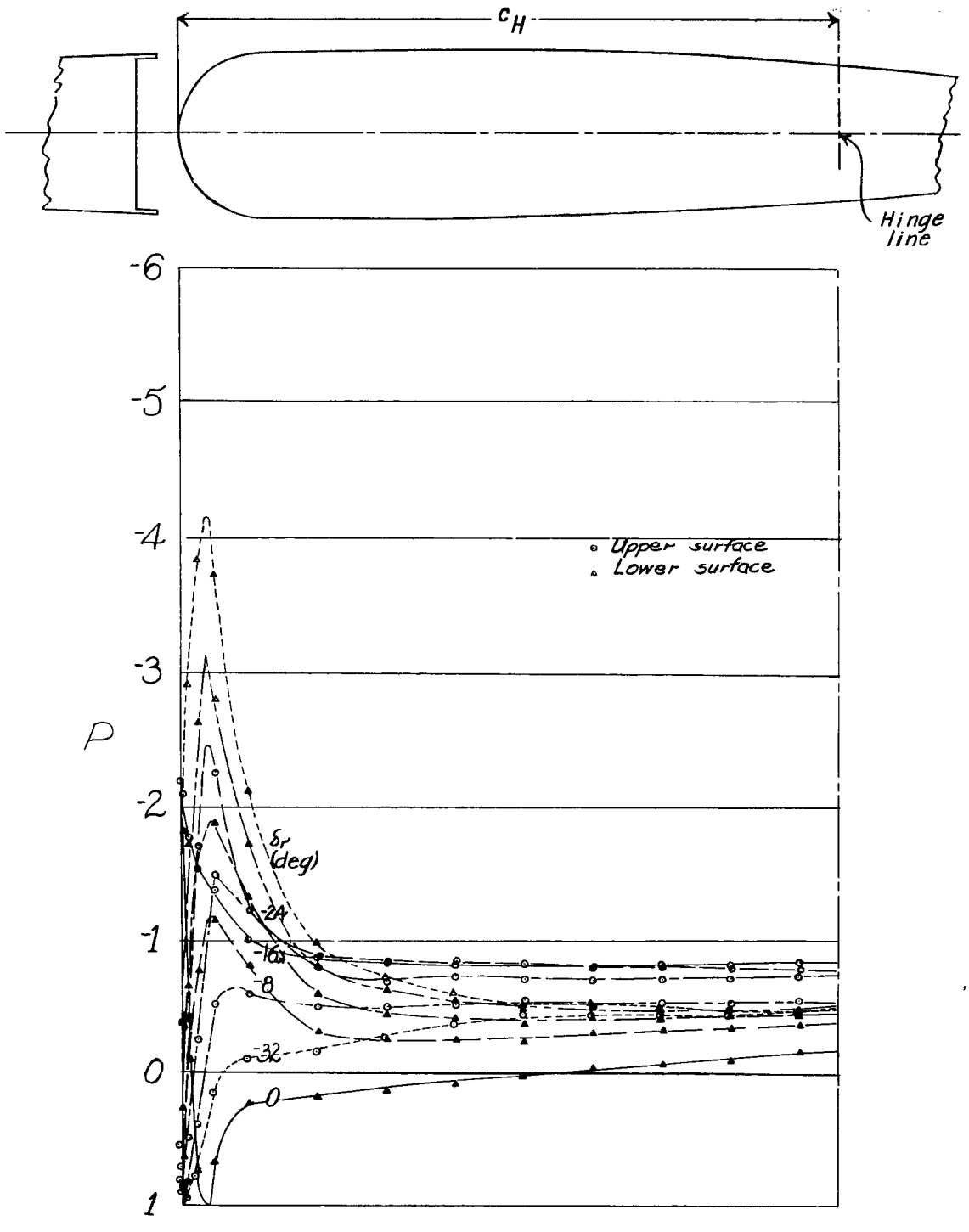

Figure 23.- Pressure distribution over horn 8-a on 0.7-scale model of XF6F vertical tail. $\alpha_c = 24°$.

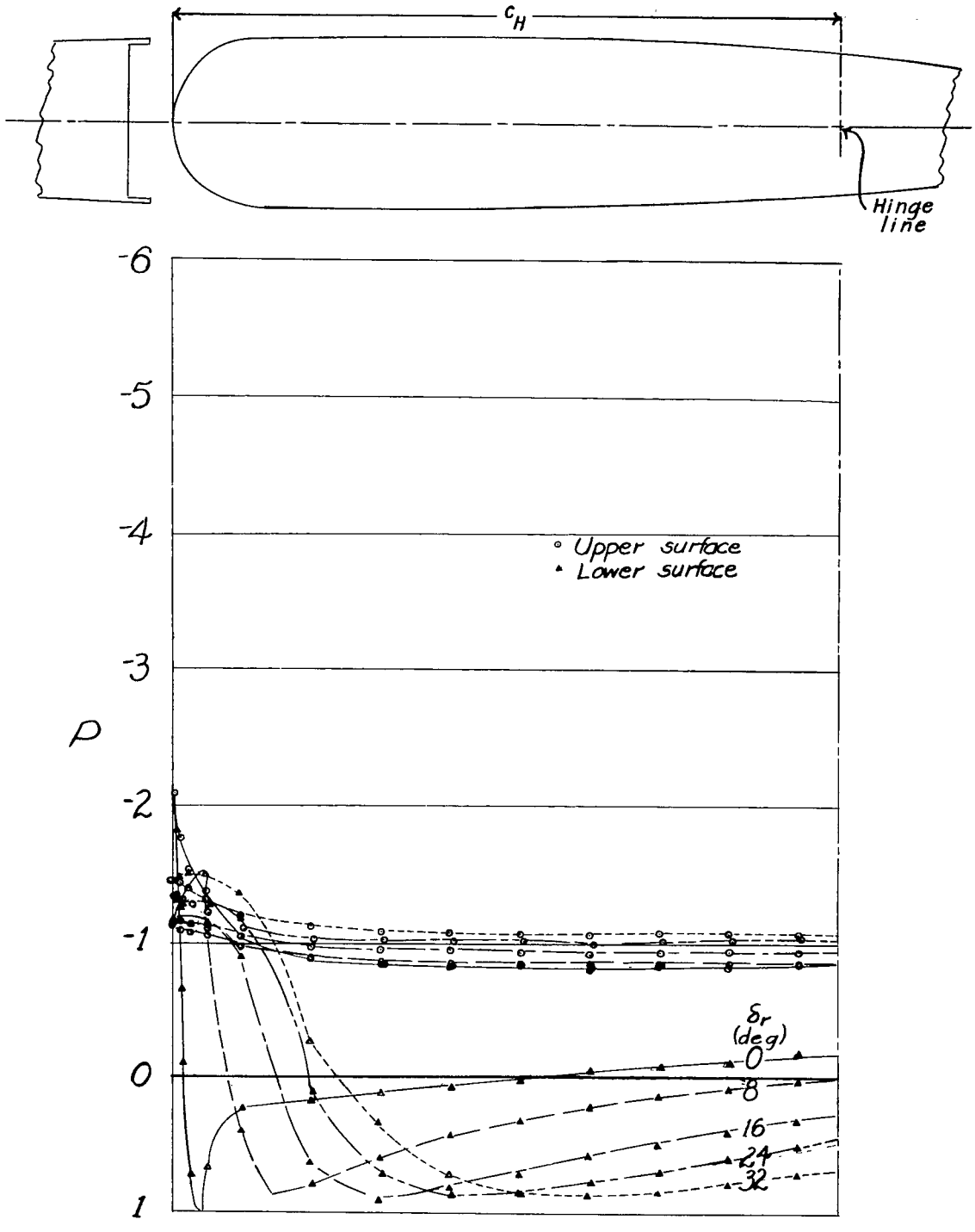

Figure 23.- Concluded.

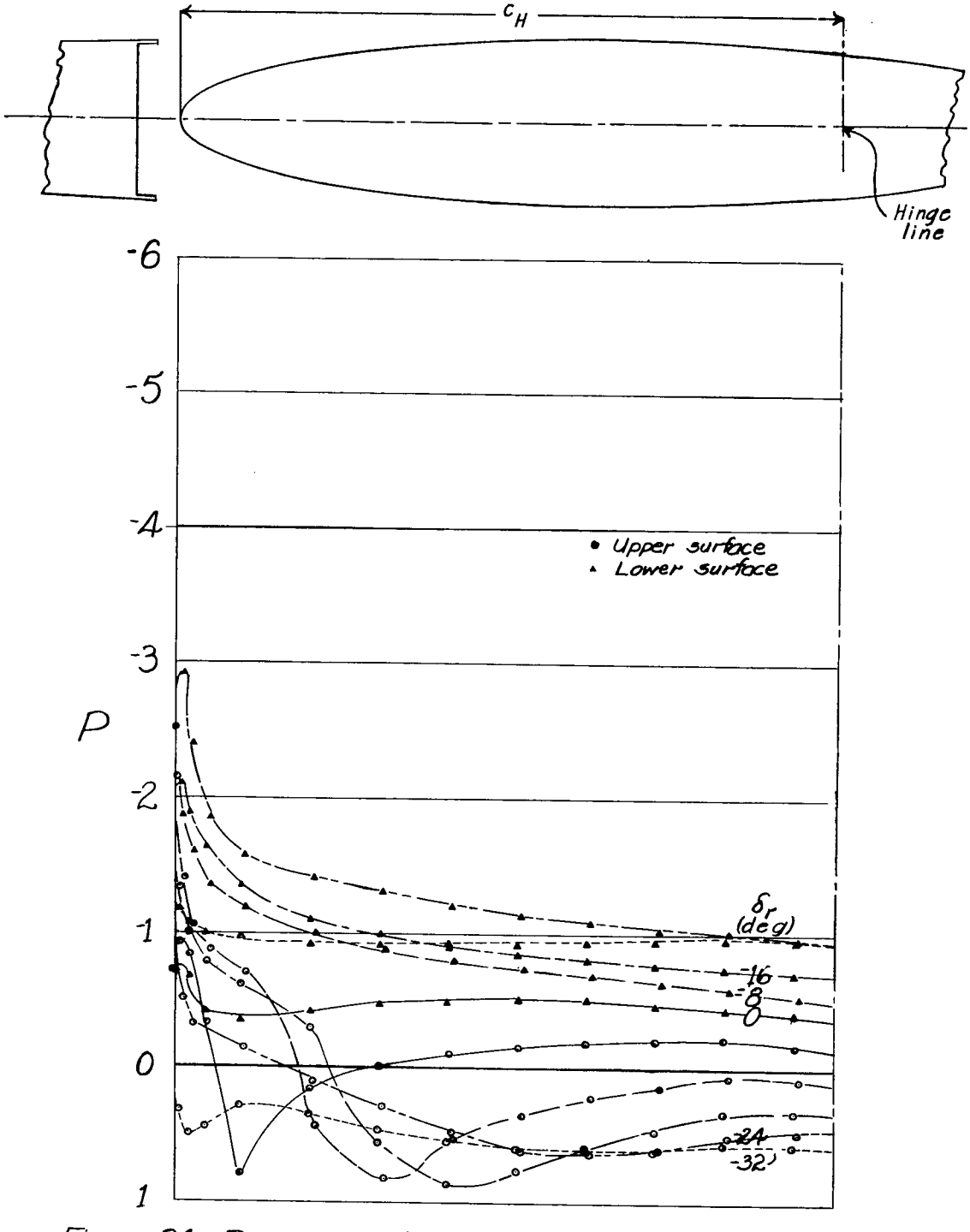

Figure 24.- Pressure distribution over horn 8-b on 0.7-scale model of XF6F vertical tail surface. $\alpha = -8°$.

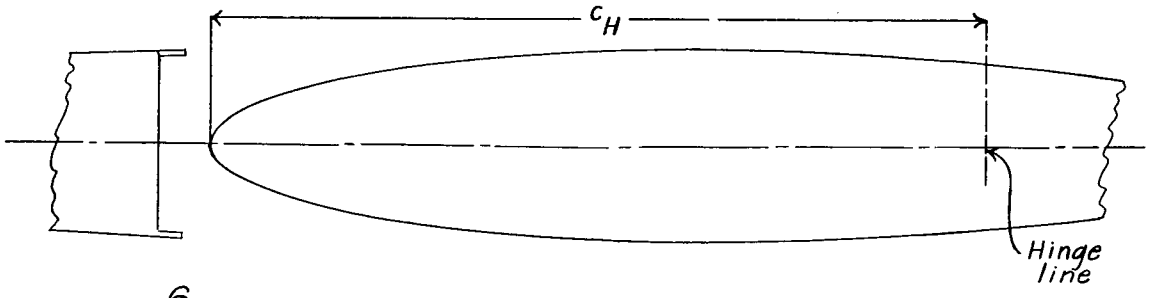

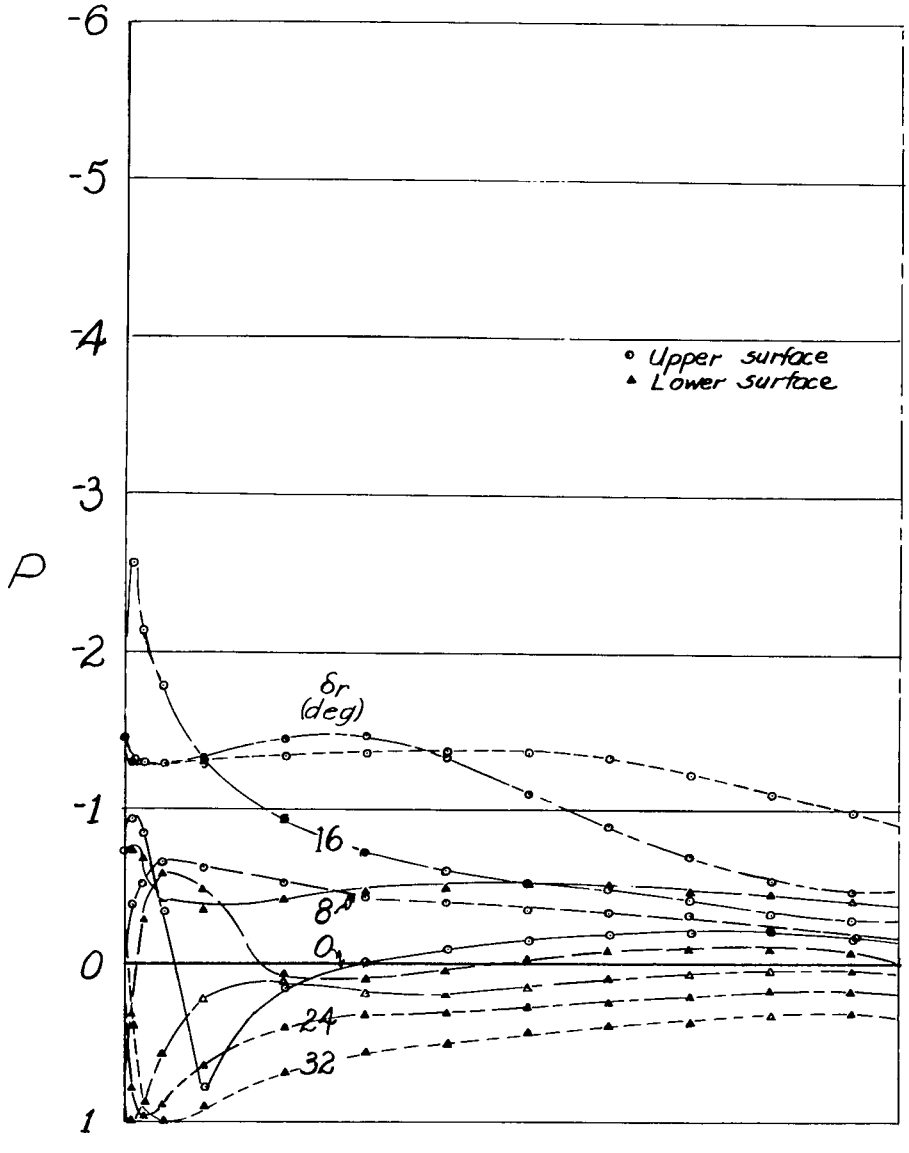

Figure 24.- Concluded.

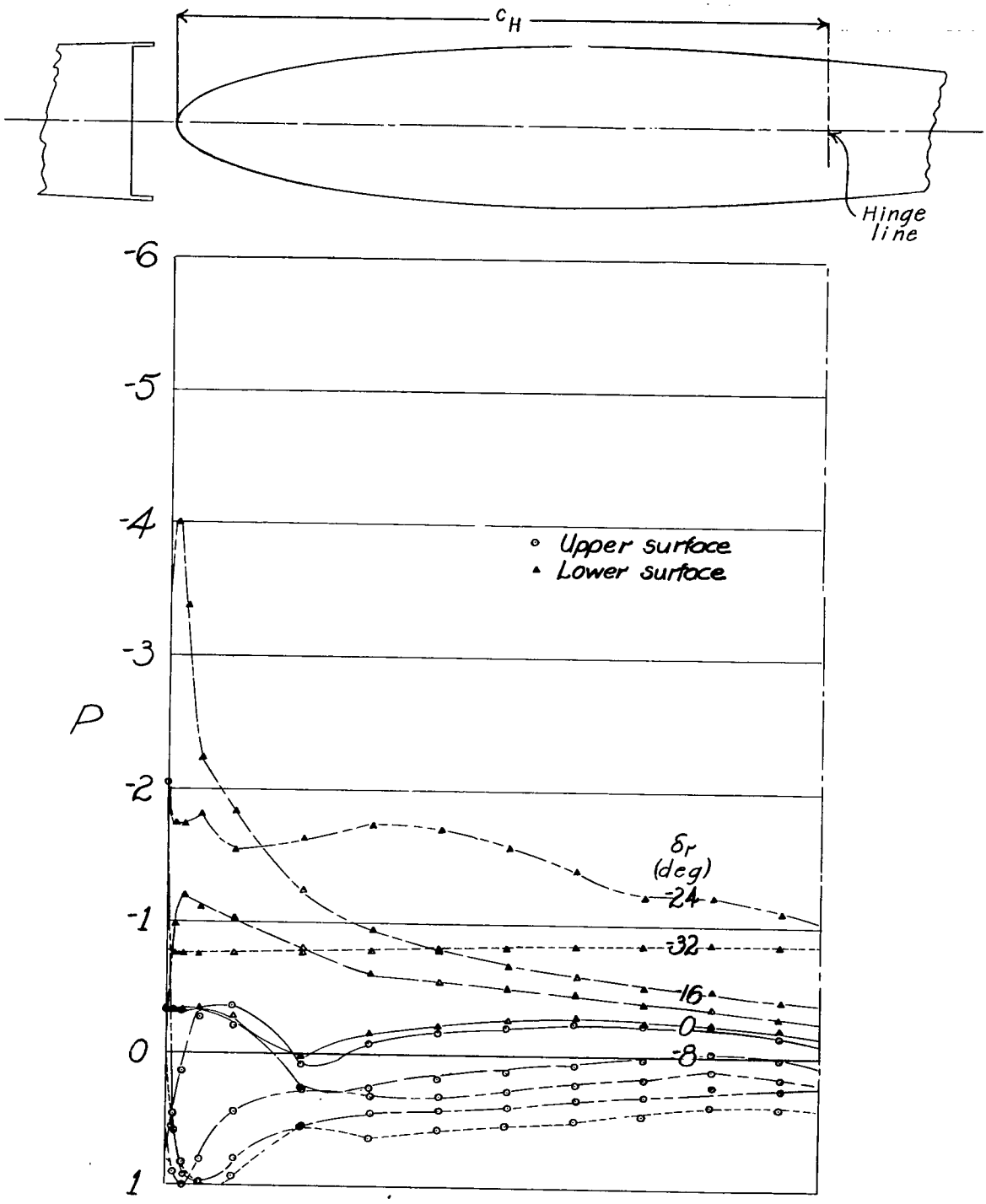

Figure 25.- Pressure distribution over horn 8-b on 0.7-scale model of XF6F vertical tail. α = 0°.

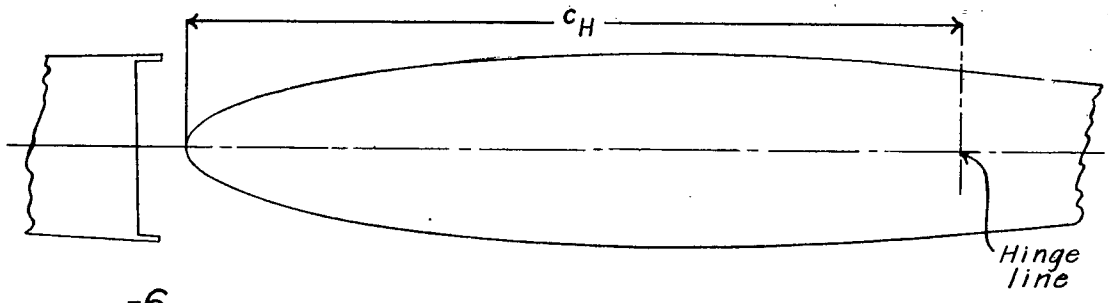

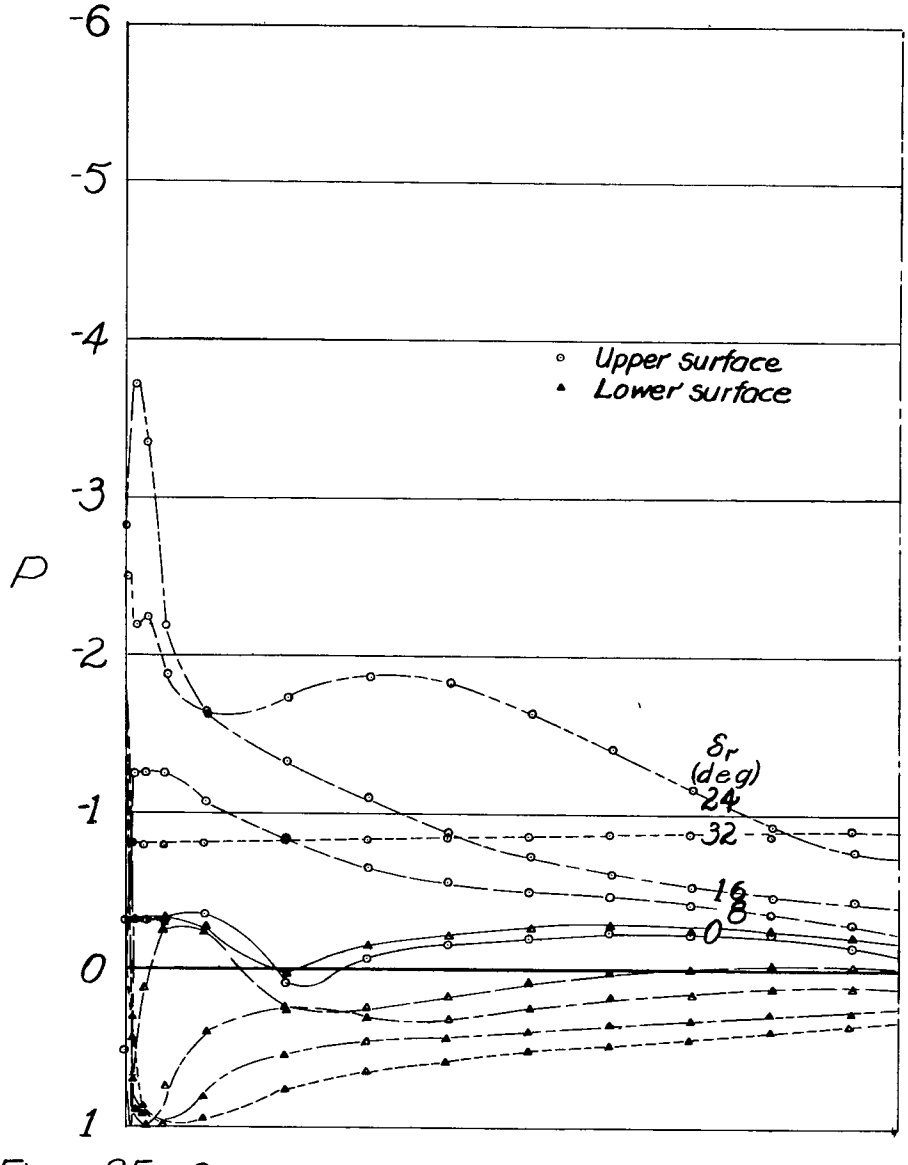

Figure 25.- Concluded.

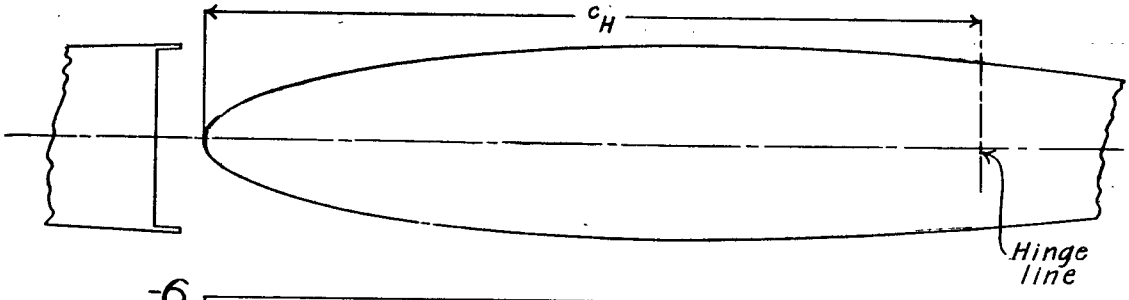

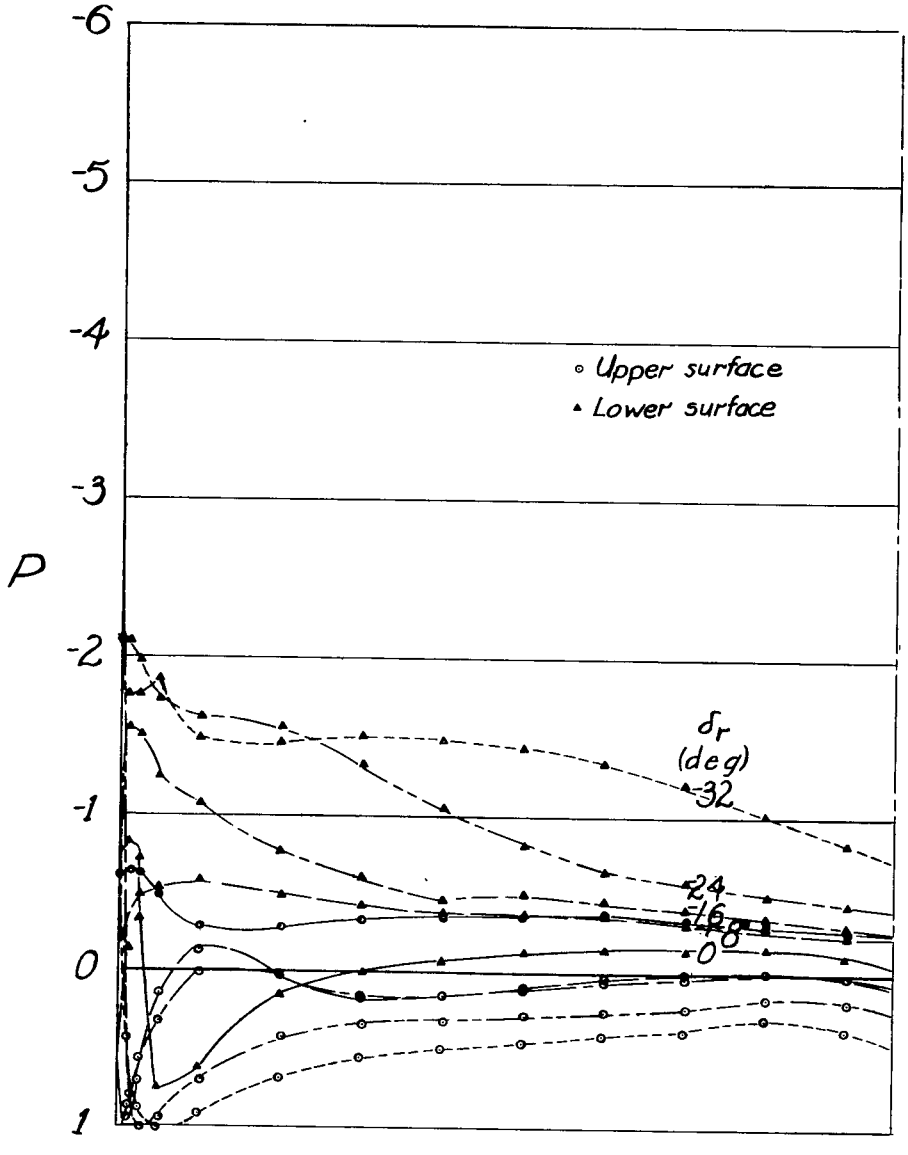

Figure 26.- Pressure distribution over horn 8-b on 07-scale model of XF6F vertical tail surface. $\alpha = 8°$.

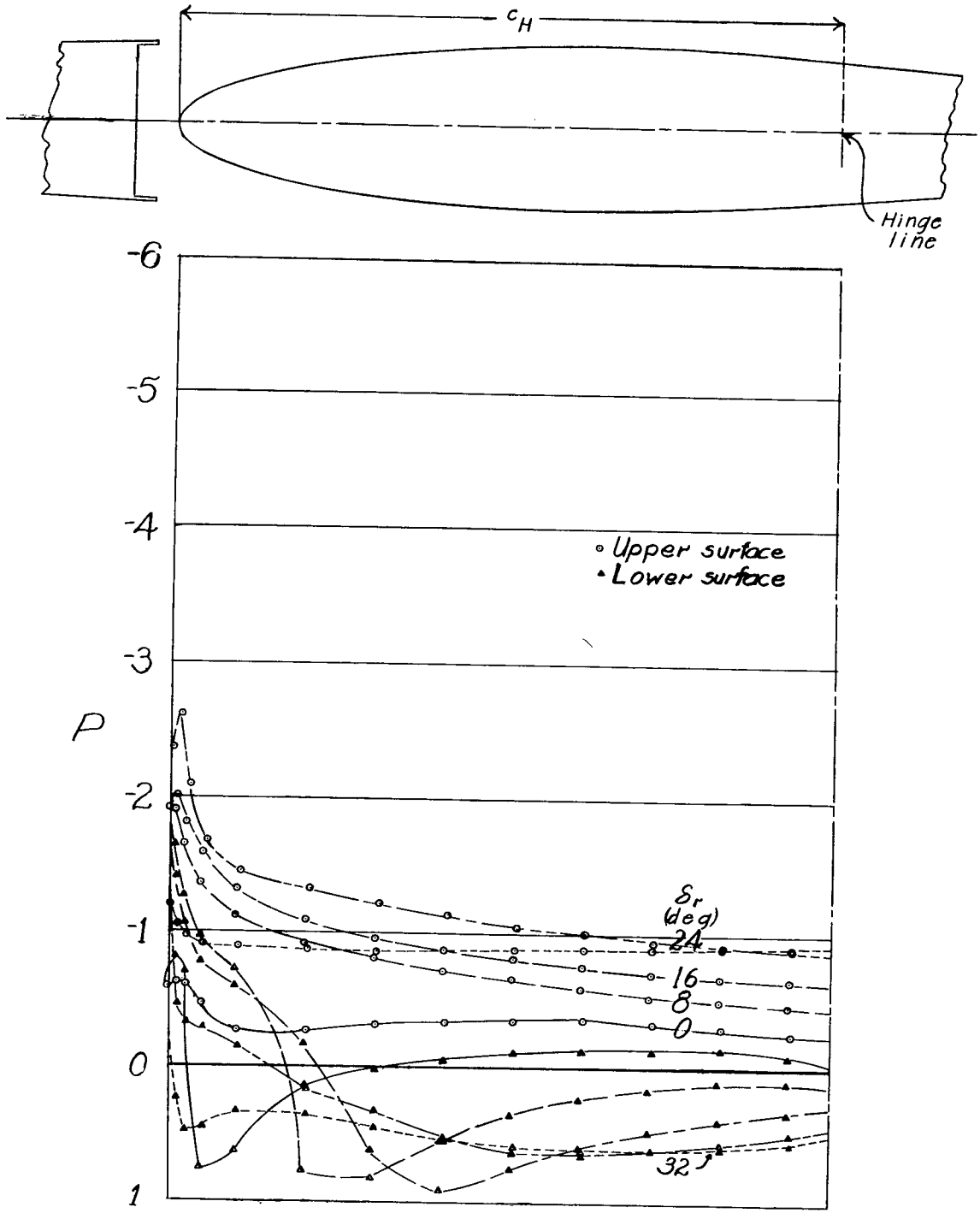

Figure 26.- Concluded.

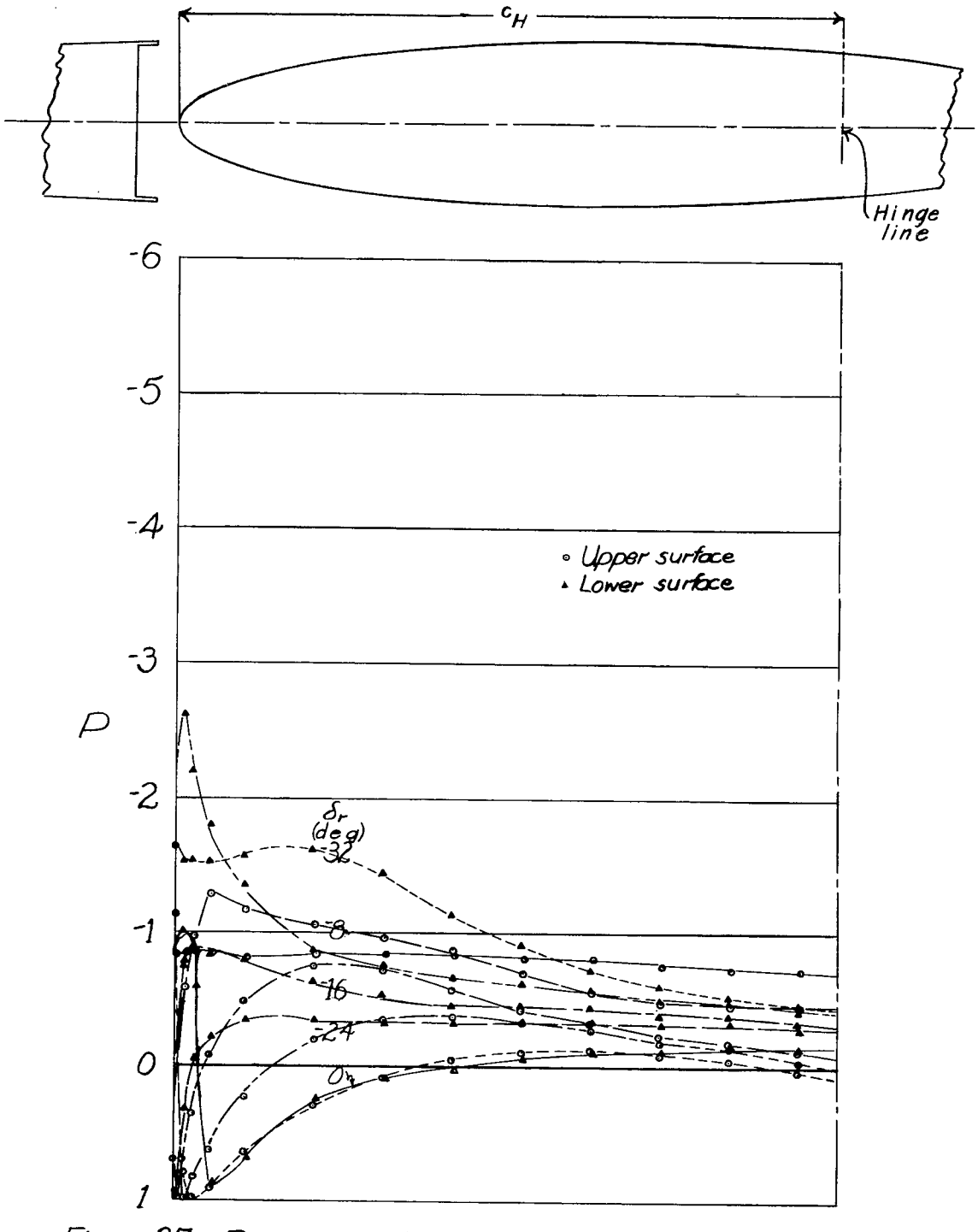

Figure 27.- Pressure distribution over horn 8-b on 0.7-scale model of XF6F vertical tail surface. $\alpha = 16°$.

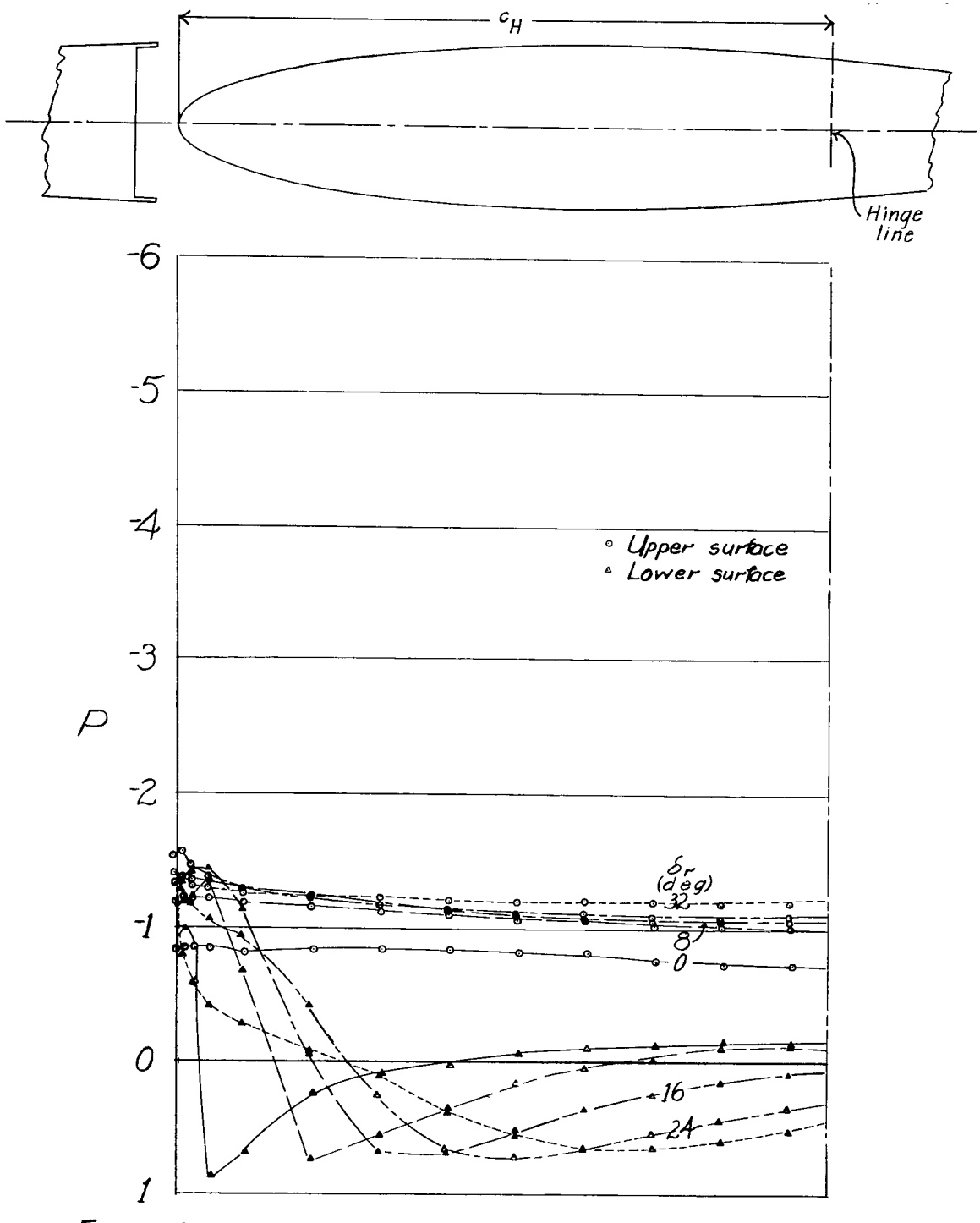

Figure 27.- Concluded.

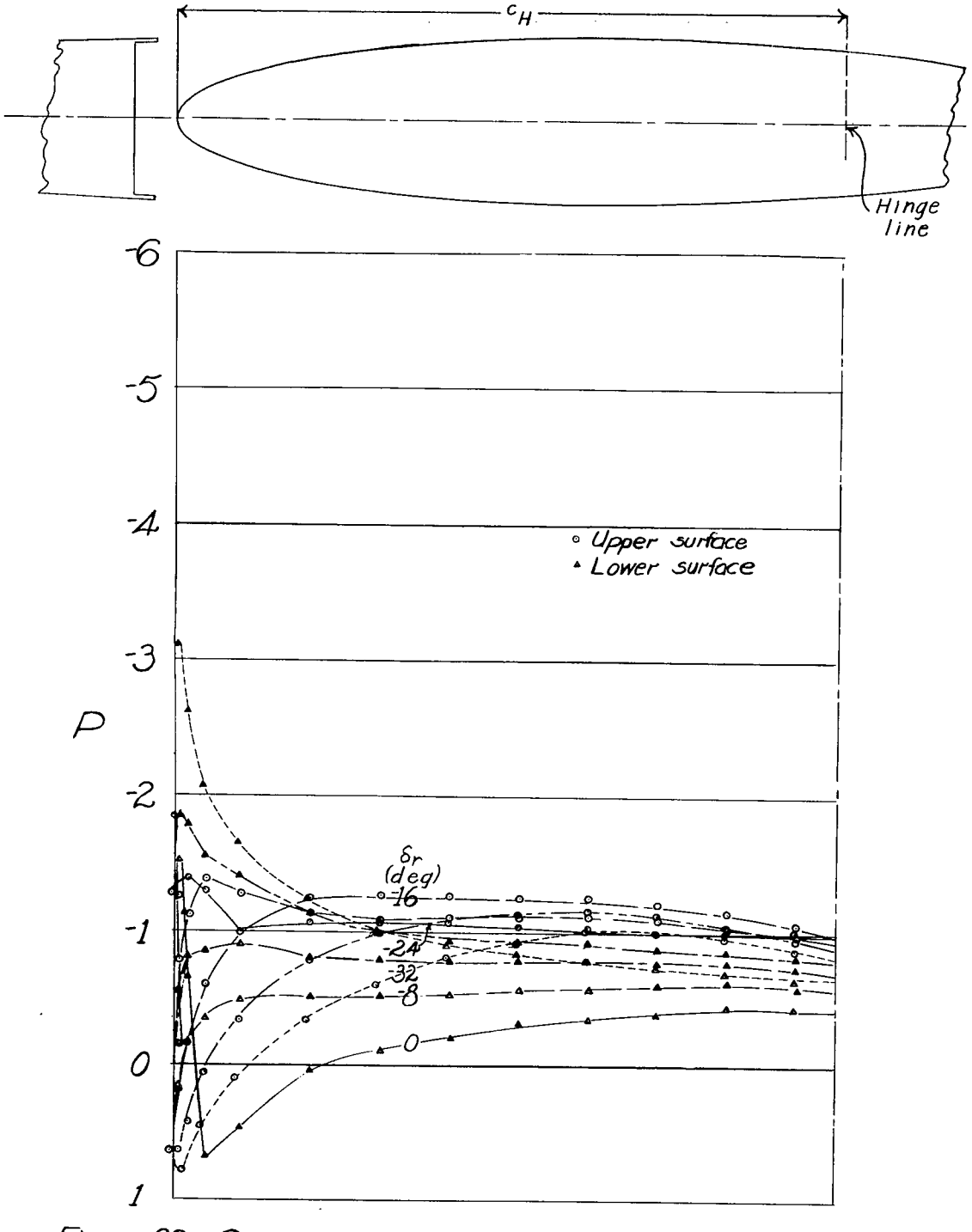

Figure 28.- Pressure distribution over horn 8-b on 0.7-scale model of XFEF vertical tail surface. $\alpha = 24°$

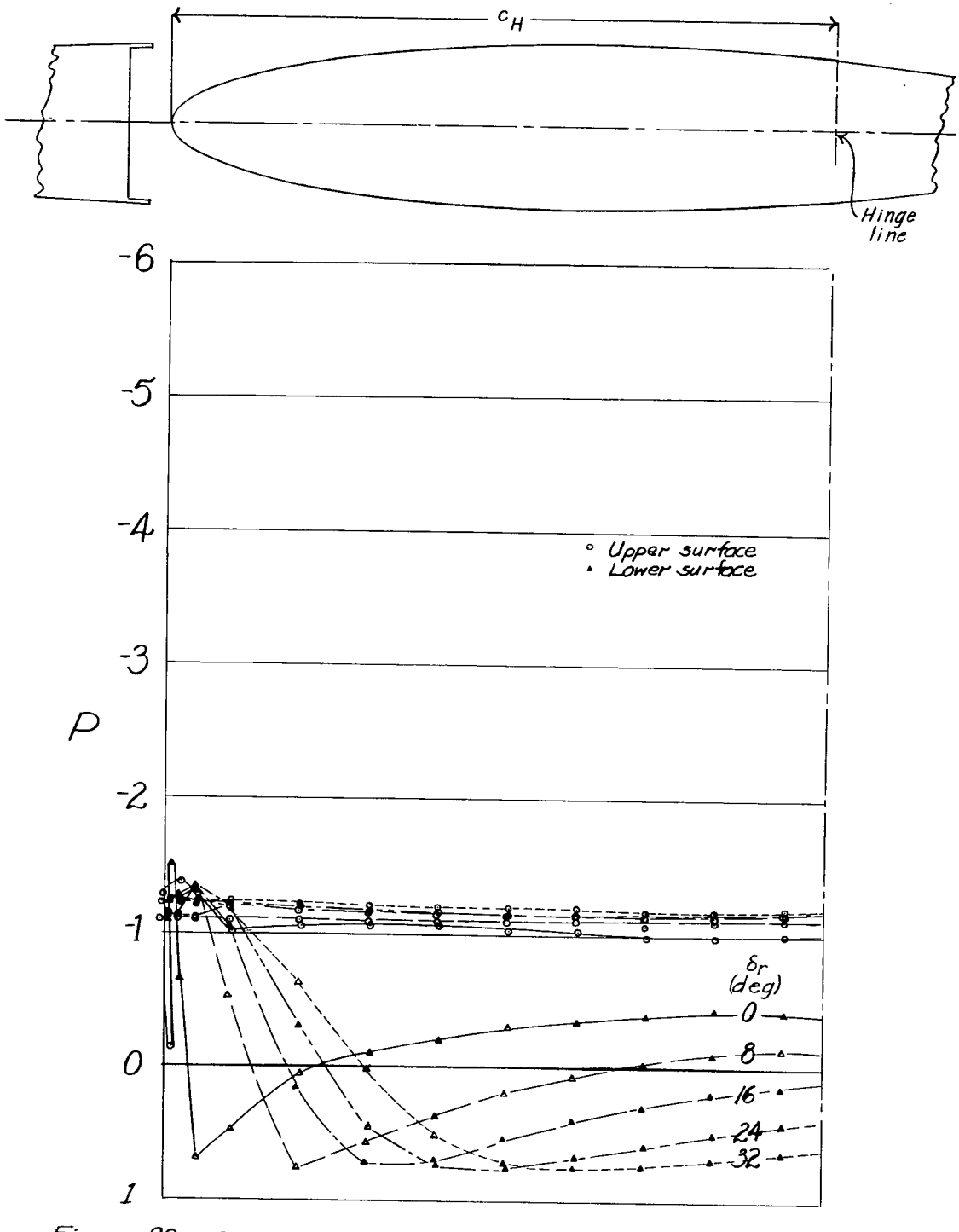

Figure 28.- Concluded.

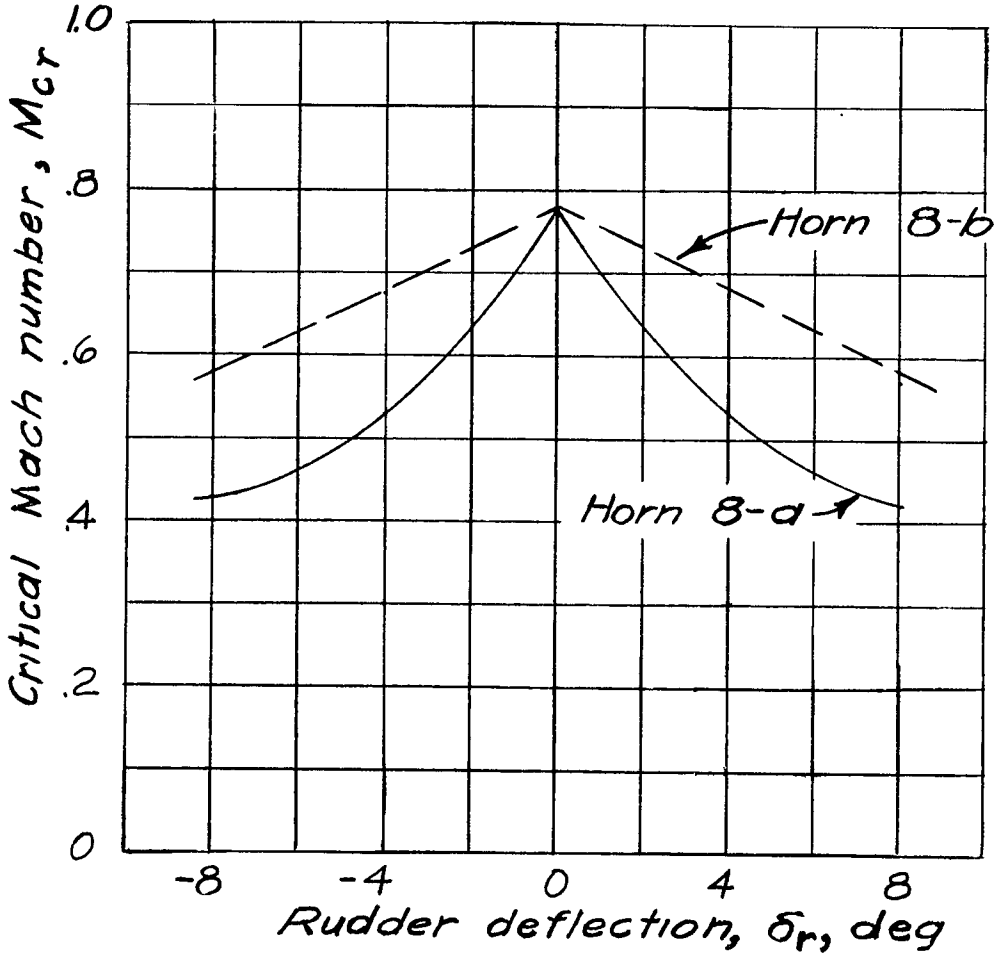

Figure 29.- Variation of critical Mach number with rudder deflection for two shielded horns on 0.7-scale model of XF6F vertical tail surface. $\alpha = 0°$.

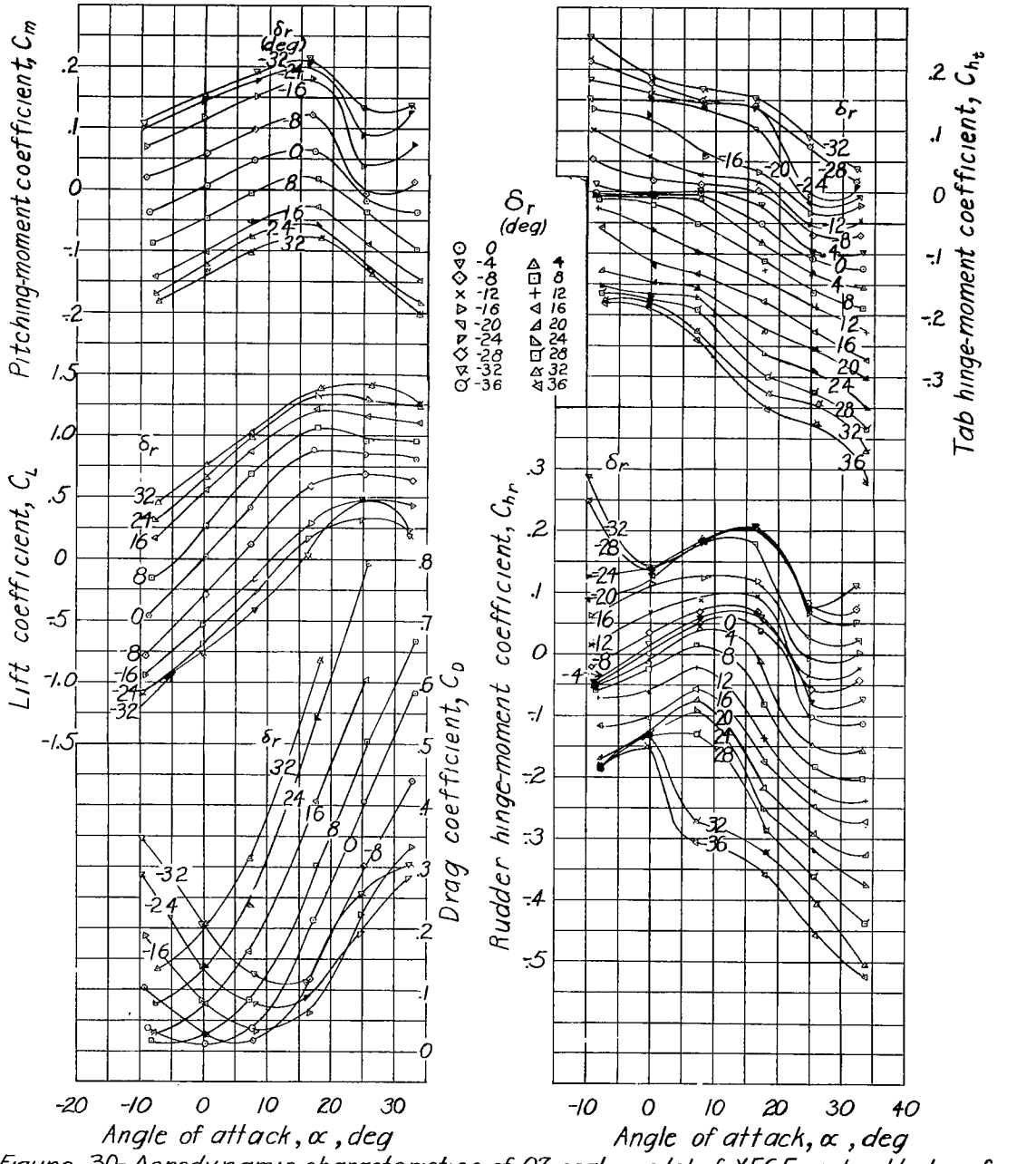

Figure 30.-Aerodynamic characteristics of 0.7-scale model of XF6F vertical tail surface with unshielded horn. Rudder gap sealed. $\delta_t = 0°$.

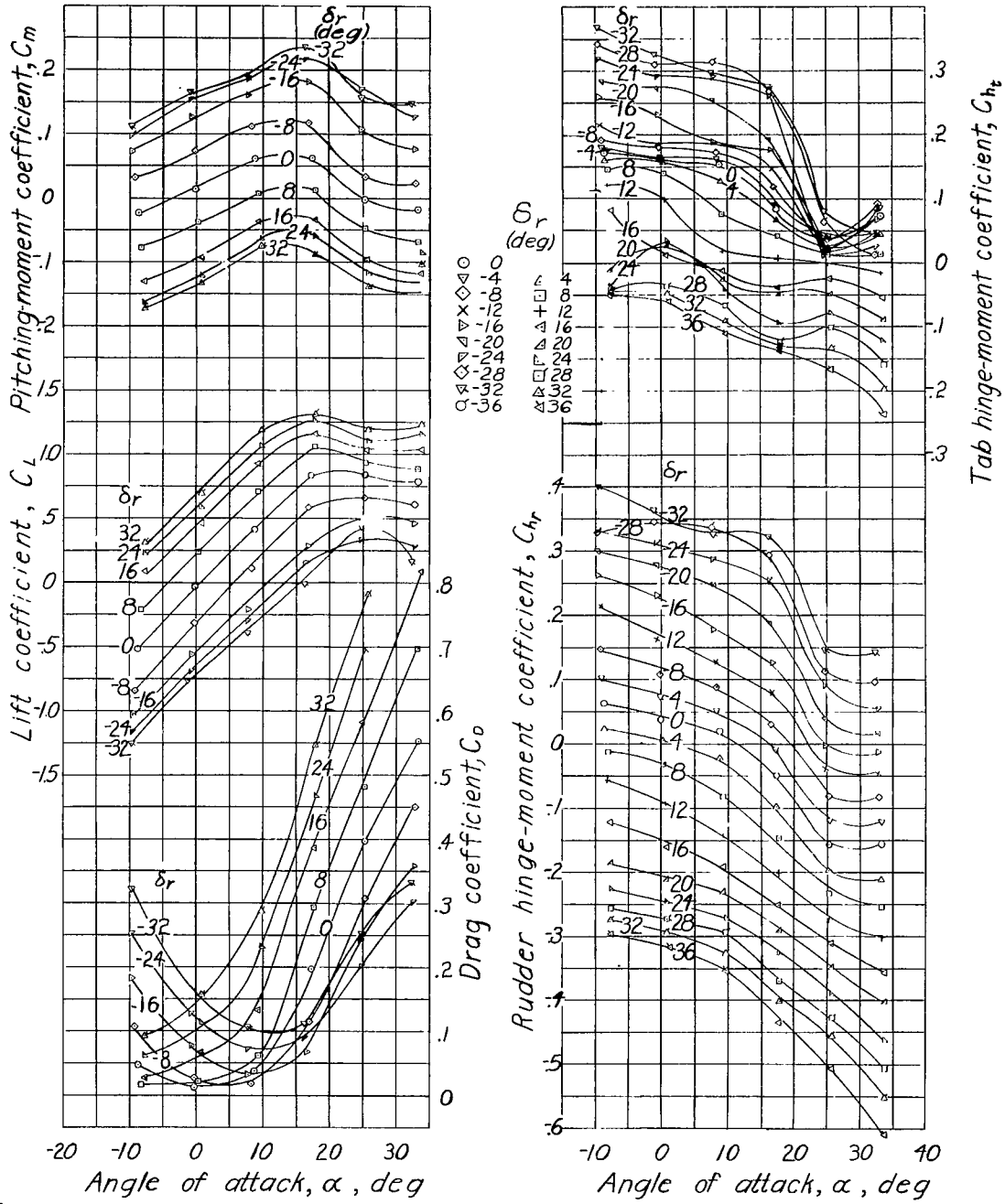

Figure 31.- Aerodynamic characteristics of 0.7-scale model of XF6F vertical tail surface. Plain sealed rudder. Original tab; $\delta_t = -20°$.

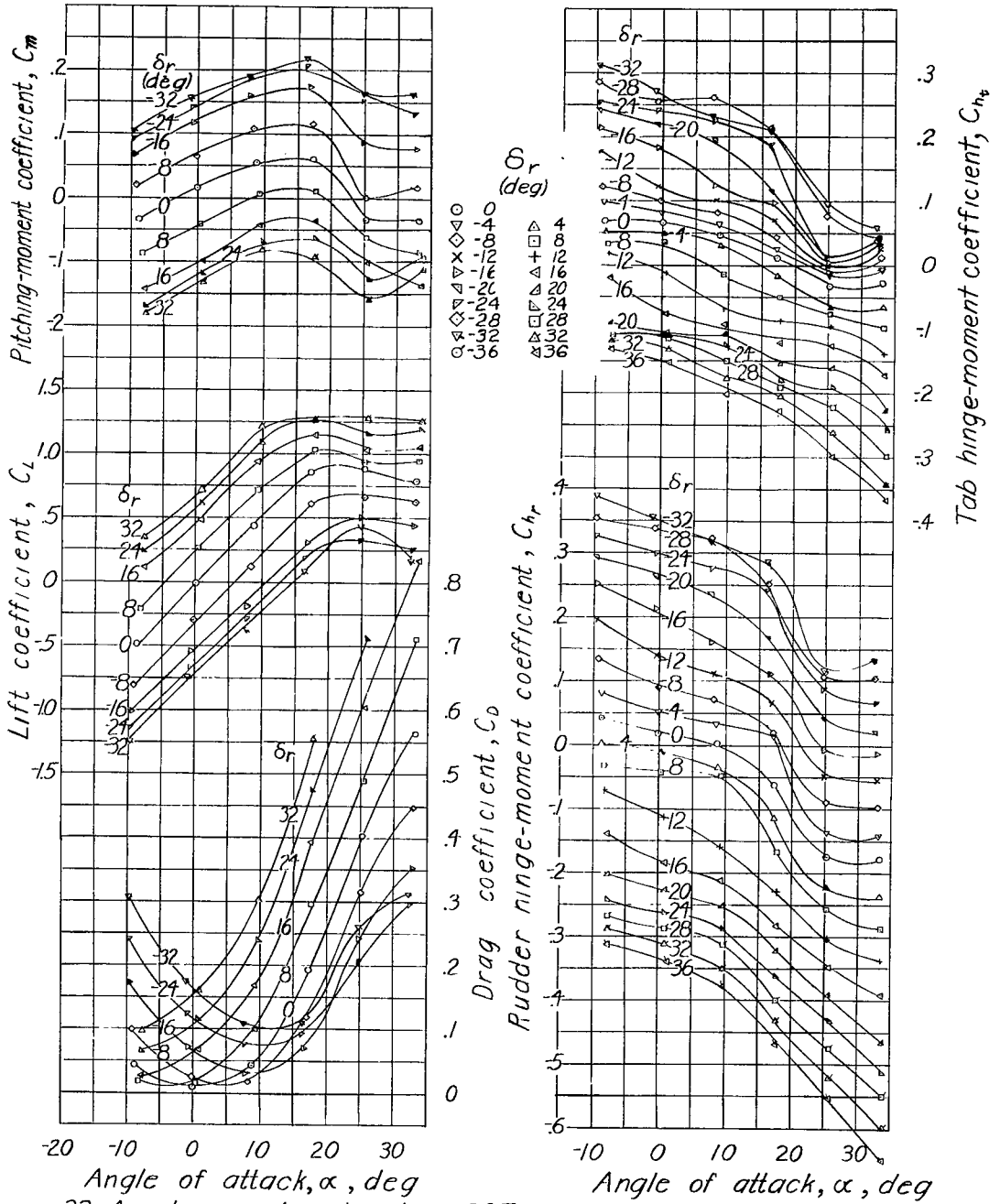

Figure 32.-Aerodynamic characteristics of 0.7-scale model of XF6F vertical tail surface. Plain sealed rudder. Original tab; $\delta_t = -10°$.

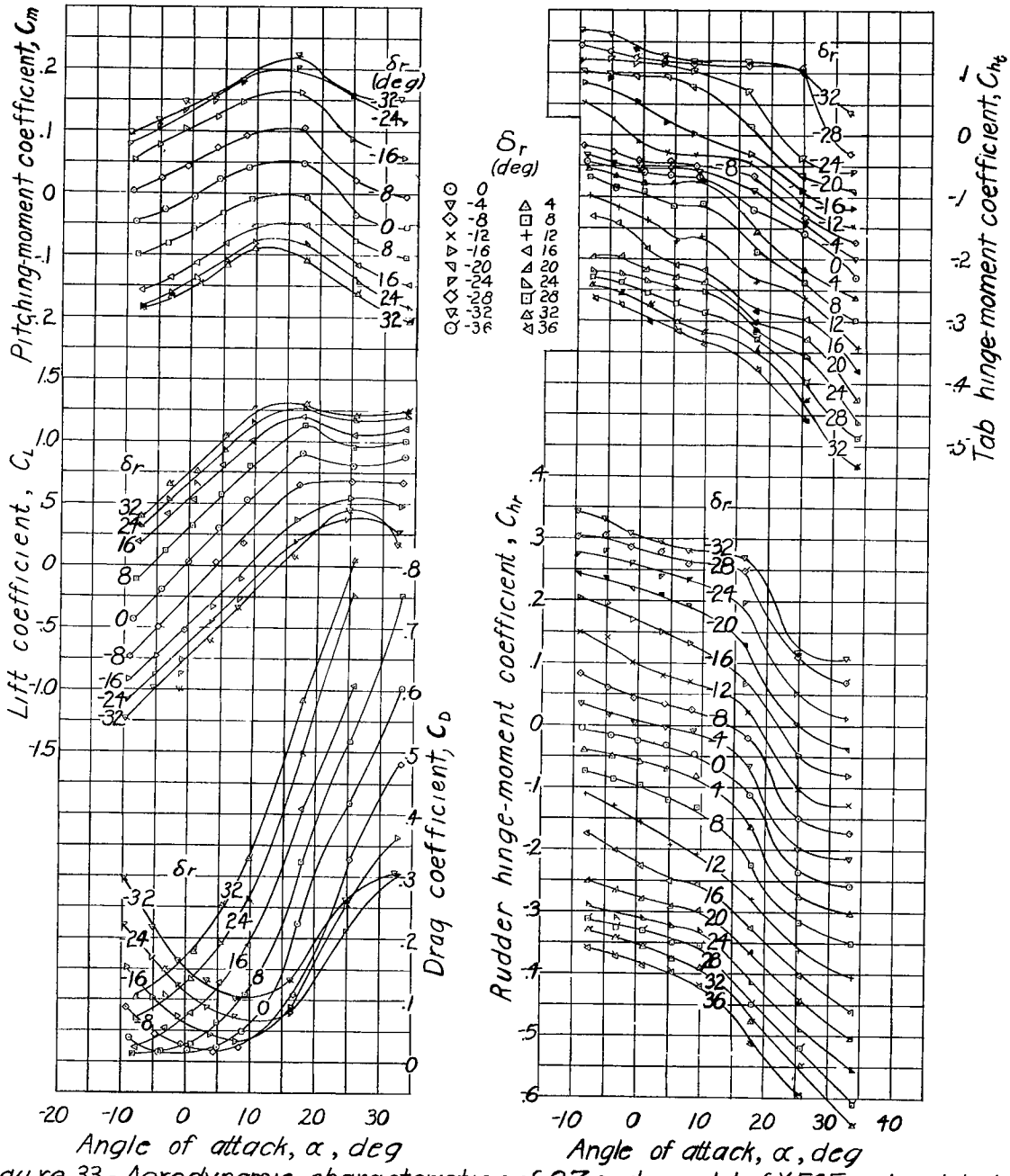

Figure 33.-Aerodynamic characteristics of 0.7-scale model of XF6F vertical tail surface. Plain sealed rudder. Original tab; $\delta_t = 10°$.

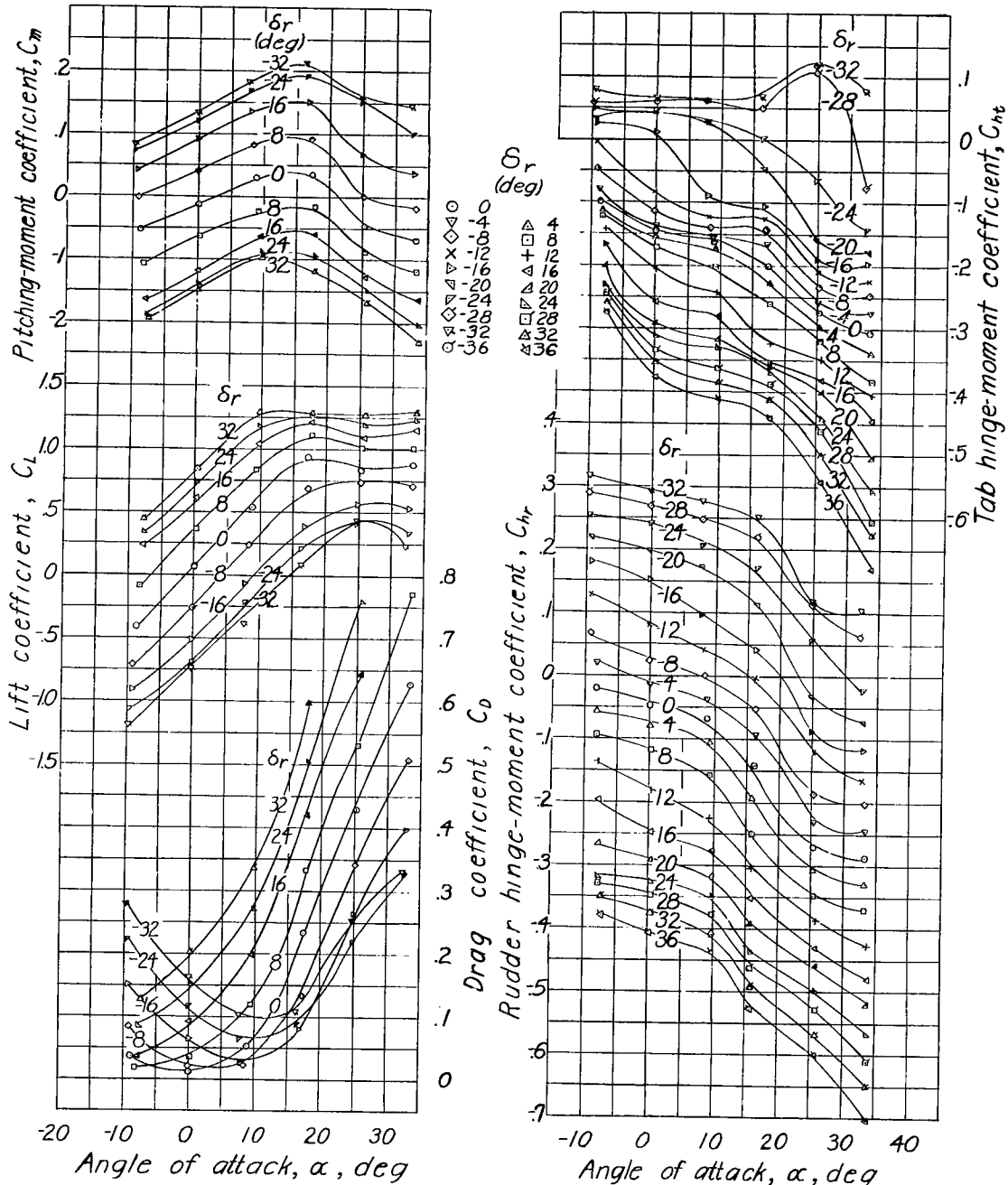

Figure 34.- Aerodynamic characteristics of 0.7-scale model of XF6F vertical tail surface. Plain sealed rudder. Original tab; $\delta_t = 20°$.

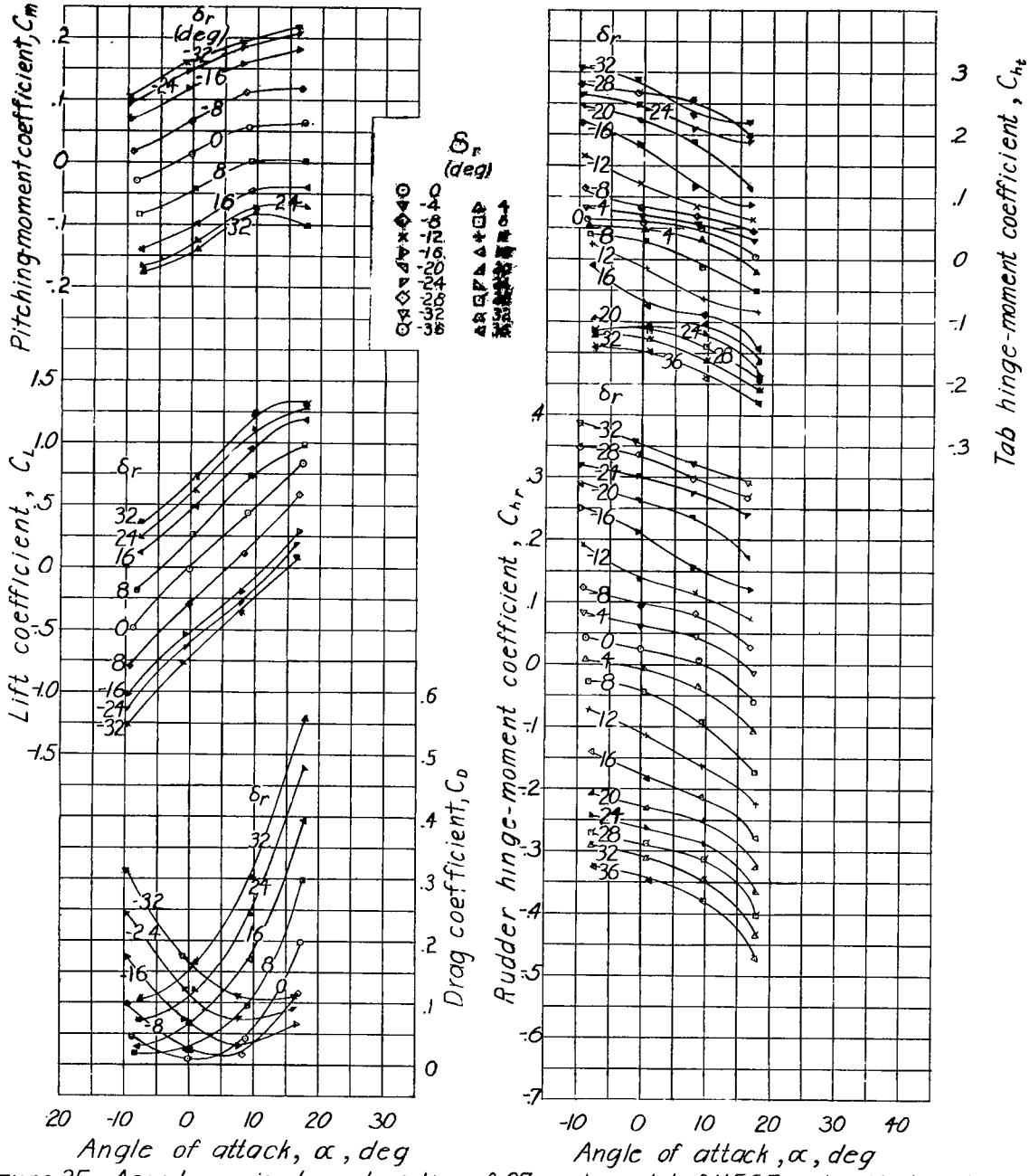

Figure 35.- Aerodynamic characteristics of 07-scale model of XF6F vertical tail surface. Plain sealed rudder. Original tab sealed; $\delta_t = -10°$.

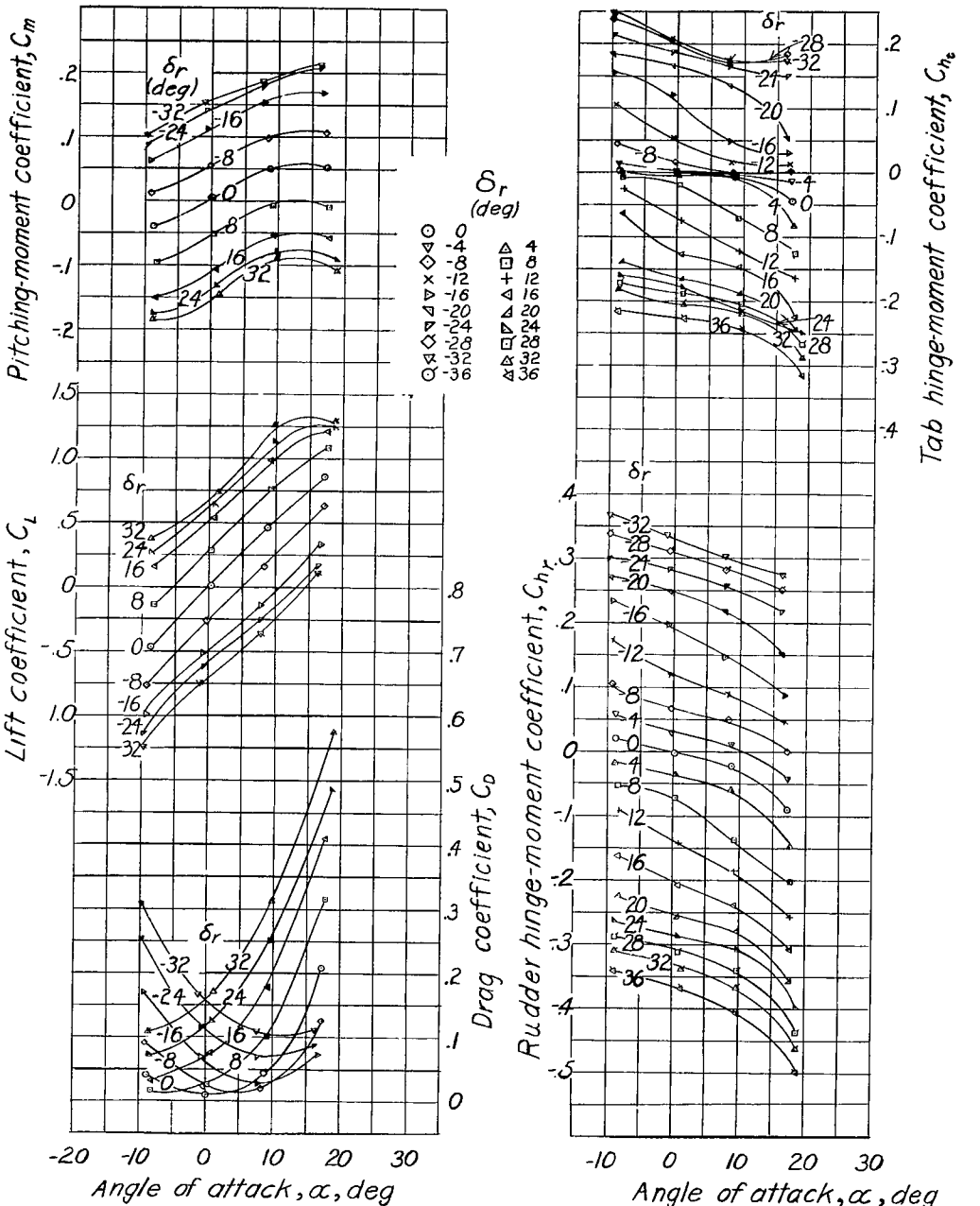

Figure 36.- Aerodynamic characteristics of 0.7-scale model of XF6F vertical tail surface. Plain sealed rudder. Original tab sealed; $\delta_t = 0°$.

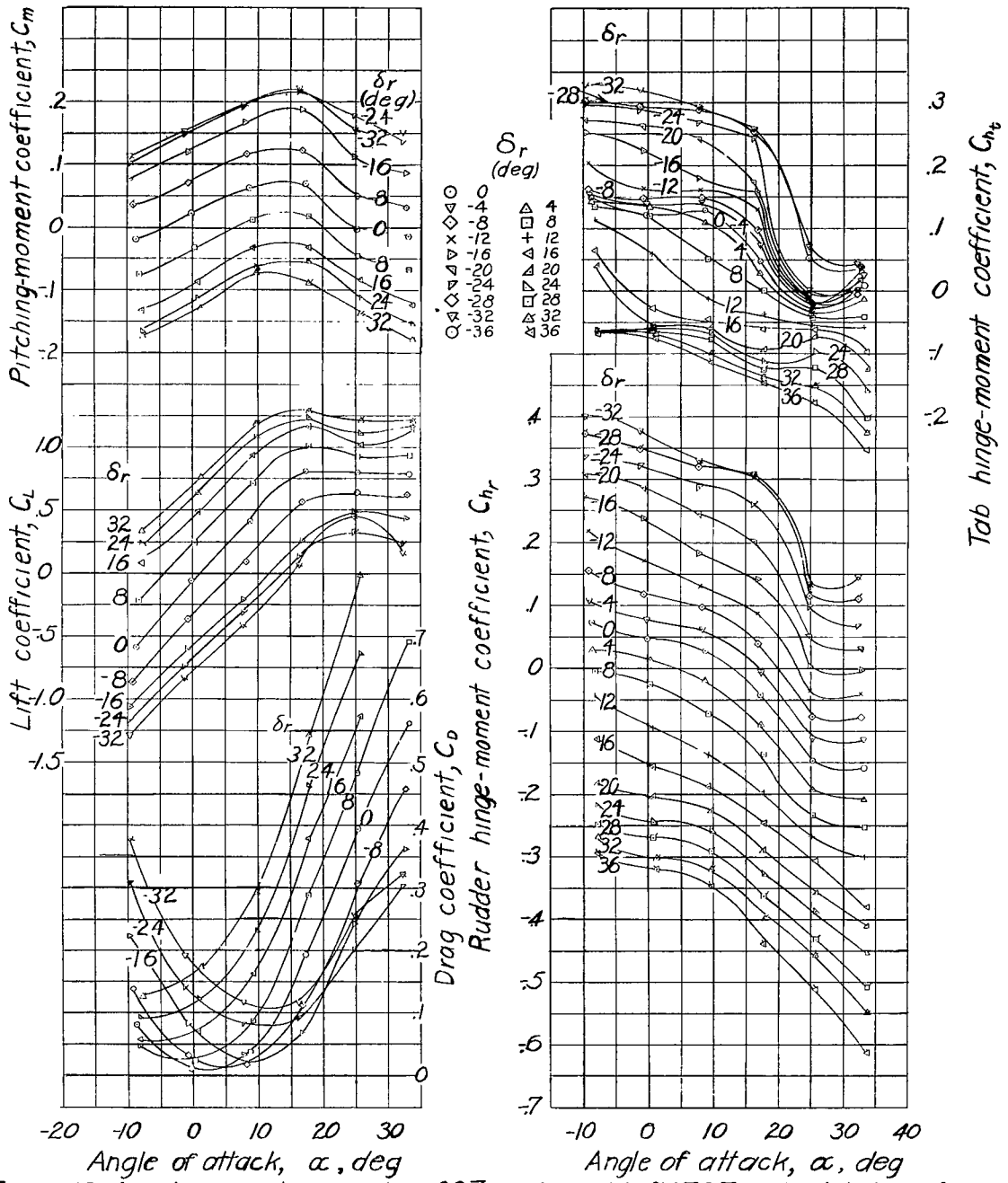

Figure 37.-Aerodynamic characteristics of 0.7-scale model of XF6F vertical tail surface. Plain sealed rudder. Round-nose tab; $\delta_t = -20°$.

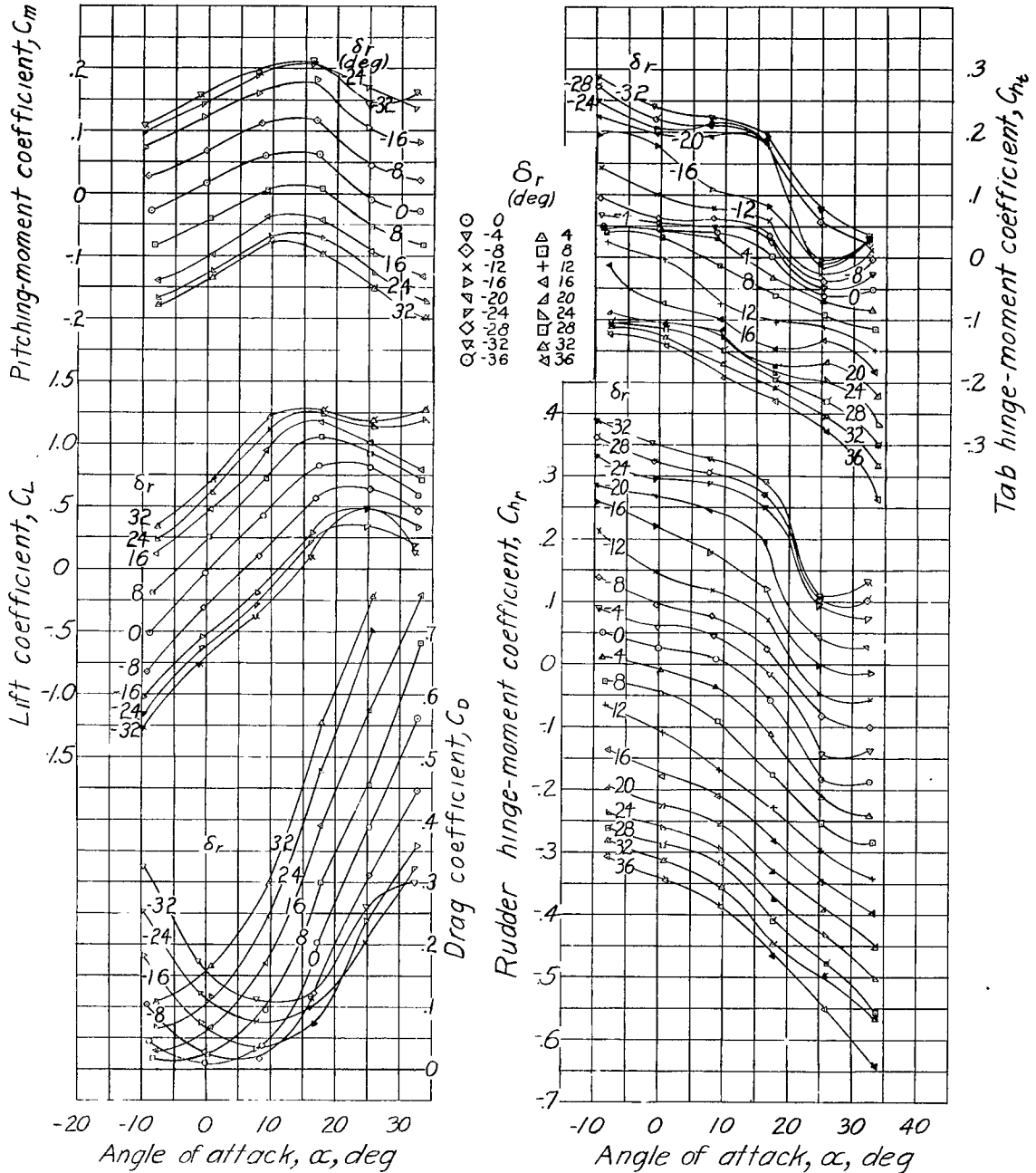

Figure 38.-Aerodynamic characteristics of 0.7-scale model of XF6F vertical tail surface. Plain sealed rudder. Round-nose tab; $\delta_t = -10°$.

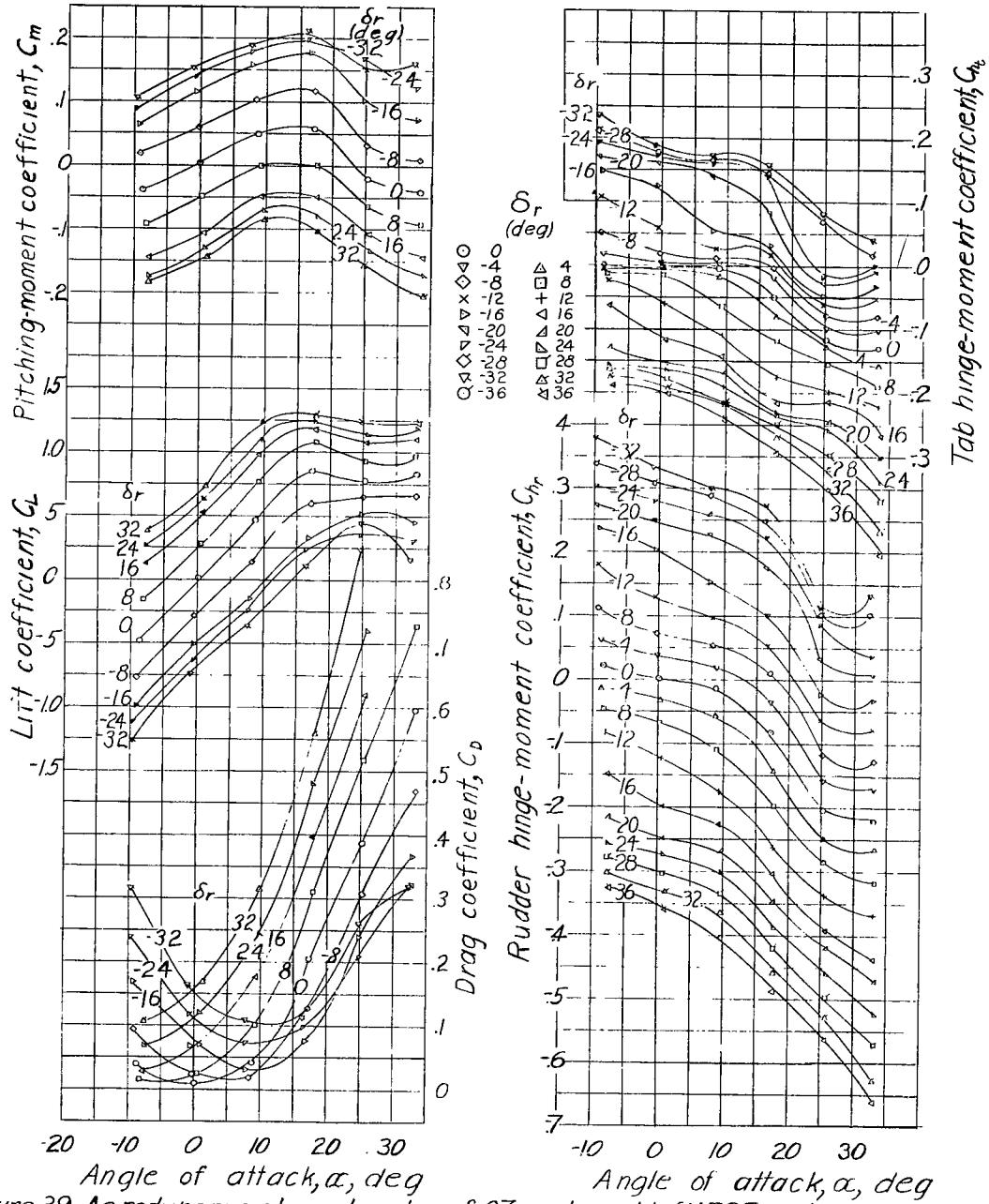

Figure 39.-Aerodynamic characteristics of 0.7-scale model of XF6F vertical tail surface. Plain sealed rudder. Round-nose tab; $\delta_t = 0°$.

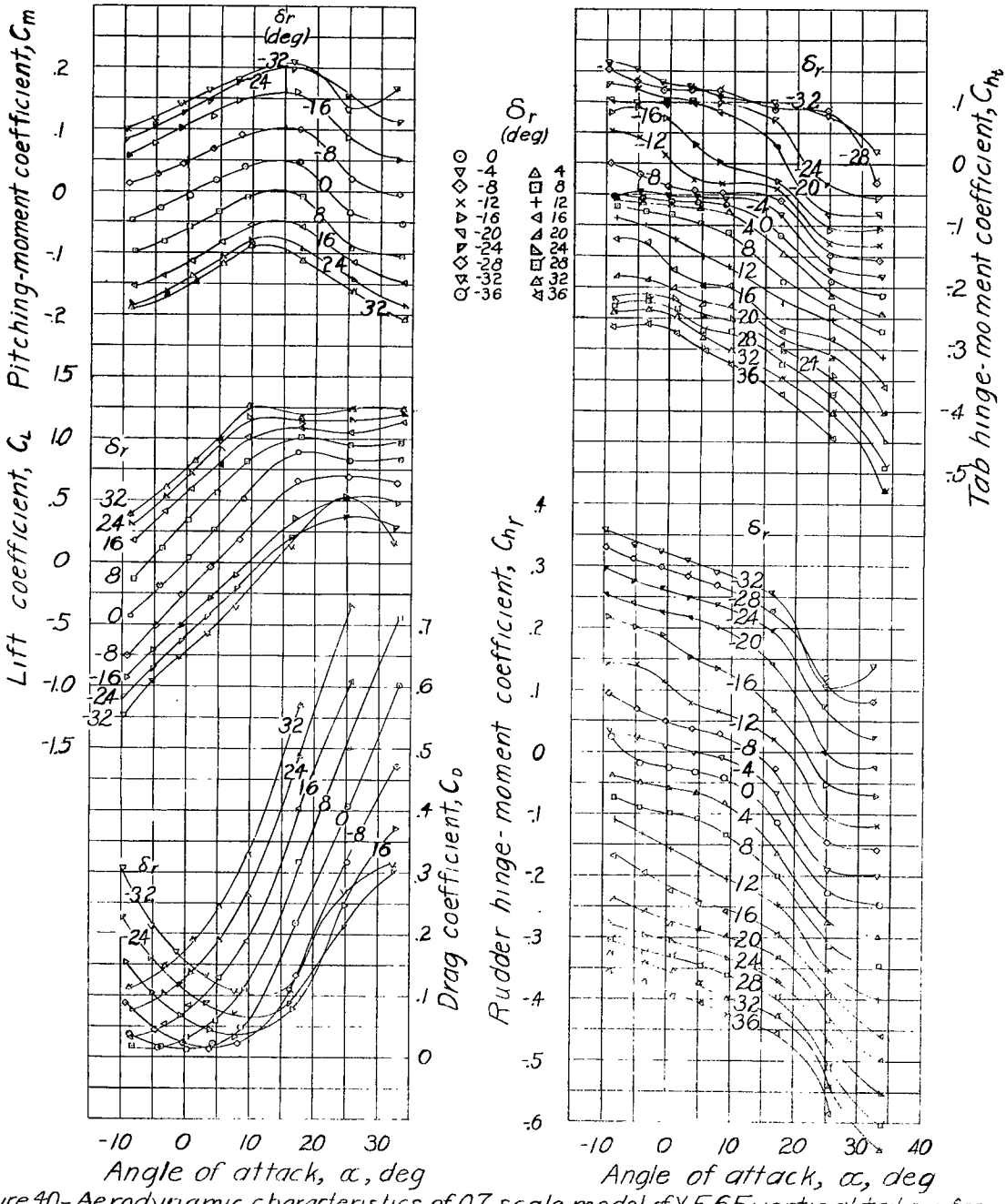

Figure 40.- Aerodynamic characteristics of 0.7-scale model of XF-6F vertical tail surface. Plain sealed rudder. Round-nose tab; $\delta_t = 10°$.

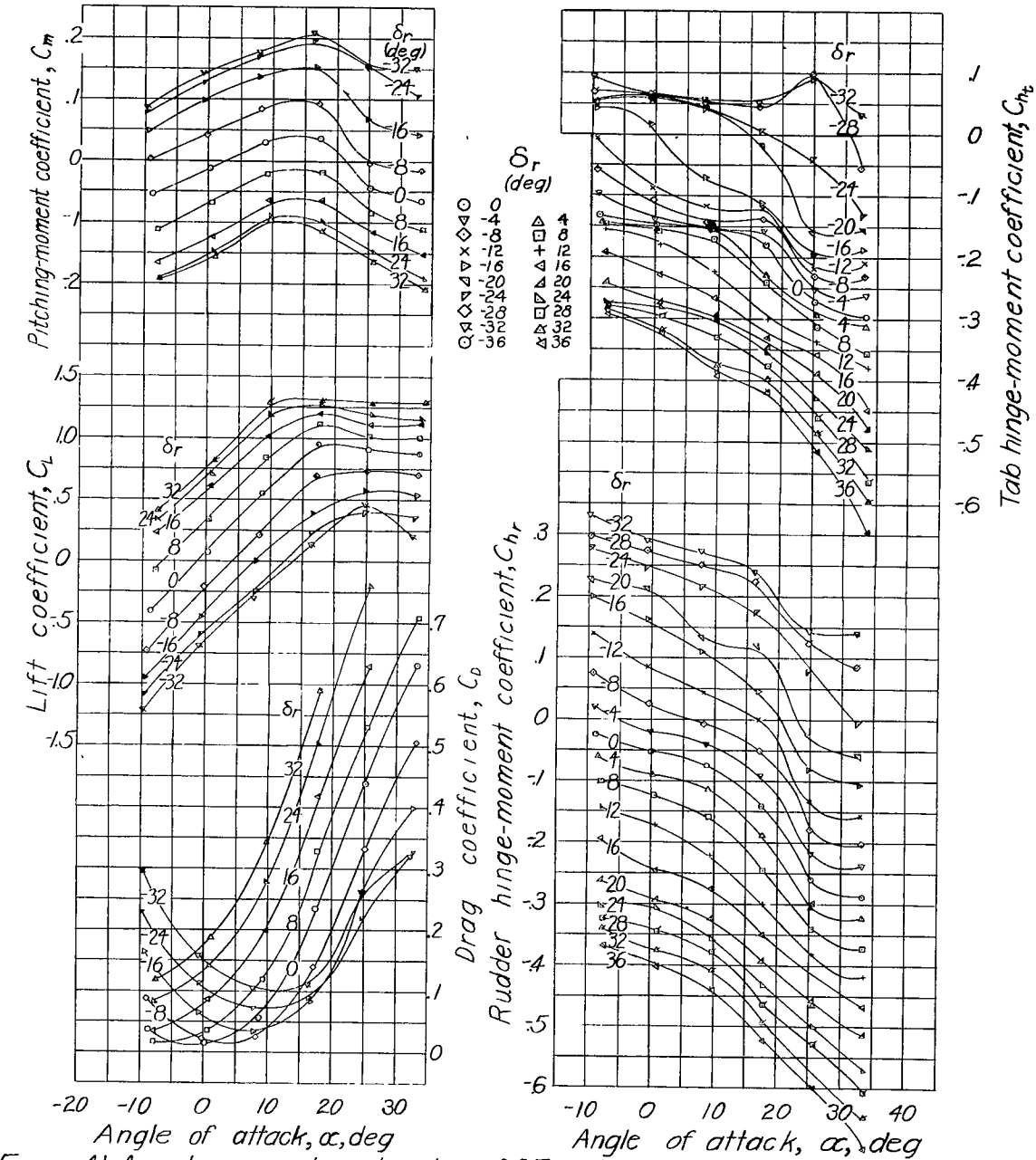

Figure 41.-Aerodynamic characteristics of 0.7-scale model of XF6F vertical tail surface. Plain sealed rudder. Round-nose tab; $\delta_t = 20°$.

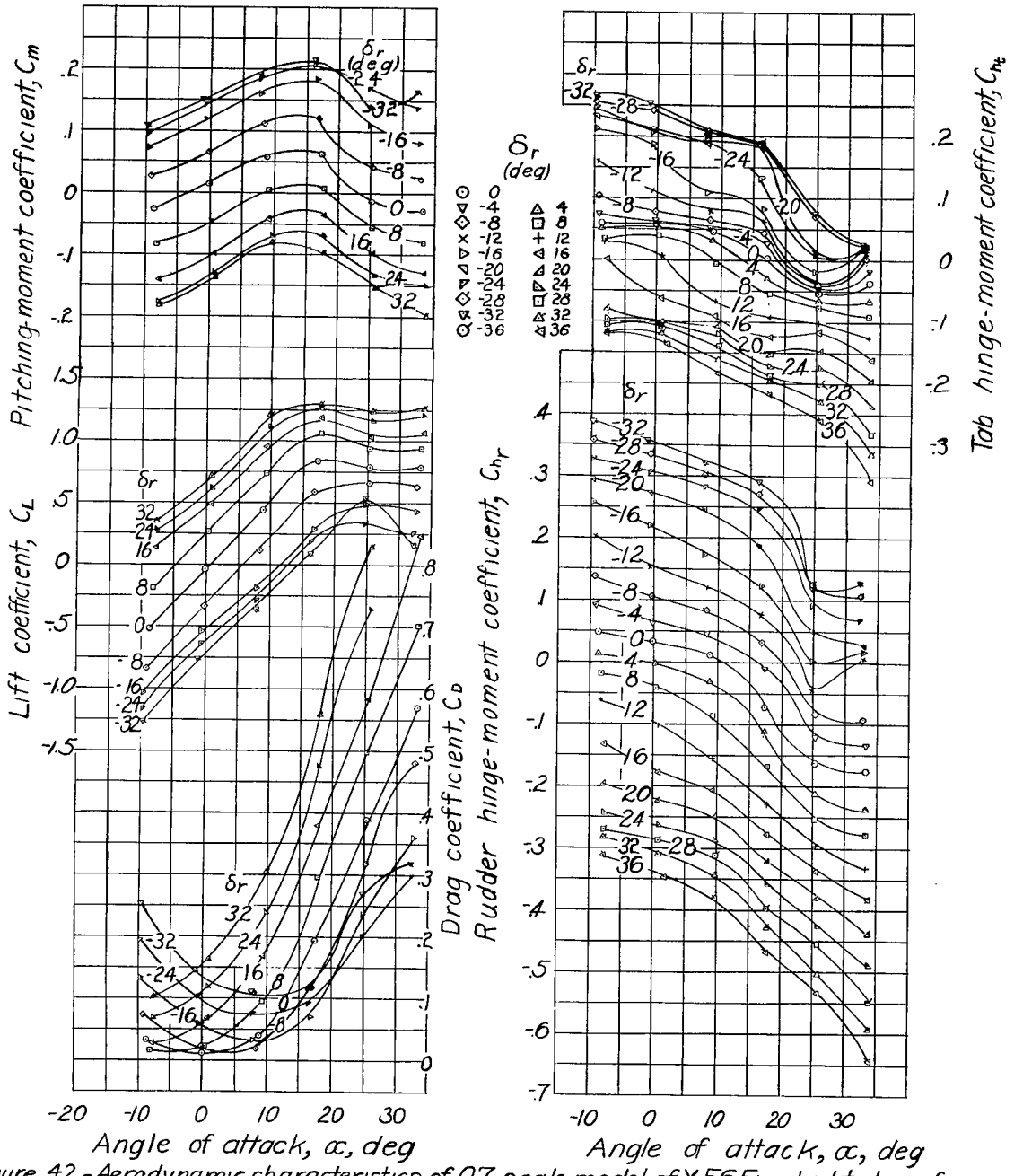

Figure 42.-Aerodynamic characteristics of 0.7-scale model of XF6F vertical tail surface. Plain sealed rudder. Round-nose tab sealed; $\delta_t = -10°$.

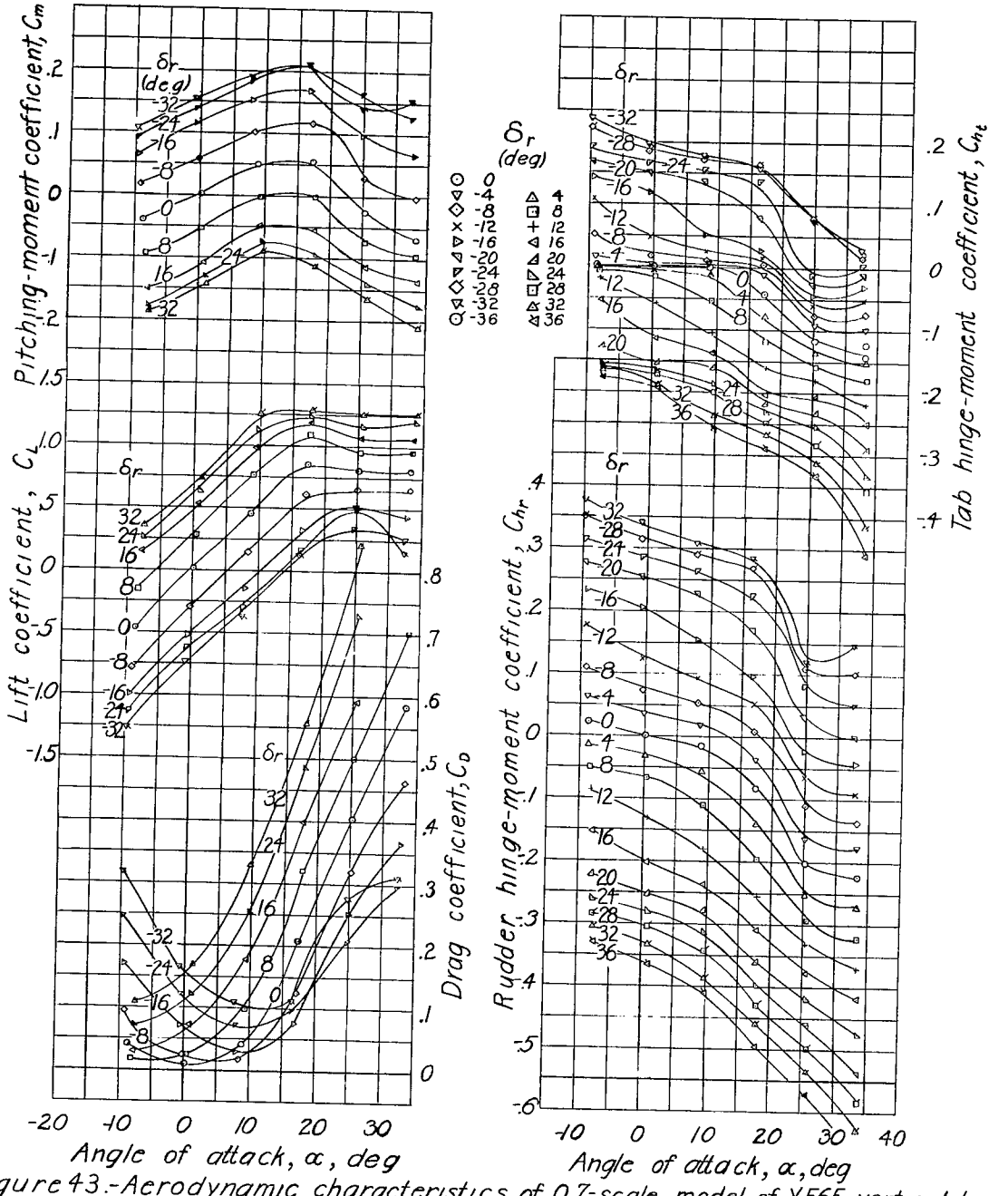

Figure 43.-Aerodynamic characteristics of 0.7-scale model of XF6F vertical tail surface. Plain sealed rudder. Round-nose tab sealed; $\delta_t = 0°$.

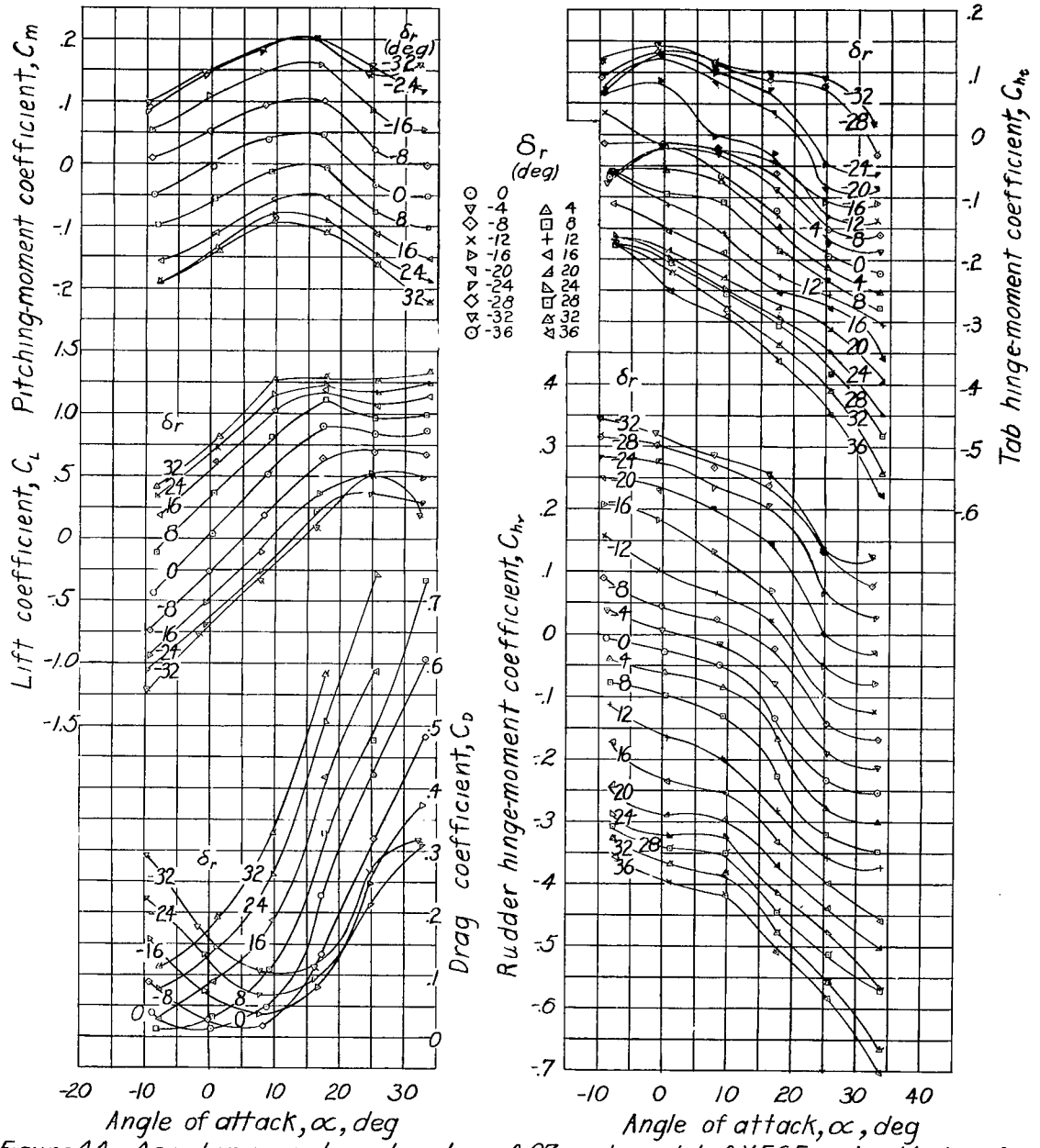

Figure 44.- Aerodynamic characteristics of 0.7-scale model of XF6F vertical tail surface. Plain sealed rudder. Round-nose tab sealed; $\delta_t = 10°$